Evaluation and Optimization of Multiple-Input Multiple-Output Antenna Schemes for Next-Generation Wireless Broadcasting

Departamento de Comunicaciones
Universitat Politècnica de València

A thesis for the degree of
Ph.D. in Telecommunications Engineering
Valencia, November 2023

Author:
Takuya Shitomi

Supervisor:
Prof. David Gómez Barquero

Academic Tutor:
Prof. Narcís Cardona Marcet

Abstract

Multiple-Input Multiple-Output (MIMO) antenna schemes in Digital Terrestrial Television (DTT) systems aim to maximize the spectral efficiency for the provision of large capacity contents in the scarce and limited DTT Radio-Frequency (RF) channel. The delivery of the emerging Ultra-High Definition TV (UHDTV) services as well as the continuous broadcast spectrum shortage due to the rapidly growing demand for wireless broadband services (4G and 5G) are the motivations for this proposal.

MIMO technologies have been firstly developed in the DTT technical specification DVB-NGH (*Digital Video Broadcasting Next Generation Handheld*) and standardized in the latest DTT standard, ATSC3.0 (*Advanced Television Systems Committee 3rd Generation*). However, MIMO broadcasting has not been commercialized due to the additional investment for both service providers and receivers. On the other hand, mobile industry has developed mobile broadcast technologies known today as 5G Broadcast based on LTE (*Long Term Evolution*). Although LTE incorporates MIMO for point to point unicast, 5G Broadcast only uses a single antenna in transmission at the moment.

The Ph.D. aims at assessing the performance of MIMO for broadcasting (*terrestrial broadcast*) for next-generation wireless broadcasting systems, including next-generation wireless broadcasting systems, both DTT and cellular system. During the standardization of MIMO DTT systems, the initial design accounts for perfect reception conditions, e.g., optimal demodulators, perfect Channel State Information (CSI), perfect noise power estimation. The main goal of this PhD is to assess and optimize the performance of MIMO wireless broadcast transmissions in realistic scenarios. This PhD proposes new models of terrestrial MIMO propagation channels based on field measurements which can be utilized for the evaluation of MIMO DTT system. Furthermore, it also optimizes the different MIMO transmission and reception configurations, such as broadcast MIMO channel estimation and signal processing. The scenarios considered in the thesis are high-power high-tower transmitter with fixed reception and characteristics of DTT networks.

The results of the PhD have contributed to the ATSC standardization forum, International Telecommunication Union Radiocommunication Sector (ITU-R), and the Japanese national research project on next generation DTT system.

Resumen

Los esquemas de antenas de múltiples entradas y múltiples salidas (MIMO) pueden maximizar la eficiencia espectral de los sistemas de Televisión Digital Terrestre (TDT) para la provisión de contenidos de gran capacidad, como los servicios emergentes de televisión de ultra alta definición (UHDTV), en el cada vez más escaso y limitado espectro radioeléctrico de la TDT debido a la creciente demanda de servicios inalámbricos de banda ancha (4G y 5G).

Las tecnologías MIMO han sido desarrolladas inicialmente en la especificación técnica de TDT DVB-NGH (*Digital Video Broadcasting Next Generation Handheld*) y estandarizadas en el último estándar de TDT, ATSC 3.0 (*Advanced Television Systems Committee 3rd Generation*). Sin embargo, no hay despliegues comerciales MIMO de TDT. Por otro lado, la industria móvil ha desarrollado una tecnología de radiodifusión móvil, conocida como hoy en día como 5G Broadcast, basado en LTE (*Long Term Evolution*). Aunque LTE incorpora MIMO para transmisiones unicast punto a punto, 5G Broadcast sólo utiliza una única antenna en transmisión.

Esta tesis doctoral tiene como objetivo evaluar el rendimiento de MIMO para radiodifusión (*terrestrial broadcast*) para sistemas inalámbricos de radiodifusión de nueva generación, tanto TDT como sistemas celulares. Durante la estandarización de los sistemas MIMO TDT, el diseño inicial tiene en cuenta condiciones de recepción perfectas, por ejemplo, demoduladores óptimos, información de estado del canal (CSI) perfecta, estimación perfecta de la potencia del ruido, etc. El objetivo principal de esta tesis doctoral es evaluar y optimizar el rendimiento de las transmisiones de radiodifusión MIMO en escenarios realistas. Esta tesis doctoral propone nuevos modelos de canales de propagación MIMO terrestres basados en medidas de campo que pueden utilizarse para la evaluación del rendimiento del sistema MIMO TDT. Además, también optimiza las diferentes configuraciones de transmisión y recepción MIMO, como la estimación de los canales MIMO en el receptor, y el procesado de señal. El escenario considerado en la tesis son torres de alta potencia con recepción fija, característico de las redes de TDT.

Los resultados de esta tesis han contribuido al foro de estandarización ATSC, al sector de radiocomunicaciones de la Unión Internacional de Telecomunicaciones (UIT-R) y al proyecto nacional japonés de investigación sobre el sistema TDT de próxima generación.

Resum

Els esquemes d‟antenes de múltiples entrades i múltiples sortides (MIMO) poden maximitzar l‟eficiència espectral dels sistemes de Televisió Digital Terrestre (TDT) per a la provisió de continguts de gran capacitat, com els serveis emergents de televisió d‟ultra alta definició (UHDTV), en el cada vegada més escàs i limitat espectre radioelèctric de la TDT a causa de la creixent demanda de serveis sense fil de banda ampla (4G i 5G).

Les tecnologies MIMO han estat desenvolupades inicialment en l'especificació tècnica de TDT DVB-NGH (*Digital Video Broadcasting Next Generation Handheld*) i estandarditzades a l'últim estàndard de TDT, ATSC 3.0 (*Advanced Television Systems Committee 3rd Generation*). No obstant això, no hi ha desplegaments comercials MIMO de TDT. D'altra banda, la indústria mòbil ha desenvolupat una tecnologia de radiodifusió mòbil, coneguda com avui dia com a 5G Broadcast, basat en LTE (*Long Term Evolution*). Tot i que LTE incorpora MIMO per a transmissions unicast punt a punt, 5G Broadcast només utilitza una única antena en transmissió.

Aquesta tesi doctoral té com a objectiu avaluar el rendiment de MIMO per a radiodifusió (*terrestrial broadcast*) per a sistemes sense fil de radiodifusió de nova generació, tant TDT com sistemes cel·lulars. Durant l'estandardització dels sistemes MIMO TDT, el disseny inicial té en compte condicions de recepció perfectes, per exemple demoduladors òptims, informació d'estat del canal (CSI) perfecta, estimació perfecta de la potència del soroll, etc. L´objectiu principal d´aquesta tesi doctoral és avaluar i optimitzar el rendiment de les transmissions de radiodifusió MIMO en escenaris realistes. Aquesta tesi doctoral proposa nous models de canals de propagació MIMO terrestres basats en mesures de camp que es poden utilitzar per a l'avaluació del rendiment del sistema MIMO TDT. A més, també optimitza les diferents configuracions de transmissió i recepció MIMO, com l'estimació dels canals MIMO al receptor, i el processament de senyal. L'escenari considerat a la tesi són torres d'alta potència amb recepció fixa, característic de les xarxes de TDT.

Els resultats d‟aquesta tesi han contribuït al fòrum d‟estandardització ATSC, al sector de radiocomunicacions de la Unió Internacional de Telecomunicacions (UIT-R) i al projecte nacional japonès de recerca sobre el sistema TDT de propera generació.

Acknowledgement

First of all, I would like to express the deepest gratitude to my advisor Prof. David Gómez Barquero for inviting me to his research team and for the continuous supervision of my Ph.D. study. I could never have achieved any of the dissertation without his constant advice and excellent guidance over the years. I am very grateful as well to Prof. Narcís Cardona Marcet for welcoming me warmly as part of the research group and giving me the remarkable opportunity to pursue my Ph.D.

I am also very grateful to Dr. David Vargas from British Broadcasting Corporation (BBC) for the valuable suggestions and great insights on MIMO broadcast as reviewer and tribunal. It is my pleasure to thank Dr. Belkacem Mouhouche from Technology Innovation Institute and Prof. Iker Sobrón Polancos from Universidad del País Vasco for acting as reviewers of this dissertation and for providing useful advice. I would also like to thank to the defense tribunals, Prof. José María Molina García-Pardo from Universidad Politécnica de Cartagena and Prof. Felipe Vico Bondia from Universidad Politécnica de Valencia for taking time to review this thesis.

Special thanks to all the Mobile Communication Group (MCG) of the Institute of Telecommunications and Multimedia Applications (iTEAM) for your help during my stay in Valencia, not only with my Ph.D. study but also with everything that happens in daily life: Jordi Joan Gimenez, Eduardo Garro, Manuel Fuentes, Carlos Barjau, Jose Luís, Gerardo Martinez, Carlos Andreu, Alejandro, Sergio, Sofía, Martina, and many others. I'm really proud to be on your team. It was truly inspiring.

I would like to express my sincere gratitude to Kenichi Murayama for arranging my research stay and generously supporting in pursuing this Ph.D. I am also very grateful to the colleagues of NHK for continually challenging me in my career and for always having my back: Masahiro Okano, Tomoaki Takeuchi, Tsuyoshi Nakatogawa, Madoka Nakamura, Kohei Kambara, Makoto Taguchi, Yoshikazu Narikiyo, Susumu Saito, Noriyuki Shirai, Shingo Asakura, Hiroaki Miyasaka, Akihiko Sato, Tomoya Ijiguchi and Yuki Hirabayashi. Special thanks also go to former members of the team Kenichi Tsuchida, Kazuhiko Shibuya, Shunji Nakahara, Masayuki Takada, Hiroyuki Hamazumi, Kotoko Furuya and Shogo Kawashima.

I would like to take this opportunity to thank my beloved parents Yoshio and Mutsuko, because I owe what I am to you. And last but not least, my sincere gratitude goes to my wife Hiromi for all her continuous support and motivation over many years. I couldn't complete this thesis without her encouragement and patience during the course of this dissertation while raising our beloved Manaya and Mai.

Contents

Acronyms

ATSC	Advanced Television Systems Committee
ATT	Attenuator
AWGN	Additive White Gaussian Noise
BER	Bit Error Rate
BICM	Bit Interleaved Coding and Modulation
CFR	Channel Frequency Response
CNR	Carrier-to-Noise Ratio
CP	Cyclic Prefix
CRC	Cyclic Redundancy Check
CSI	Channel State Information
CTI	Convolutional Time Interleaver
DBPSK	Differential Binary Phase-Shift Keying
DD	Digital Dividend
DEMUX	Demultiplexer
DFT	Discrete Fourier Transform
DT	Decision Threshold
DTMB	Digital Terrestrial Multimedia Broadcast
DTT	Digital Terrestrial TV
DTTB	Digital Terrestrial TV Broadcasting
DUR	Desired-to-Undesired signal Ratio
DVB	Digital Video Broadcasting
DVB-NGH	DVB Next Generation Handheld

DVB-T	DVB Terrestrial
DVB-T2	DVB Terrestrial 2nd Generation
eMBMS	Evolved Multimedia Broadcast Multicast Services
eNB	evolved Node B
E.R.P.	Effective Radiation Power
eSFN	enhanced Single Frequency Network
eSM-PH	Enhanced Spatial Multiplexing with Phase Hopping
FDM	Frequency Division Multiplexing
FEC	Forward Error Correction
FFT	Fast-Fourier Transform
FeMBMS	Further evolved Multimedia Broadcast Multicast Service
FIL	Frequency Interleaving
GI	Guard Interval
GPS	Global Positioning System
HDTV	High-Definition TV
HEVC	High Efficiency Video Coding
HPHT	High Power High Tower
ICI	Inter-Carrier Interference
IF	Intermediate Frequency
IFFT	Inverse Fast Fourier Transform
IF-TTL	Intermediate Frequency Transmitter-to-Transmitter Link
IMT	International Mobile Telecommunications
IQPI	IQ Polarization Interleaving
IRA	Irregular Repeat Accumulate
ISDB-T	Integrated Services Digital Broadcasting Terrestrial

ISI	Inter-Symbol interference
iTEAM	Instituto de Telecomunicaciones y Aplicaciones Multimedia
ITU	International Telecommunications Union
ITU-R	International Telecommunication Union Radiocommunication Sector
LDPC	Low Density Parity Check
LLR	Log Likelihood Ratio
LNA	Low Noise Amplifier
LOS	Line-of-Sight
LS	Least Square
LTE	Long Term Evolution
LTE-A	Long Term Evolution - Advanced
MBSFN	Multimedia Broadcast multicast service Single Frequency Network
MET	Multi Edge Type
MIMO	Multiple Input Multiple Output
MISO	Multiple Input Single Output
ML	Maximum Likelihood
MLD	Maximum Likelihood Detection
MLSE	Maximum Likelihood Sequence Estimation
MMSE	Minimum Mean Square Error
MODCOD	Modulation and Coding
MRC	Maximum Ratio Combining
MSE	Mean Square Error
NHK	Nippon Hoso Kyokai (Japan Broadcasting Corporation)
NLOS	non Line-of-Sight
NP	Null Pilot

NUC	Non-Uniform Constellation
NUQAM	Non-Uniform Quadrature Amplitude Modulation
OFDM	Orthogonal Frequency Division Multiplexing
PAM	Pulse Amplitude Modulation
PH	Phase Hopping
PI	Power Imbalance
PP	Pilot Pattern
QAM	Quadrature Amplitude Modulation
QEF	Quasi Error Free
QPSK	Quadrature Phase Shift Keying
Rb	Rubidium
RF	Radio Frequency
SC	Stream Combining
SFBC	Space Frequency Block Coding
SFN	Single Frequency Network
SHF	Super High Frequency
SISO	Single Input Single Output
SM	Spatial Multiplexing
SNR	Signal-to-Noise Ratio
SP	Scattered Pilot
STC	Space Time Coding
STBC	Space Time Block Coding
T-DMB	Terrestrial - Digital Multimedia Broadcasting
TIL	Time Interleaving
TLV	Type Length Value

TMCC	Transmission and Multiplexing Configuration Control
TTL	Transmitter-to-Transmitter Link
TV	Television
Tx	Transmitter
UE	User Equipment
UHDTV	Ultra-High Definition TV
UHF	Ultra-High Frequency
VHF	Very High Frequency
VVC	Versatile Video Coding
WH	Walsh-Hadamard
WiMAX	Worldwide interoperability for Microwave Access
WRC	World Radiocommunication Conference
XPD	Cross Polarization Discrimination
XPI	Cross Polarization Isolation
ZF	Zero Forcing
3GPP	Third Generation Partnership Project
5G	Fifth Generation of Wireless Systems
5G-PPP	the 5G Infrastructure Public Private Partnership
5G-Xcast	Broadcast and Multicast Communication Enablers for the Fifth Generation of Wireless Systems

Chapter 1 Introduction

1.1. State-of-the-Art of DTT Systems

Terrestrial broadcasting is the primary means of delivering Television (TV) service in many countries as it can provide near-universal coverage to a potentially unlimited number of users by means of point-to-multipoint transmissions since the 1950s. The switch from analogue to digital processing in the 1990s brought various benefits, such as increased spectral efficiency, noise-free viewing, enhanced video and sound quality known as High Definition TV (HDTV), flexible broadcasting networking configurations (e.g., coverage area, multiple bitrates for video/audio services, multiple robustness services for mobile/fixed receivers) and the introduction of multimedia or interactive contents.

The utilization of broadcasting systems for the delivery of Digital Terrestrial TV (DTT) has grown very strongly during the last decade, and Digital Terrestrial TV Broadcasting (DTTB) networks are already in place in many countries all over the world. Several first-generation broadcasting standards are available today for the provision of DTT services: Advanced Television Systems Committee (ATSC) in North America [1], Integrated Services Digital Broadcasting - Terrestrial (ISDB-T) in Japan [2], Terrestrial - Digital Multimedia Broadcasting (T-DMB) in Korea [3], Digital Terrestrial Multimedia Broadcast (DTMB) in China, and Digital Video Broadcasting - Terrestrial (DVB-T) [4] in Europe. As to second-generation DTT system, DVB - Terrestrial 2nd Generation (DVB-T2) [5] was developed in Europe, and Advanced Television Systems Committee 3rd Generation (ATSC 3.0) has started commercialization in Korea and in the U.S progressively. Figure 1.1 shows the distribution of all DTT systems mentioned above that have been currently implemented (or adopted) in the world [6].

On the other hand, the mobile broadband demand is increasing in the last years due to the penetration of new devices in the market, such as smart phones or tablets. At the moment, mobile broadband system is not still perceived as viable alternatives to DTTB systems. The reasons derived from broadband cannot support large-scale consumption of TV services, and newly deployed Fifth Generation of Wireless Systems (5G) mobile broadcasting networks are expensive to deploy due to the large investment in

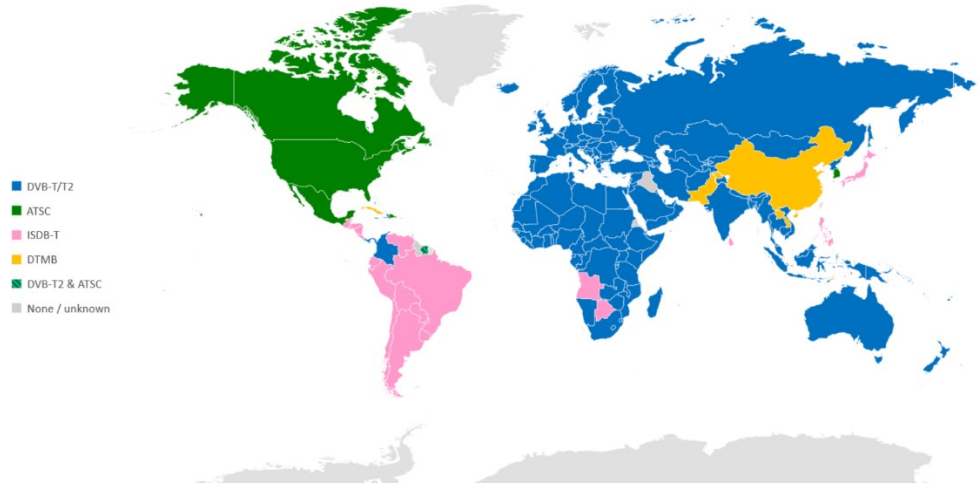

Figure 1.1 DTT system implemented or adopted by the different countries in the world [6].

infrastructure required to provide acceptable coverage levels [7]. Hence, it is expected that terrestrial broadcasting will remain very important at least on medium term. Due to this situation, a new generation of DTT standards is emerging. Today, it is already available a second generation of DVB system, DVB-T2 standard [5], which provides a 50% increase of spectral efficiency over its predecessor [4][8]. Moreover, the U.S. broadcasting standardization body, Advanced Television Systems Committee (ATSC), initiated the study of new technical approaches to evolve its terrestrial broadcasting standards to a new version, known as ATSC 3.0 in 2013. It aims at developing an advanced standard combining the most advanced transmission technologies that could exploit the optimum combination among large coverage, large capacity and efficient use of the scarce spectrum involving worldwide manufactures, broadcasters and research institutes [9].

Due to the continuous demand of spectrum by mobile broadband communications [10], further efficient utilization of the DTT spectrum has been required. The adoption of the DTT led to the release of a number of frequency channels over the Very High Frequency (VHF) and Ultra High Frequency (UHF) bands, formerly assigned to broadcasting services, known as Digital Dividend (DD) [11]. In the World Radiocommunication Conference (WRC) of 2007, the International Telecommunications Union (ITU) decided to allocate the upper part of the TV broadcasting band to International Mobile

Telecommunications (IMT) technologies. Hence, Regions 1[i] and 3[ii] allocated the 800 MHz band (790-862 MHz, channels 61-69) for Long Term Evolution (LTE) services [12] with a guard band of only 1 MHz, and Region 2[iii] allocated the 700 MHz band (698-806 MHz, channels 52-69) with a guard band of 5 MHz. In addition, the ITU WRC-12 [13] concluded with a decision to allocate additional UHF spectrum to mobile services and invited to perform further coexistence studies and report the results to the WRC-15. The new mobile allocation, also known as Second Digital Dividend (DD2), was made in Region 1 in the 700 MHz band. Implementing the DD2 within ITU Region 1 may affect up to eleven more DTT channels (49-60), creating several challenges. The DD2 may be particularly problematic in countries where terrestrial television is the main distribution platform, such as the United Kingdom, France, Spain, Portugal and Italy. For most countries, releasing the 700 MHz band will require a new re-tune of existing DTTB networks. As for the WRC-23, agenda item 1.5, which reviews the spectrum use and spectrum needs of existing services in the frequency band 470-960 MHz in Region 1, was set and broadcasters have been conducting studies on the spectrum requirements [14]. The agenda item considers possible regulatory actions in the frequency band 470-694 MHz in Region 1 on the basis of the review in accordance with Resolution 235 (WRC-15) [15].

Additional demand on DTT spectrum is the higher data rates needed for the delivery of new content such as 4K/8K Ultra-High Definition TV (UHDTV) [16] and multi-dimensional audio system [17]. It is obvious that in this time of competitiveness, DTTB networks should significantly increase their spectrum efficiency to cope with the limited spectrum use. To cope with these demands ATSC 3.0 has been developing new DTT technologies in North America [18]. Higher spectral efficiencies are achieved by the utilization of new technological, i.e., more sophisticated Modulation and Coding (MODCOD) schemes [19]. The use of advanced Low Density Parity Check (LDPC) codes [20] greatly improves the performance close to the theoretical limits [21] in Additive White Gaussian Noise (AWGN). Further improvement in performance, i.e., spectral efficiencies, for the next generation DTT system is difficult by developing the

[i] Europe, Africa, the Commonwealth of Independent States, Mongolia, and the Middle East west of the Persian Gulf, including Iraq
[ii] most of non-FSU Asia east of and including Iran, and most of Oceania
[iii] Americas including Greenland, and some of the eastern Pacific Islands

modulation and coding schemes. On the other hand, the progress in video compression technologies significantly reduces the bit rate with the High Efficiency Video Coding (HEVC) which can reduce by 50% the video bit rate compared with the previous H.264/AVC codec version for the same video quality [22]. The next-generation video coding standard, versatile video coding (VVC), has been developed [23]. The coding efficiency of VVC has been targeted to be 30% better than that of HEVC.

As a background for this thesis, an overview of the first generation and the second generation DTT systems are briefly described below.

1.1.1. First generation DTT systems

DVB-T is the first-generation International DTT standard developed in Europe. It is the most widely deployed DTT system in the world [6], including Spain. The standard is aimed at providing services for fixed rooftop to migrate from analogue to digital television service. It is assumed that the transmit and receive antenna in DVB-T have single element as analogue television system, i.e., DVB-T is a standard for Single-Input Single-Output (SISO) transmission. DVB-T is the first DTT system which utilizes Orthogonal Frequency Division Multiplexing (OFDM) [24][25] to cope with the signal distortion caused by multipath echoes in terrestrial transmission channel. The degradation of the reception performance by multipath echoes has been considered as a significant problem for analogue television system and for the first ATSC DTT standard [1]. Due to the robustness for the multipath echoes, Single Frequency Network (SFN) is applied in DVB-T system, in which a couple of adjacent transmitters can provide DTT services in the same spectrum. Although the transmitters should be synchronized to configure SFN, further efficient utilization of the DTT spectrum was achieved in DVB-T.

1.1.2. Second generation DTT systems

DVB-T2 is the second-generation International DTT standard developed in Europe. It offers more robustness, flexibility and at least 50% more spectrum efficiency than the first-generation DTT standard. The waveform in DVB-T2 is based on OFDM as DVB-T and more flexible DTTB network including SFN can be configured. DVB-T2 incorporates some important features in terms of the spectrum efficiency. DVB-T2 is the first DTT system which adopted LDPC codes [26] for the Forward Error Correction (FEC) to improve its robustness. It is known that LDPC codes greatly improve the transmission performance

compared with convolutional codes which is used in DVB-T, not only in AWGN channel but also in an actual propagation channel [27].

Additionally, DVB-T2 adopted a Multiple-Input Single-Output (MISO) scheme based on a site distributed configuration with Space Frequency Block Coding (SFBC) reusing the existing transmitter infrastructure and the existing receive antenna installations. The SFBC scheme adopted in DVB-T2 is based on Alamouti coding [28] defined to exploit only diversity gain. The Alamouti code is designed for achieving full diversity with reduced linear complexity at the receiver side with two transmit antennas. By using the Alamouti code in a distributed manner, it is possible to improve the performance in SFN transmission. The Alamouti code requires orthogonal pilot patterns between antennas which imposes doubling the number of transmitted pilots to achieve the same resolution of channel estimation as with single antenna transmissions. Despite the potential improvements shown in theory by the distributed MISO scheme in SFN scenarios, results from simulation in [29] and field measurements carried out in Germany in portable and mobile scenarios [30] do not recommend the use of MISO based on Alamouti coding.

DVB-NGH [31][32] is the first broadcast system to employ Multiple-Input Multiple-Output (MIMO), i.e. with Spatial Multiplexing (SM) gains, as key technology exploiting the benefits of the MIMO channel. DVB-NGH is the handheld evolution of DVB-T2. While the core of the system is based on DVB-T2, two types of MIMO schemes are specified in the specification of DVB-NGH [33]. The first type of techniques is known in DVB-NGH as MIMO rate 1 codes, which exploit the spatial diversity of the MIMO channel without the need of multiple antennas at the receiver side. They can be applied across the transmitter sites of SFNs to reuse the existing network infrastructure, i.e., DVB-T and DVB-T2, as well as to an individual transmitter site equipped with multiple transmit antennas. These codes include the Alamouti code, already featured in DVB-T2, together with a scheme known as enhanced Single Frequency Network (eSFN). The second type of techniques is known in DVB-NGH as MIMO rate 2 codes, which exploit the diversity and multiplexing capabilities of the MIMO channel. In this category DVB-NGH has adopted a novel scheme known as Enhanced Spatial Multiplexing with Phase Hopping (eSM-PH). The eSM-PH was designed to overcome the spatial correlation in the MIMO channel retaining the multiplexing capabilities of SM MIMO. With eSM-PH the information symbols are weighted and combined before their transmission across the

antennas according to a specified rotation angle. This rotation angle has been tuned for every combination of constellation order and deliberated transmit Power Imbalance (PI). To ease dual polar operation, MIMO rate 2 codes can be transmitted with deliberated PI between the transmit antennas with values of 0 dB, 3 dB and 6 dB. In addition, eSM-PH includes a periodical Phase Hopping (PH) term to the second antenna to randomize the code structure and avoid the negative effect of certain channel realizations. To demodulate an eSM-PH signal it is necessary to employ orthogonal pilot patterns (as for the Alamouti code) between antennas.

During the standardization process of DVB-NGH, a channel sounding campaign took place in July 2010 in Helsinki, Finland, focusing on cross-polar UHF transmission and reception in order to compare candidate schemes in simulation with a realistic measurement-based channel model [34]. The trials included a number of practical designs for antennas suitable for a handheld terminal. From the measurements, the following channel models were developed: an outdoor mobile model, an outdoor portable model and an indoor portable model. For the mobile case, user velocities of 60 km/h or 300 km/h were considered, whereas for the portable case, user velocities of 0 km/h or 3 km/h were considered.

ATSC 3.0 is the current state-of-the art DTT system developed as the U.S. terrestrial broadcasting standard, which aims at becoming the reference terrestrial broadcasting technology, outperforming DVB-T2 and DVB-NGH in terms of coverage and capacity. It is focused on the efficient delivery of emerging UHDTV services as well as to cope with the broadcast spectrum shortage due to the rapidly growing demand for wireless broadband services. The standardization process started in Oct. 2013 [9]. MIMO technology has been further developed and fully standardized in ATSC 3.0 [35] not only for mobile broadcasting. The higher flexibility of MIMO antenna technology allows broadcasters to select the configuration that better suits the capacity and coverage requirements per service. In practice, MIMO in DTT is implemented using cross-polarized 2×2 MIMO, i.e., horizontal and vertical polarization to decorrelate the channel even in Line-of-Sight (LOS) reception conditions [36]. This means that at least two antenna elements are equipped at both transmitter and receiver sides.

Figure 1.2 illustrates the ATSC 3.0 MIMO transmission chain standardized in [37]. The MIMO profile re-uses as much as possible the SISO baseline profile. The main new

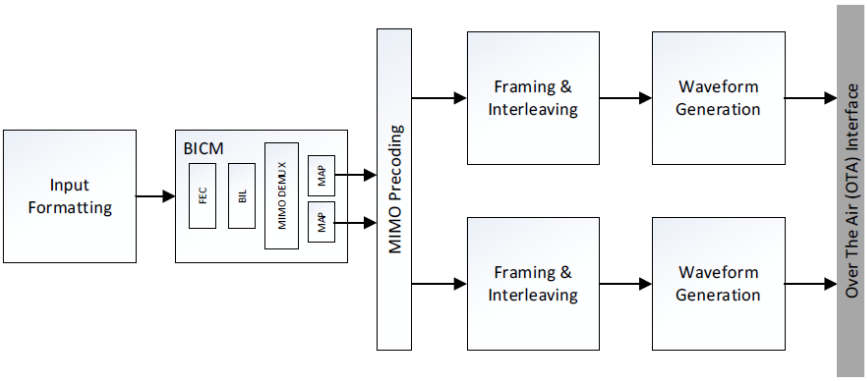

Figure 1.2 MIMO block diagram in ATSC 3.0 [37].

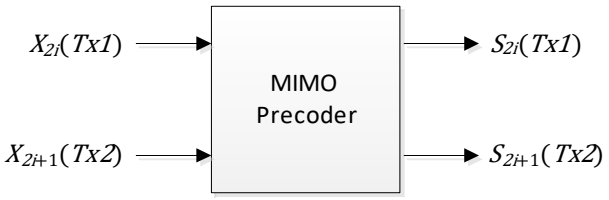

Figure 1.3 Generic MIMO Pre-coder block diagram in ATSC 3.0 [37].

block compared to SISO is so cold the MIMO Demultiplexer (DEMUX) and MIMO precoding. In addition, 2×2 SM MIMO requires doubling the pilot overhead compared to SISO to keep the channel estimation performance. DVB-NGH adopted an orthogonal Scattered Pilot (SP) encoding scheme, namely Walsh-Hadamard (WH) encoding, which is the same configuration used in DVB-T2 for MISO mode [5]. ATSC 3.0 adopted WH encoding for MIMO channel estimation together with another SP encoding algorithm known as Null Pilot (NP) encoding [35]. The NP encoding scheme was firstly adopted in LTE [38] for MIMO mode. However, the scheme was modified and it was the first time ever to be introduced in DTT specification ATSC 3.0. The MIMO pilot positions in LTE are different from SISO depending on the antenna configuration. On the other hand, the MIMO pilot positions in ATSC 3.0 are located at the same positions as SISO and the pilot positions are selectable out of 16 pilot patterns. Another novelty of pilot configuration in ATSC 3.0 is that the pilot boosting is selectable out of five pilot boosting values.

The MIMO precoding in ATSC 3.0 acts on a pair of input constellation symbols (X_{2i}, X_{2i+1}), where i is the index of the cell pair within the FEC block, and creates a pair of output constellation symbols as depicted in Figure 1.3 [37]. Encoded cell pairs (S_{2i}, S_{2i+1}) shall be transmitted on the same OFDM symbol and carrier from transmit antenna #1

(Tx1) and transmit antenna #2 (Tx2), respectively. The MIMO pre-coder is based on SM, and consists of three different steps, Stream Combining (SC), IQ Polarization Interleaving (IQPI), and PH. The SM encoding scheme in DVB-NGH was simplified not to have the transmit PI function and standardized as the SC in ATSC 3.0. The PH in ATSC 3.0 is standardized as that in DVB-NGH. Note that MIMO profile for mobile broadcasting service was optimized in DVB-NGH, whereas MIMO was fully standardized for fixed/mobile reception scenario in ATSC 3.0. Regarding the implementation, it should be noted that MIMO signal processing requires higher-spec hardware compared with the conventional SISO transmitter/receiver for the higher computational complexity.

1.1.3. Mobile broadband systems

From 3G cellular networks, mobile industry has developed several mobile broadcast technologies to support large-scale consumption of mass multimedia services on mobile devices. The broadcast capabilities are referred to as Evolved Multimedia Broadcast Multicast Services (eMBMS) from Release 9 [12]. The higher potential of eMBMS together with the increase of video traffic demand have led to the first trials and commercial eMBMS networks in 2014 [39]. As some examples, in January 2014, Verizon Wireless used the Super Bowl in New York as a test case for eMBMS technology and Korea Telecom completed the world's first commercial launch of LTE Broadcast services using eMBMS technology.

One of the most important means to achieve the high data rate objectives for LTE is MIMO transmission [40]. In LTE downlink it is supported one, two or four transmit antennas at the evolved Node B (eNB) and one, two or four receive antennas at the User Equipment (UE). In LTE-Advanced, the maximum number of antennas is increased up to eight. Multiple antennas can be used in different ways. When the Signal-to-Noise Ratio (SNR) is high, MIMO can be used to increase the data rate by creating several parallel channels with SM. For situations with low SNR, it is better to use other types of multi-antenna techniques to obtain additional transmit/receive diversity and improve the SNR. Third Generation Partnership Project (3GPP) has not standardized any MIMO scheme for multicast broadcast transmissions, and LTE/LTE-A does not include MIMO for its extension eMBMS. Therefore, eMBMS data are provided using single antenna mode. However, the MIMO schemes adopted for DVB-NGH and ATSC 3.0 share similar technologies with LTE/LTE-A open loop single user downlink schemes as the way to exploit the benefits of the MIMO channel. Regarding the number of transmitting elements,

MIMO DTTB systems define a maximum of two transmit antennas, while for LTE the maximum number is four, and eight for LTE-A. Increasing the number of transmit antennas generally improves the system performance at expense of higher system complexity.

In LTE-Advanced Pro Release 14, 3GPP completed the standardization of a DTTB-like mode (e.g., receive-only, broadcast and downlink only, free to air, support for high-power high-tower (HPHT) infrastructure, etc.) based on eMBMS [41]. In Release 14, the eMBMS radio interface efficiency and flexibility are greatly enhanced by introducing a new type of subframe without unicast control region and removing the restriction that up to 60% subframe can be allocated for broadcast [42]. Thus, the name has been updated as Further evolved to Multimedia Broadcast Multicast Service (FeMBMS). However, MIMO technology was not introduced to the FeMBMS. Release 16 defines a so-called LTE-based 5G Terrestrial Broadcast solution based on the work in Release 14 [43],[44]. The target is to enable a Multimedia Broadcast multicast service Single Frequency Network (MBSFN) to support SFN with a cell coverage range of up to 100 km and mobile reception with speeds up to 250 km/h [45]. However, Release 16 doesn't support MIMO broadcasting either.

1.2. Motivation and Problem Statement

1.2.1. Motivation

In Japan, research on transmission methods for next-generation terrestrial broadcasting started within a national program in 2014 [P1] and further developed [P2] with the participation of broadcasters, manufacturers, and universities. The objective is to study technologies that improve transmission efficiency while inheriting the features of the current DTTB system and to establish an SFN that promotes the effective use of the radio spectrum. The projects have explored different ways of advancing the current DTTB system, Integrated Services Digital Broadcasting-Terrestrial (ISDB-T), to provide UHDTV and HDTV services within a single 6-MHz channel [46]. To provide 4K/8K UHDTV services through terrestrial broadcasting in a 6-MHz channel, the transmission capacity should be further increased. One option being considered for increasing the capacity is to introduce MIMO antenna schemes with SM [47].

The main requirement for the next generation broadcasting system is high spectral efficiency, due to the increase of the data traffic and the scarcity of other recourses such

as bandwidth or transmitting power. The MIMO technology has emerged as one of the most promising technologies [48], since this technology allows to increase the transmission capacity, reliability and coverage without the need of extra bandwidth or power cost. In fact, MIMO technology has been adopted by many wireless standards such as LTE [49], LTE-Advanced (LTE-A) [50], Worldwide interoperability for Microwave Access (WiMAX) [51], IEEE 802.11n/ac [52], and 5G systems [53].

MIMO refers to a transmission technology employing at least two transmit antennas and two receive antennas. A conventional topology for DTT comprising a single transmit antenna and a single receive antenna is referred to as SISO. The increasing interest in MIMO systems has given rise to its consideration for terrestrial broadcasting and its performance was evaluated [54] by information-theoretical study and simulations. The utilization of MIMO for broadcasting systems was discussed in the ATSC 3.0 standardization process to expand the transmission capacity, however MIMO broadcasting has not been commercialized mainly due to the absence of a strong market at the present moment. Many of the state-of-the-art DTT standards has been developed with new technologies to improve the performance, mainly to increase the capacity at a certain SNR. Even though MIMO broadcasting system requires additional investments for both service providers and receivers, MIMO has been recognized as a breakthrough to greatly increase transmission capacity.

1.2.2. Problem Statement

During the standardization of new DTT systems the initial design accounts for perfect reception conditions, e.g., optimal demodulators, perfect Channel State Information (CSI), perfect noise power estimation, and infinite-precision number representations. For instance, that was the approach to design DVB-T2, DVB-NGH and ATSC 3.0. However, due to complexity constraints for practical use, it is crucial for the overall system performance to carefully design receiver algorithms. MIMO channel estimation is one of the factors that increase complexity because of the MIMO pilots decoding at the receiver. MIMO transmit/receive signal processing also increases complexity.

The previous research in iTEAM aimed at studying fundamental MIMO performance for ATSC3.0 with ideal channel estimation. On the other hand, the practical 2×2 SM MIMO system requires doubling the pilot overhead compared to SISO to keep the channel estimation performance. To evaluate the MIMO system performance including

channel estimation overhead and channel estimation errors, MIMO pilot schemes for ATSC3.0 should be evaluated with the physical layer simulator focusing on the encoding scheme, pilot boosting and frequency interpolation. ATSC 3.0 adopted WH encoding and NP encoding for MIMO channel estimation, and the selection of the optimum MIMO pilot configuration (pilot encoding scheme, pilot pattern and pilot boosting) is not straightforward. The optimum configuration represents a trade-off between quality of the channel estimation and overhead. The pilots should be sufficiently dense to follow channel fluctuations, but the denser pilots reduce the net transmission capacity. Although different studies have shown the pilot optimization for SISO in ATSC 3.0, e.g. [55], the impact of pilot encoding for MIMO transmission has not been fully evaluated. Indeed, the two pilot encoding algorithms were not deeply compared in the standardization process in terms of the channel estimation algorithms and channel conditions [35]. Moreover, the MIMO pilots are directly standardized so as to have the same positions (pilot patterns) and the same amplitudes (pilot boosting) as SISO.

To improve the spectral efficiency and/or the transmission robustness of 2×2 MIMO, DVB-NGH introduced eSM-PH as the MIMO precoding scheme, which consists of a spatial multiplexing precoding followed by an additional phase hopping [56]. The MIMO precoding adopted in ATSC 3.0 is based on SM and consists of three different steps known as SC, IQPI and PH. Each of the three steps of the MIMO precoding is optional. SC and PH are based on the precoding scheme in DVB-NGH, however the IQPI precoding component is completely novel, being the first time introduced in a DTT specification. Although different studies have analyzed the MIMO precoding performance in DVB-NGH, see e.g. [57], the impact of each component of the MIMO precoding in ATSC 3.0 has not been yet fully evaluated. Indeed, the MIMO precoding scheme has not been compared in terms of practical cross-polarized 2×2 MIMO configuration and practical channel conditions. For more efficient use of the broadcast spectrum, Non-Uniform Quadrature Amplitude Modulation (NUQAM) also called one-dimensional Non-Uniform Constellation (NUC) has been firstly introduced in DVB-NGH, and two-dimensional NUC has been implemented in ATSC 3.0. NUCs reduce the gap between conventional uniform Gray-labelled Quadrature Amplitude Modulation (QAM) constellations and the theoretical Shannon limit. The challenge is to design constellations that improve the system performance, and to use simplified sub-optimum

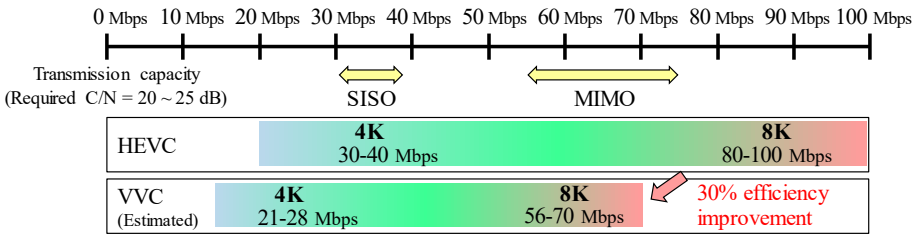

Figure 1.4 Relationship between transmission capacity and maximum video bit rate for broadcasting emission.

demappers that reduce the demapping complexity at the receiver without any significant loss.

Terrestrial MIMO TV broadcasting in the low UHF band has been demonstrated in field trials by the public broadcasters BBC (U.K.) [58], [59] and NHK (Japan) [60], [61], in which a cross-polarized (horizontal and vertical) antenna was introduced to retain full spatial multiplexing capabilities in LOS conditions. Although a MIMO TV broadcasting system requires updating both transmit and receive antennas, the enhancement of the transmission system allows broadcasters to select the configuration that better suits the capacity and coverage requirements per service. In an earlier study, NHK conducted preliminary field experiments to evaluate the transmission performance of MIMO by using small-scale experimental test stations built in a rural area and confirmed the feasibility of MIMO broadcasting [36]. Although the feasibility of MIMO technology in DTT system was confirmed, further experiment and analysis should be conducted at more reception points under a wider range of conditions to assess the MIMO capacity gain obtained in practical DTTB reception scenario.

As for the MIMO channel model, various 2×2 channel models have been proposed for system performance evaluation by simulations [62]. As a fixed reception model, the MGM (Modified Guilford Model) [63], which is a cross-polarized 2×2 MIMO fixed reception channel model for broadcasting, has been introduced by BBC based on field measurements in UK [59], [64]. The MGM was defined as a stochastic model and used in the standardization process of DVB-NGH and ATSC 3.0. However, since the MGM has many parameters to be set and its implementation takes some efforts, it is desirable to construct a simple deterministic model for practical use.

Figure 1.4 shows the relationship between the transmission capacity and the maximum video bit rate for broadcasting emission. The recommended video bit rates when using

HEVC/H.265 standard is 30-40 Mbps for 4K and 80-100 Mbps for 8K [65]. The coding efficiency of VVC [23] is 30 percent better than that of HEVC, and the required video bit rates when using VVC can be estimated as 21-28 Mbps for 4K and 56-70 Mbps for 8K. The next generation broadcasting system considered in Japan, so called advanced ISDB-T, is capable of transmitting one UHDTV 4K program by using HEVC in a single 6-MHz channel for fixed SISO reception. When VVC is introduced, it is expected that an UHDTV 8K program can be transmitted in a single 6-MHz channel by 2×2 SM MIMO transmission with the progress of methods for improving the video coding efficiency [66].

1.3. Objectives and Scope

The author aims at investigating and assessing MIMO for next generation broadcasting not only by simulations but also laboratory and field experiments. The main goals of the thesis are focused on evaluating the MIMO gains in comparison with SISO in practical scenarios, i.e., not in perfect reception conditions. To clarify the benefits of MIMO, the work is divided into several phases. For practical use, a cross-polarized 2×2 SM with horizontal and vertical polarizations is analyzed. Currently, an advanced ISDB-T system is being developed to provide simultaneously 4K terrestrial broadcasting service for fixed reception and 2K service for mobile reception. We evaluate the transmission parameters that are candidates for practical use for the required Carrier-to-Noise Ratio (CNR) of 20 dB, which is equivalent to the operational parameters for fixed reception of the current DTTB in Japan.

MIMO performance has been evaluated mainly in fixed reception environment targeting 4K/8K UHDTV transmission assuming fixed roof top receiving antenna in terms of the following scopes.

1.3.1. Broadcast MIMO channel estimation

We assess the MIMO performance by simulations and provide an optimum configuration for MIMO regarding the waveform parameters, Pilot Pattern (PP), Fast-Fourier Transform (FFT) size and Guard Interval (GI) with the signal structure of ATSC 3.0. 2×2 MIMO requires doubling the pilot overhead compared to SISO to keep the resolution of channel estimation. The performance evaluation and optimization of MIMO channel estimation are performed in fixed/mobile reception scenarios with a practical receiver implementation including channel interpolation. Details are provided in Chapter 3.

1.3.2. Broadcast MIMO signal processing

A study of the MIMO transmit/receive signal processing, for instance MIMO precoding and demapping complexity reduction, is carried out. The MIMO precoding blocks standardized in ATSC3.0, i.e., SC, IQPI and PH, are evaluated in several reception conditions for cross-polarized 2×2 MIMO by simulations. A Space Time Coding (STC) based 4×2 MIMO SFN scheme is evaluated based on the signal structure of an advanced ISDB-T in laboratory and field experiments. Details are provided in Chapter 4.

1.3.3. Broadcast MIMO practical gain and channel modeling

We compare the performance of SISO and MIMO in a large-scale HPHT network in in Tokyo and Osaka using the signal structure of an advanced ISDB-T system studied in Japan [46]. The amount of improvement in transmission capacity and required CNR due to the introduction of MIMO is verified. We evaluate the fixed reception performance by computer simulations using 101 channel responses captured in real environment in Osaka. We create a simple terrestrial MIMO channel models which can be utilized for DTT system performance evaluation. The channel model is derived from the MIMO channel snapshots captured in Osaka area. Details are provided in Chapter 5.

1.4. Thesis Outline and Contributions

With this Ph.D. thesis, the investigations have been performed in the context of the next-generation U.S. DTT system ATSC 3.0, which was being updated. The author takes advantage of the fact that the iTEAM Research Institute of the Universitat Politècnica de València is a full member of the U.S. digital television standardization forum ATSC [F1]. The author also has been working on specifications and verification of advanced ISDB-T as a member of Japanese national research projects funded by the Ministry of Internal Affairs and Communications [P1], [P2]. Additionally, iTEAM was the project manager of the 5G Infrastructure Public Private Partnership (5G-PPP) project Broadcast and Multicast Communication Enablers for the Fifth Generation of Wireless Systems (5G-Xcast) [P3]. Hence, this thesis can contribute to the framework of the standardization processes of ATSC 3.0, advanced ISDB-T and 5G Broadcast systems.

This thesis is divided into six chapters and one appendix. The thesis is structured as follows.

Chapter 2 Background and Methodology

This chapter describes an overview of the system model and DTTB system studied in the thesis. The methodologies and the setup, e.g., channel models, signal processing at the receivers, simulations, laboratory experiments and field experiments are presented.

Chapter 3 Broadcast MIMO Channel Estimation

Regarding MIMO channel estimation, two pilot encoding algorithms known as Walsh-Hadamard encoding and Null Pilot encoding are possible in ATSC 3.0. The two MIMO pilot algorithms are standardized so as to have the same pilot positions and the same pilot boosting as SISO, and the optimum pilot configuration has not been fully evaluated for MIMO. This chapter focuses on the performance evaluation and optimization of the pilot boosting, pilot pattern and pilot encoding in ATSC 3.0 using physical layer simulations. This chapter provides a great benefit to broadcasters to select the MIMO pilot configuration including pilot boosting, pilot pattern and pilot encoding algorithm that better suits their service requirements. Several channel interpolation algorithms have been considered as a typical receiver implementation in both fixed SFN reception and mobile reception.

The results showed that the encoding scheme and the frequency interpolation do not make much difference in lower SNR region. The Mean Square Error (MSE) between the estimated channel and the real channel indicated that NP encoding and linear frequency interpolation is the best combination in mobile and fixed reception scenario for SNRs below 10 dB. On the other hand, WH encoding can provide a better performance in mobile reception conditions especially at high SNRs. Linear frequency interpolation is not suited for SFNs with long delay echoes at high SNRs.

Chapter 4 Broadcast MIMO Signal Processing

We evaluated the transmission performance of NUQAMs with a simplified demapping algorithm that approximates the Log Likelihood Ratio (LLR) as a simple distance from a boundary of only the in-phase or quadrature component. Simulations using the MIMO channel response captured in an urban area demonstrated that the higher-order NUQAMs mitigate the degradation caused by the LLR approximation compared with conventional QAMs. The results show that the degradation in the simplified demapping algorithm in the required CNR is approximately 0.4 dB and that the LLR approximation is applicable to transmission systems with high-order NUQAMs.

Regarding MIMO precoding, three precoding blocks, so called SC, IQPI and PH, are possible in ATSC 3.0. The three MIMO precoding blocks are standardized as optional, but the performance has not been fully evaluated. We focus on the performance evaluation of the three MIMO precoding blocks in ATSC 3.0 using physical layer simulations. Potential gains in required SNR for several MODCOD combinations have been evaluated in a fundamental cross-polarized 2×2 MIMO transmission model and MIMO channel snapshots actually captured in an urban area. The simulation results showed that SC provides some gain with QPSK and 16QAM in a PI channel and that IQPI provides small gain only in an extremely high PI channel. SC and PH provide some gains in a small Cross Polarization Discrimination (XPD) case. The study based on the practical MIMO channel snapshots concluded that SC potentially provides some gains especially with QPSK and high code rate, but IQPI and PH are less likely to beneficial in an actual static reception scenario. The main contribution is to provide an analysis on MIMO precoding in practical reception scenarios for the potential MIMO ATSC3.0 broadcasters.

To evaluate DTTB network for 2×2 cross-polarized MIMO, two experimental stations composed of an advanced SFN using STC technology were set up in Hitoyoshi area, Kumamoto, Japan. The transmission capacity of each experimental station is a maximum of 91.8 Mbps when using dual-polarized MIMO and 4096 QAM modulation. To evaluate an advanced SFN with a 4×2 MIMO system, we conducted field experiments in Hitoyoshi area to compare two SFN schemes: STC-SFN and conventional SFN without coding. The results of the field tests showed that the required received power of the STC-SFN is lower than that of the conventional SFN, and the amount of improvement is up to 3 dB when the power ratio of the main wave and the SFN wave is 6 dB.

Chapter 5 Broadcast MIMO Practical Gain and Channel Modeling

The transmission performance of 2×2 cross-polarized MIMO is studied to determine how to increase the capacity of DTTB and make it more robust. In this chapter, the performance was evaluated in laboratory experiments and large-scale field experiments in central Tokyo under three deployment scenarios. The results showed that the required received power can be improved by 7.3 dB when MIMO is introduced to enhance transmission robustness, i.e., maintaining the same transmission capacity as SISO. Alternatively, the transmission capacity can be doubled by introducing MIMO for the same robustness as SISO, requiring a slight increase in received power of 0.9 dB

compared with SISO. The field experiments were performed by using a prototype advanced ISDB-T system developed in Japan, however the results obtained are also valid for 5G Broadcast systems. Regarding the feasibility of the DTTB system operating at a target bit rate of about 60 Mbps to distribute a VVC-based 8K program within a 6-MHz channel bandwidth, an increased received power of 3.7 dB compared with SISO was required for MIMO to achieve 60 Mbps order transmission capacity in the worst case for 28 reception points evaluated in urban areas.

In previous studies [58] and [59], the performance of MIMO transmission was evaluated with a MODCOD having the same robustness as the reference SISO configuration. In other studies, e.g., [60], [36], the MIMO transmission performance was evaluated with several MODCOD, however the performance was not compared with SISO. In this chapter, it is clarified that the amount of degradation in the required received power for MIMO is higher than that for SISO with several MODCOD having different levels of robustness. As a follow-up verification to the field experiments, we conducted performance evaluation with channel snapshots captured in the field experiments, removing uncertainties such as a fluctuation in the electric field strength or the effect of man-made noise occurring at the time of measurement. The results of the field experiments and the follow-up laboratory experiments confirmed that the degradation in MIMO transmission performance was not negligible compared with SISO. In addition, the field experiments have the novelty of being a feasibility study on a DTTB system that operates at a target bit rate of about 60 Mbps so that a VVC-based 8K program can be distributed within a single 6-MHz channel.

The fixed reception performance of MIMO transmission was verified in simulations with the MIMO channel snapshots of 101 points captured in Osaka. When compared with MIMO with a required CNR of 18 dB, which provides almost the same robustness as SISO with a required CNR of 20 dB, the transmission capacity increases approximately 1.8 times. The MIMO parameters that have the same transmission capacity as SISO, the gain in transmission robustness was approximately 7 dB. Note that when comparing SISO and MIMO with a constant transmission power, the amount of improvement decreases by 3 dB, and the MIMO gain is reduced to about 4 dB.

We created 8-tap fixed rooftop reception MIMO channel models based on 101 snapshots captured in the field experiments. The MIMO capacity gain obtained at the

Table 1.1 Summary of evaluation and optimization of each component

Methodology	Components	System	Subsection
Simulations	Pilot encoding/decoding	ATSC 3.0	3.3.1 3.3.2 3.3.3
	Pilot boosting		3.3.1
	Frequency interpolation		3.3.2
	FFT size, GI, Pilot pattern		3.3.3
	Stream combining		4.2.2
	IQ polarization interleaving		
	Phase hopping		
	demapping	Advanced ISDB-T	4.1.2
	Modulation and coding		5.2.2 5.2.4
Laboratory experiments	Space Time Coding		4.3.2
	Modulation and coding		5.1.1 5.1.3
Field experiments	Space Time Coding		4.3.2
	Modulation and coding		5.1.2 5.2.1

required CNR of 10 dB was 1.5 to 1.7 times in 50, 80, 90 and 95-percentile channels. The gain at 20 dB and 30 dB was 1.7 to 1.8 times in 50, 80, 90 and 95-percentile channels. The results concludes that the MIMO practical gain obtained in the current fixed rooftop reception of DTTB assuming a required CNR of 20 dB is roughly 1.7 times.

Chapter 6 Conclusions and Future Work

The conclusions and future work are summarized in this chapter reviewing the results of the simulation, laboratory and field experiments. The methodologies and systems used for evaluation and optimization of each component are summarized in Table 1.1.

1.5. List of Publication

1.5.1. International Journals

[J1] S. Saito, **T. Shitomi**, S. Asakura, A. Sato, M. Okano, K. Murayama and K. Tsuchida, “8K Terrestrial Transmission Field Tests Using Dual-Polarized MIMO and Higher-Order Modulation OFDM,” in IEEE Transactions on Broadcasting, vol. 62, no. 1, pp. 306-315, Mar. 2016.

[J2] C. Barjau, M. Fuentes, **T. Shitomi** and D. Gomez-Barquero, "MIMO Sphere Decoding With Successive Interference Cancellation for Two-Dimensional Non-Uniform Constellations," in IEEE Communications Letters, vol.21, no. 5, pp. 1015-1018, May 2017.

[J3] **T. Shitomi**, E. Garro, K. Murayama and D. Gomez-Barquero, "MIMO Scattered Pilot Performance and Optimization for ATSC 3.0," in IEEE Transactions on Broadcasting, vol. 64, no. 2, pp. 188-200, June 2018.

[J4] **T. Shitomi**, S. Asakura, S. Kawashima, A. Sato, H. Miyasaka, N. Shirai, Y. Narikiyo, T. Takeuchi, K. Kambara, M. Nakamura, T. Nakatogawa, K. Murayama, M. Okano and K. Tsuchida, "Fixed Reception Performance of FDM-based Transmission System for Advanced ISDB-T," in SET International Journal of Broadcast Engineering, vol.2020 (6), pp. 9-20, Dec. 2020.

[J5] **T. Shitomi**, N. Shirai, A. Sato, S. Kawashima, T. Ijiguchi, H. Miyasaka, S. Asakura, T. Takeuchi, K. Kambara, M. Nakamura, T. Nakatogawa, M. Okano and K. Tsuchida, "Performance evaluation of MIMO broadcast systems for advanced digital terrestrial TV," in EURASIP Journal on Wireless Communications and Networking, Article number 89, Apr. 2021.

[J6] **T. Shitomi**, T. Nakatogawa, A. Sato, K. Furuya, and M. Okano, "Spectral Efficiency Evaluation of an NR-Based 5G Terrestrial Broadcast System for Fixed Reception," in IEEE Transactions on Broadcasting, vol. 68, no. 2, pp. 487-500, June 2022.

[J7] **T. Shitomi**, Y. Hirabayashi, A. Sato, S. Asakura, M. Okano and D. Gomez-Barquero, "Cross-polarized 2×2 MIMO Fixed Reception Broadcast Channel Models - Osaka Model for HPHT DTTB network -," to be submitted.

1.5.2. Papers in International Conference Proceedings

[C1] **T. Shitomi,** A. Satou, S. Asakura, S. Saito, T. Takeuchi, M. Okano and K. Tsuchida, "Evaluation of Simplified Demapping Algorithm for NUQAMs Using MIMO Channel Response," 2016 IEEE International Symposium on Broadband Multimedia Systems and Broadcasting (BMSB), Nara, Japan, 2016.

[C2] **T. Shitomi,** E. Garro, K. Murayama and D. Gomez-Barquero, "Performance Evaluation of MIMO Channel Estimation for ATSC 3.0," 2017 IEEE International Symposium on Broadband Multimedia Systems and Broadcasting (BMSB), Cagliari, Italy, 2017.

[C3] **T. Shitomi,** C. Barjau, K. Murayama and D. Gomez-Barquero, "Performance Evaluation of ATSC 3.0 MIMO Precoding," 2018 IEEE International Symposium on Broadband Multimedia Systems and Broadcasting (BMSB), Valencia, Spain, 2018.

[C4] M. Nakamura, A. Sato, H. Miyasaka, S. Asakura, **T. Shitomi,** N. Shirai, T. Takeuchi, M. Okano, K. Tsuchida, Y. Narikiyo and K. Muaryama, "A Study on the Transmission System for Advanced ISDB-T," 2019 IEEE International Symposium on Broadband Multimedia Systems and Broadcasting (BMSB), Jeju, South Korea, 2019.

[C5] N. Shirai, S. Kawashima, T. Ijiguchi, Y. Yamakami, A. Sato, H. Miyasaka, S. Asakura, **T. Shitomi,** T. Takeuchi, N. Madoka, T. Nakatogawa, M. Okano, Y. Narikiyo, K. Suzuki, A. Mizuguchi, N. Sato, R. Watanabe and K. Tsuchida, "Laboratory Experiments and Large-Scaled Field Trials for Evaluating the Advanced ISDB-T," 2019 IEEE International Symposium on Broadband Multimedia Systems and Broadcasting (BMSB), Jeju, South Korea, 2019.

[C6] **T. Shitomi,** A. Sato, N. Shirai, T. Nakatogawa, M. Okano, S. Kawashima, T. Ijiguchi, H. Miyasaka, S. Asakura, T. Takeuchi, M. Nakamura and K. Tsuchida, "Field Trials for Evaluating Advanced Digital Terrestrial MIMO TV Broadcasting System," European Conference on Networks and Communications (EuCNC), Valencia, Spain, 2019.

1.5.3. Contributions to Standardization Activities

[S1] 1 contribution to the Working Party 6A on terrestrial broadcasting in ITU-R Study Group 6 for broadcasting service.

Contribution to add the latest information on 4K/8K field trials in Japan to the Report ITU-R BT.2343-5: Collection of field trials of UHDTV over DTT networks, July 2019.

[S2] 1 contribution to the S32 Specialist Group on Physical Layer for ATSC3.0.

Contribution to create a new section on MIMO operation in the guidelines for physical layer mode in the ATSC Recommended Practice: Guidelines for the Physical Layer Protocol (A/327), June 2020.

Chapter 2 Background and Methodology

This chapter presents fundamental concepts on wireless communications utilized in this thesis. Theoretical definitions presented in this chapter constitute the background of the following Chapter 3, Chapter 4 and Chapter 5. Section 2.1 provides a system model overview and consists of the fundamentals of MIMO wireless communications looking at the channel matrix representation. The basics of DTTB systems used in this thesis are explained in Section 2.2 to describe the different transmit/receive components providing a general description of the Bit Interleaved Coding and Modulation (BICM) and waveform generation. Section 2.3 introduces channel models used for the system performance evaluation. Section 2.4 consists of the fundamentals of MIMO signal processing at the receiver side, which describes practical receiver implementations. Section 2.5, 2.6 and 2.7 are devoted to the methodologies for simulation, laboratory experiments and field experiments.

2.1. System Model Overview

This section presents the fundamental ideas and concepts on broadcasting communications used in this thesis. Figure 2.1 shows a simplified broadcasting transmission system model, in which the channel $h(t)$ distorts the characteristics of the transmitted signal $s(t)$ producing the received signal $y(t)$. The channel $h(t)$ is different for each possible receiver, and the received signal $y(t)$ is also different for each receiver. The received signal is expressed as:

$$y(t) = h(t) * s(t) + w(t) \tag{2.1}$$

where $w(t)$ represents an additive noise at the receiver and the operator $*$ denotes the convolution. The noise is caused by thermal noise of the receiver and/or external noise such as man-made noise in urban areas. The receiver then recovers the transmitted information. It is assumed that the information is transmitted every T second in digital communications, which produces an information rate of $1/T$ Hz proportional to the signal bandwidth. To retrieve the transmitted information, receivers need to sample the signal

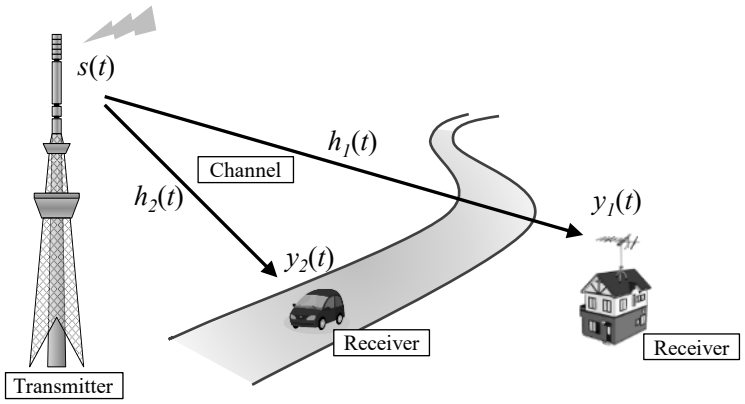

Figure 2.1 DTTB transmission system model.

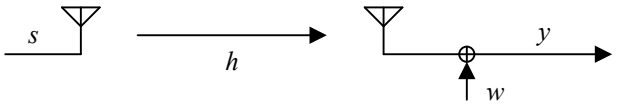

Figure 2.2 Simplified transmission system diagram.

$y(t)$ at every 0, T, $2T$, …period. Assuming that the Nyquist rate signaling criterion [67] is fulfilled, the digital received signal can be represented by the discrete time baseband model:

$$y[n] = h[n]s[n] + w[n] \tag{2.2}$$

where n represents the nth sample. The noise $w[n] \sim \mathcal{CN}(0, \sigma^2)$ is modeled as additive circularly symmetric complex Gaussian noise, where σ^2 represents the noise power.

The described system can be modeled using a basic transmission system diagram as shown in Figure 2.2. From the sampled received signal $y[n]$ the receiver corrects part of the received information which is corrupted due to the $h[n]$ and $w[n]$ terms.

When N_t transmit antennas and N_r receive antennas are used in a multi-antenna transmission system, the discrete received signal is modeled as:

$$\mathbf{y}[n] = \mathbf{H}[n]\mathbf{s}[n] + \mathbf{w}[n] \tag{2.3}$$

where $\mathbf{s}$ is the $N_t \times 1$ transmitted vector, $\mathbf{y}$ is the $N_r \times 1$ received vector, $\mathbf{H}$ is the $N_r \times N_t$ channel matrix and $\mathbf{w} \sim \mathcal{CN}(\mathbf{0}, \sigma^2\mathbf{I})$ is the $N_r \times 1$ additive circularly symmetric complex Gaussian noise. $\mathbf{H}$ is represented by the expression

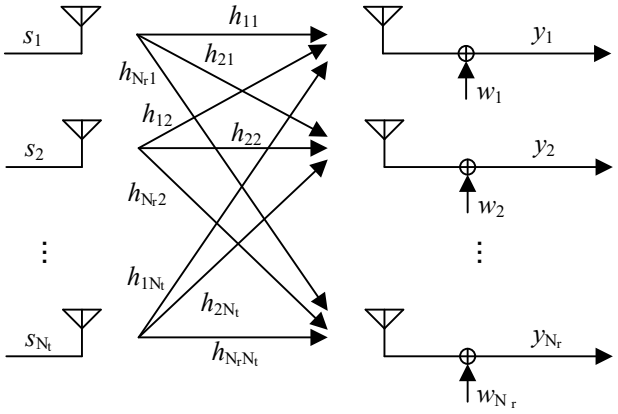

Figure 2.3 MIMO transmission system diagram.

$$\mathbf{H} = \begin{bmatrix} h_{11} & h_{12} & \cdots & h_{1N_t} \\ h_{21} & h_{22} & \cdots & h_{2N_t} \\ \vdots & \vdots & \ddots & \vdots \\ h_{N_r1} & h_{N_r2} & \cdots & h_{N_rN_t} \end{bmatrix} \tag{2.4}$$

where h_{ij} is the channel coefficient between the *i*th receive antenna and *j*th transmit antenna. The index n is omitted for simplicity in the rest the thesis. The $N_r \times N_t$ MIMO transmission system is also shown in Figure 2.3. At the *i*th receive antenna the signal is represented as:

$$y_i = \sum_{j}^{N_t} h_{ij} s_j + w_i\,, \qquad \text{for } i = 1, 2, \ldots, N_r \tag{2.5}$$

where the received signal at the *i*th antenna is the combination of all the signals from all the transmit antennas plus the AWGN. At the *i*th receive antenna, the symbol from the *j*th transmit antenna when $i = j$ is considered as the desired message and the other transmitted symbols $i \neq j$ behave as interference. The received signal y can be decomposed as:

$$y_i = h_{ii} s_i + \sum_{j \neq i}^{N_t} h_{ij} s_j + w_i\,, \qquad \text{for } i = 1, 2, \ldots, N_r \tag{2.6}$$

where we can observe the inter-antenna interference, which need to be considered at the receiver.

All h coefficients are distributed as $\mathcal{CN}(0, 1)$. SISO refers to the case when a single antenna is used at both sides, i.e., the number of transmit (N_t) and receive (N_r) are equal

to 1. In this thesis, only 2×2 MIMO systems are considered. This implies the transmitted vector **s** with 2×1 elements, the received vector **y** with 2×1 elements, and the channel **H** with 2×2 elements as follows.

$$\mathbf{H} = \begin{bmatrix} h_{11} & h_{12} \\ h_{21} & h_{22} \end{bmatrix} \tag{2.7}$$

In this thesis, the channel power is defined as the squared Frobenius matrix norm as follows:

$$\|\mathbf{H}\|_F^2 = \sum_{i,j}^{N_r,N_t} \left|h_{ij}\right|^2 \tag{2.8}$$

where $\left|h_{ij}\right|$ denotes the modulus of each channel coefficient. Note that the channel power is normalized to N_r.

$$\|\mathbf{H}\|_F^2 = \sum_{i,j}^{N_r,N_t} \left|h_{ij}\right|^2 = N_r \tag{2.9}$$

For instance, the channel power of 1×1 SISO system is equal to 1. The channel power of 2×2 MIMO system is equal to 2 as shown in (2.10).

$$\|\mathbf{H}\|_F^2 = |h_{11}|^2 + |h_{12}|^2 + |h_{21}|^2 + |h_{22}|^2 = 2 \tag{2.10}$$

In this thesis, the matrix **H** considers that one transmit/receive antenna has horizontal polarization, and the other transmit/receive antenna has vertical polarization, or vice-versa. Additionally, PI and XPD for the two receive antennas are introduced. The matrix **H** can be multiplied by two additional factors, obtaining a modified channel matrix $\widetilde{\mathbf{H}}$:

$$\widetilde{\mathbf{H}} = \mathbf{PX} \odot \mathbf{H} \tag{2.11}$$

where the matrix **P** is the PI between two recived signals caused by the difference in the receiving system, e.g., antenna gain or feeder loss, **X** is the XPD factor, **H** is the channel model matrix, and ⊙ represens the Hadamard element-wise multiplication. The PI is modeled using one configuration parameter: p [dB], which defines the power ratio of vertical polarization to horizontal polarization as shown in (2.12)(2.12). In this thesis, intentional PI at the transmitter is not included in the modified channel matrix $\widetilde{\mathbf{H}}$ and can be introduced as part of the transmitted vector **s** if needed. When p is a positive value in (2.12), it means that the received power of vertical polarization is high. The factor 2 is

introduced in (2.12) to make the channel models easier to understand in Section 2.3 satisfying the channel power constraint in (2.10). Note that the factor 2 can be omitted because the normalization in (2.9) applies to the modified channel matrix $\tilde{\mathbf{H}}$.

$$\mathbf{P} = \begin{bmatrix} \sqrt{2/\left(1+10^{\frac{p}{10}}\right)} & 0 \\ 0 & \sqrt{\left(2\times 10^{\frac{p}{10}}\right)/\left(1+10^{\frac{p}{10}}\right)} \end{bmatrix} \tag{2.12}$$

On the other hand the XPD is modeled using one configuration parameter: x [dB], which represents the average power ratio of the co-polar channel coefficient and the cross-polar channel coefficient. For the 2×2 cross-polarized MIMO under study in this thesis, the matrix $\mathbf{X}$ is expressed as follows.

$$\mathbf{X} = \begin{bmatrix} \sqrt{1/\left(1+10^{-\frac{x}{10}}\right)} & \sqrt{10^{-\frac{x}{10}}/\left(1+10^{-\frac{x}{10}}\right)} \\ \sqrt{10^{-\frac{x}{10}}/\left(1+10^{-\frac{x}{10}}\right)} & \sqrt{1/\left(1+10^{-\frac{x}{10}}\right)} \end{bmatrix} \tag{2.13}$$

High or low XPD values x represent low or high coupling between polarizations, respectively. For the extreme case with full coupling, i.e., pure co-polarized case, the XPD parameter x is set to 0 [dB]. While for no coupling, i.e., two isolated parallel channels, x is set to ∞ [dB]. The last element of $\tilde{\mathbf{H}}$ is the matrix $\mathbf{H}$, which depends on the channel model itself used, and is elaborated in Section 2.3. Note that 1×1 SISO system simplifies the channel model as $\tilde{h} = h$, since no PI and XPD factors are considered.

In the rest of the thesis the following notation is used: lower case letters z denotes scalars, boldface lower case letters $\mathbf{z}$ denote column vectors, boldface upper case letters $\mathbf{Z}$ denote matrices, the superscripts $^{-1}$, ^{T}, ^{H} denote matrix inversion, transposition and Hermitian transposition, the operator $E_z\{\cdot\}$ denotes the expectation over the variable z, N_t and N_r are the number of transmit and receive antennas, respectively.

2.2. DTTB System Overview

This section describes a channel coding scheme developed in ATSC 3.0 [9] and national research projects funded by the Ministry of Internal Affairs and Communications in Japan[68],[69].

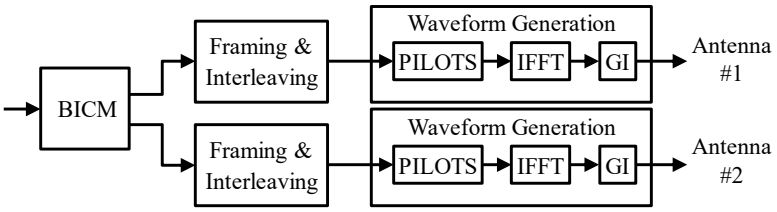

Figure 2.4 Block diagram of ATSC 3.0 MIMO transmitter.

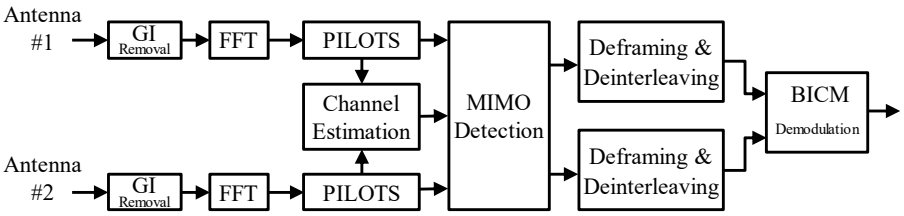

Figure 2.5 Block diagram of ATSC 3.0 MIMO receiver.

2.2.1. ATSC3.0 System Overview

Figure 2.4 presents the block diagram of 2×2 MIMO transmitter in ATSC 3.0. The input bit stream passes through a BICM chain that is a pragmatic approach where a bit-wise interleaver permits the independent design of modulation and coding. The details of the BICM is described in 2.2.2. The BICM provides two symbol streams to be transmitted on antenna #1 and #2. In the Framing & Interleaving chain, the input symbol streams are time-interleaved and frequency-interleaved. The Framing & Interleaving chains of both antennas have the same configuration. The Waveform Generation chain is composed of pilots insertion, Inverse Fast Fourier Transform (IFFT) and GI insertion blocks. Figure 2.5 shows the block diagram of the receiver. The active symbol period is extracted from the received signals, which are then converted into frequency domain signals by the FFT. The channel estimation is conducted using the MIMO pilots. The received signals are equalized and demultiplexed by MIMO detection. The details of the Waveform Generation parameters are described below.

A. Pilots

Table 2.1 gives an overview of the different types of pilots and the corresponding MIMO pilot encoding mechanism per antenna. Pilots for MIMO fall on exactly the same positions as for SISO, but the amplitudes and/or phases of the scattered, continual, edge, and subframe boundary pilots may be modified compared to SISO. The SPs are used for channel estimation, and they are regularly inserted in time and frequency direction. The

Table 2.1 MIMO pilots overview of ATSC 3.0

Pilot Encoding Algorithm	Antenna	Scattered Pilot	Common Continual Pilot	Additional Continual Pilot	Edge Pilot	Subframe Boundary Pilot
WH	#1	SISO	SISO	SISO	SISO	SISO
	#2	WH	SISO	SISO/WH	WH	WH
NP	#1	NP	SISO	SISO	SISO	SISO
	#2	NP	SISO	SISO/NP	WH	WH

Table 2.2 Allowed SP patterns for Walsh-Hadamard encoding

GI Pattern	GI Samples	8K FFT	16K FFT	32K FFT
GI1_192	192	MP16_2, MP16_4, MP8_2, MP8_4	MP16_2, MP16_4	MP16_2
GI2_384	384	MP8_2, MP8_4, MP4_2, MP4_4	MP16_2, MP16_4, MP8_2, MP8_4	MP16_2
GI3_512	512	MP6_2, MP6_4, MP3_2, MP3_4	MP12_2, M12_4, MP6_2, MP6_4	MP12_2
GI4_768	768	MP4_2, MP4_4	M8_2, M8_4, MP4_2, MP4_4	MP16_2, MP8_2
GI5_1024	1024	MP3_2, MP3_4	MP6_2, MP6_4, MP3_2, MP3_4	MP12_2, MP6_2
GI6_1536	1536	N/A	MP4_2, MP4_4	MP8_2, MP4_2
GI7_2048	2048	N/A	MP3_2, MP3_4	MP6_2, MP3_2
GI8_2432	2432	N/A	MP3_2, MP3_4	MP6_2, MP3_2
GI9_3072	3072	N/A	N/A	MP3_2
GI10_3648	3648	N/A	N/A	MP3_2
GI11_4096	4096	N/A	N/A	MP3_2
GI12_4864	4864	N/A	N/A	MP3_2

common and additional continual pilots are transmitted on predefined carriers, and they are basically used for synchronization at the receiver. The edge pilots are transmitted on both edge carriers to complete the frequency interpolation procedure in the channel estimation. The subframe boundary pilots are transmitted on the last OFDM symbol of a subframe to terminate the time interpolation procedure in the channel estimation. The WH algorithm differs from NP only in the scattered and the additional continual pilots. In Table 2.1, SISO indicates that the pilots are not modified compared to the pilots used in SISO configuration. The details of pilot encoding algorithms WH and NP are described in Section 3.1.3.

The terminology employed for the MIMO pilot patterns is described as MPa_b, where a=D_X and b=D_Y are defined. D_X is the number of carriers between the scattered pilot bearing carriers and D_Y is the number of symbols between the scattered pilots in a single pilot bearing carrier. Taking the Nyquist limits into account, the SP patterns allowed for the GI/FFT combinations with WH encoding for MIMO are presented in Table 2.2.

Table 2.3 Allowed SP patterns for Null Pilot encoding

GI Pattern	GI Samples	8K FFT	16K FFT	32K FFT
GI1_192	192	MP32_2, MP32_4, MP16_2, MP16_4	MP32_2, MP32_4	MP32_2
GI2_384	384	MP16_2, MP16_4, MP8_2, MP8_4	MP32_2, MP32_4, MP16_2, MP16_4	MP32_2
GI3_512	512	MP12_2, MP12_4, MP6_2, MP6_4	MP24_2, MP24_4, MP12_2, MP12_4	MP24_2
GI4_768	768	MP8_2, MP8_4, MP4_2, MP4_4	MP16_2, MP16_4, MP8_2, MP8_4	MP32_2, MP16_2
GI5_1024	1024	MP6_2, MP6_4, MP3_2, MP3_4	MP12_2, MP12_4, MP6_2, MP6_4	MP24_2, MP12_2
GI6_1536	1536	MP4_2, MP4_4	MP8_2, MP8_4, MP4_2, MP4_4	MP16_2, MP8_2
GI7_2048	2048	MP3_2, MP3_4	MP6_2, MP6_4, MP3_2, MP3_4	MP12_2, MP6_2
GI8_2432	2432	N/A	MP6_2, MP6_4, MP3_2, MP3_4	MP12_2, MP6_2
GI9_3072	3072	N/A	MP4_2, MP4_4	MP8_2, MP3_2
GI10_3648	3648	N/A	MP4_2, MP4_4	MP8_2, MP3_2
GI11_4096	4096	N/A	MP3_2, MP3_4	MP6_2, MP3_2
GI12_4864	4864	N/A	N/A	MP6_2, MP3_2

Compared with the table for SISO [55], D_X is reduced to half to keep the Nyquist limits for WH. The SP patterns for NP encoding is shown in Table 2.3. The combination of D_X and D_Y are the same as in SISO.

B. Inverse Fast Fourier Transform

ATSC 3.0 has adopted three different FFT sizes: 8k, 16k and 32k. OFDM systems are sensitive to inter-carrier interference (ICI), and the sensitivity depends on the FFT size. The smaller the FFT size, the more ICI the system can withstand. On the other hand, the smaller FFT size has a drawback to introduce the higher overhead of GI compared with the higher FFT size.

C. Guard Interval

ATSC 3.0 has adopted twelve GI lengths: 192, 384, 512, 768, 1024, 1536, 2048, 2432, 3072, 3648, 4096, and 4864 samples. GI length must be, at least, equal to the length of the delay time between the multipath signals in order to eliminate inter-symbol interference (ISI), which is also important for SFN. The further separation between the transmitters is allowed with the longer GI duration, i.e., the larger SFN area can be realized. However, the longer GI also increases the overhead. Thus, not all GI lengths are allowed for the three FFT sizes.

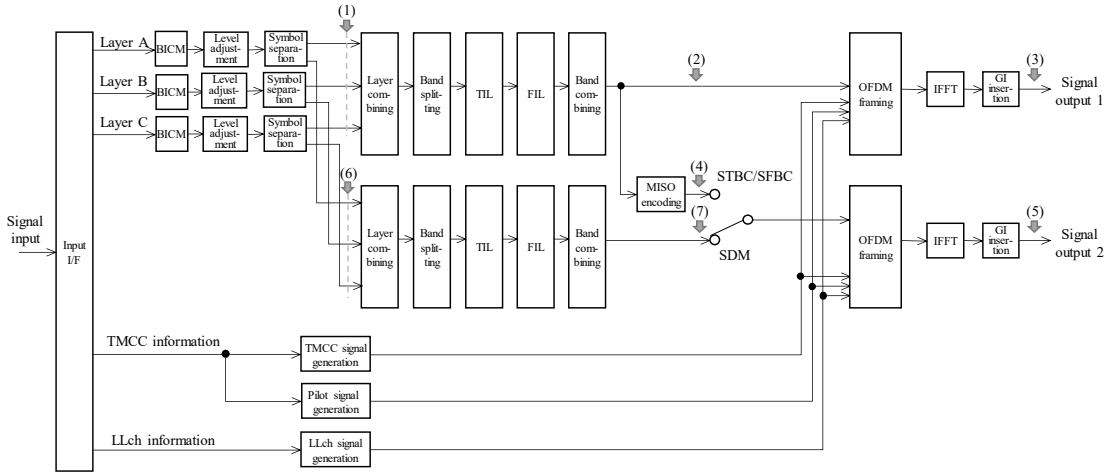

Figure 2.6 Block diagram of channel coding in advanced ISDB-T.

2.2.2. Advanced ISDB-T System Overview

This subsection presents an overview of the advanced ISDB-T system examined in this thesis. This system adopts frequency division multiplexing (FDM) based on a segment structure, which is a feature of the current terrestrial broadcasting transmission system, ISDB-T [70]. The segment structure is similar to the resource block structure introduced in the downlink physical channel in LTE [71]. The carrier modulation of advanced ISDB-T ranges from QPSK to 4096 QAM with non-uniform constellations [72] to improve the robustness performance. The system also supports MIMO transmission in order to provide large capacity content. An open-loop plain spatial multiplexing with cross-polarized 2×2 MIMO can be configured.

A. Basic Configuration of Channel Coding

The basic configuration of the channel coding of advanced ISDB-T is shown in Figure 2.6. Three hierarchical-frame signals (on layers A, B, and C), transmission and multiplexing configuration control (TMCC) information, and low latency channel (LLch) information are output from the input interface (Input I/F). The former signals are input into BICM blocks and are subjected to error-correction coding and mapping to carrier symbols. Furthermore, the power for each layer is adjusted, e.g., the power of layer A can be boosted, at the level-adjustment blocks. After that, the layer combining blocks combine the carrier symbols for hierarchical layers A, B, and C. Then, band splitting, time interleaving (TIL), frequency interleaving (FIL), and band combining are performed to form data segments.

To achieve low-latency transmission, processing that differs from the hierarchical frame of the three layers is applied to LLch information, and differential binary phase-shift keying (DBPSK) modulation is performed after the differential reference bit is added to the beginning of the LLch. Some predetermined carriers are assigned to LLch for each OFDM segment, and these carriers can be used for various purposes according to service requirements. At the OFDM framing blocks, a pilot signal, LLch signal, and TMCC signal are added to the data segments to construct an OFDM frame. OFDM modulation is then applied to the frame by using an IFFT, a GI is added, and the output OFDM signal is generated. The signal for SISO transmission is generated via path (1)-(2)-(3) in Figure 2.6

In the case of MISO transmission, the MISO encoding unit applies STBC [28] or SFBC to the carrier symbols for data after band combining. The OFDM frame is then formed and subjected to OFDM modulation. Signal output 1 for MISO transmission is generated by the same path (1)-(2)-(3) as for SISO transmission, and signal output 2 is generated by path (1)-(4)-(5). MISO encoding aims to improve the transmission robustness by exploiting the transmission-diversity in a poor reception environment, and the transmission capacity is equivalent to that in the case of SISO.

Moreover, in the case of advanced ISDB-T, it is possible to configure SM MIMO [73], which transmits different information from signal outputs 1 and 2, to expand the transmission capacity. For MIMO transmission, it is advantageous that the transmission capacity can be doubled compared with that possible with SISO; however, to achieve satisfactory transmission characteristics by reducing the correlation between propagation paths 1 and 2 in a LOS reception environment, it is necessary to install transmit and receiving antennas that support orthogonal polarization (horizontal and vertical polarization), which requires an initial cost for broadcasters and viewers. In MIMO transmission, the level-adjusted carrier symbols are separated by symbol-separation blocks into two streams, OFDM frames are formed and subjected to OFDM modulation, and the two signals are output. Signal outputs 1 and 2 of the MIMO transmission are generated via paths (1)-(2)-(3) and (6)-(7)-(5), respectively. For the FIL in MIMO transmission, different interleaving processes are applied for signal outputs 1 and 2 to improve the interleaving effect.

Although SISO, 2×1 MISO, and 2×2 MIMO are introduced in advanced ISDB-T, in the case of using one transmit antenna, it is supposed that all layers are transmitted via SISO. In the case where two transmit antennas are available, MISO or MIMO can be selected for each layer. For example, it is possible to improve the reception robustness with layer A (for mobile reception) using MISO and to expand the transmission capacity with layer B (for fixed reception) using MIMO.

B. Bit-Interleaved Coded Modulation

A detailed configuration of the BICM block is shown in Figure 2.7. For FEC, a combination of concatenated codes (with the LDPC code as the inner code and BCH code as the outer code) is adopted. Transmission capacity close to the Shannon limit [74] can be obtained by optimizing LDPC codes in combination with bit interleaving and NUC. For high code rates of 8/16 or higher, the irregular repeat accumulate (IRA) type parity check matrix is used [75]. For low coding rates of 7/16 or less, the multi edge type (MET) parity check matrix characterized by a structure in which two parity check matrices are combined is used [76].

In the block for FEC block encapsulation shown in Figure 2.7, the variable-length Type Length Value (TLV) packet [77], which is the input data, is encapsulated in a fixed-length FEC block. The configuration of the FEC block is shown in Figure 2.8. In the case of advanced ISDB-T, to increase the error-correction capability, codes were designed with an FEC block length of 69,120 bits. This block length is longer than that of ISDB-S3 [78], DVB-T2 [79], and ATSC3.0 [37]. The parity length of the LDPC code is determined according to the code rate of the LDPC code. The information bits of the LDPC code include the parity of the BCH code, and the length of the BCH parity is 192 bits regardless of the code rate of the LDPC code.

The variable-length TLV packets are stored in the main data area shown in Figure 2.8. When a TLV packet cannot fit in this area, it is divided and partly stored there, while the rest is stored in the main data area of the next FEC block. At that time, the start position of the TLV packets in each FEC block is designated by the TLV packet pointer in the FEC block header shown in Figure 2.8. The bit length of each part of the FEC block of advanced ISDB-T is listed in Table 2.4

In general, as the number of decoding iterations and the block length of the LDPC code increase, a larger amount of calculation is required at the receiver. Although it depends

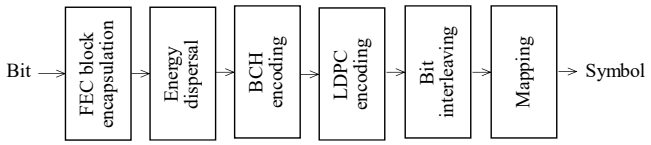

Figure 2.7 Configuration of BICM block.

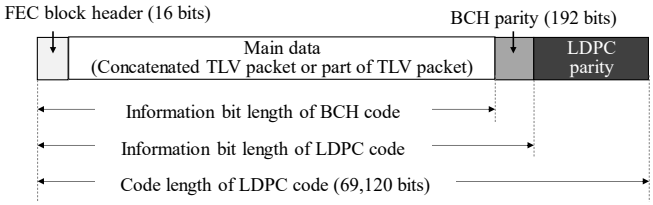

Figure 2.8 Configuration of FEC block.

Table 2.4 Bit length of FEC block for each code rate

LDPC code				BCH code		FEC block header	Main data
Code rate	Code length	Parity bit length	Information bit length	Parity bit length	Information bit length		
2/16	69,120	60,480	8,640	192	8,448	16	8,432
3/16	69,120	56,160	12,960	192	12,768	16	12,752
4/16	69,120	51,840	17,280	192	17,088	16	17,072
5/16	69,120	47,520	21,600	192	21,408	16	21,392
6/16	69,120	43,200	25,920	192	25,728	16	25,712
7/16	69,120	38,880	30,240	192	30,048	16	30,032
8/16	69,120	34,560	34,560	192	34,368	16	34,352
9/16	69,120	30,240	38,880	192	38,688	16	38,672
10/16	69,120	25,920	43,200	192	43,008	16	42,992
11/16	69,120	21,600	47,520	192	47,328	16	47,312
12/16	69,120	17,280	51,840	192	51,648	16	51,632
13/16	69,120	12,960	56,160	192	55,968	16	55,952
14/16	69,120	8,640	60,480	192	60,288	16	60,272

on the decoding algorithm, the computational complexity of LDPC code decoding in advanced ISDB-T is considered larger than that of Viterbi decoding in ISDB-T.

Table 2.5 Transmission Parameters of advanced ISDB-T and ISDB-T

		Advanced ISDB-T		ISDB-T
Channel bandwidth		6 MHz		
Number of segment divisions		36		14
Bandwidth of segment		166.7 kHz		428.6 kHz
Number of segments		35	33 + adjusting band	13
Signal bandwidth		5.83 MHz	5.57 MHz	5.57 MHz
Number of layers		Up to 3 layers		
Number of segments in partial reception band		9		1
FFT size (N_{FFT})		8,192, 16,384, 32,768		2,048, 4,096, 8,192
FFT sampling frequency		6.321 MHz (=512/81)		8.127 MHz (=512/63)
Guard interval ratio (GI ratio)		1/4, 1/8, 1/16, 1/32, 800/N_{FFT}		1/4, 1/8, 1/16, 1/32
Carrier modulation		QPSK, 16QAM, 64QAM, 256QAM, 1024QAM, 4096QAM (Non-uniform)		DQPSK, QPSK, 16QAM, 64QAM (Uniform)
FEC	Inner code	LDPC code		Convolutional code
	Outer code	BCH code		RS code
System configuration		SISO, 2×1 MISO, 2×2 MIMO		SISO

C. Waveform Generation

The transmission parameters of advanced ISDB-T are listed in Table 2.5. Although the new scheme attempts to expand the transmission capacity compared with that of ISDB-T by enhancing the frame structure (by increasing the FFT size and reducing the GI ratio while inheriting the functions of hierarchical transmission), considering the migration from the current terrestrial broadcasting to the next-generation system, a GI ratio of $800/N_{FFT}$ was included for setting the GI length to 126 μs, which is the same as the operational parameter used in Japan for the current ISDB-T. Here, N_{FFT} indicates the FFT size, which is 8,192 (8k), 16,384 (16k), or 32,768 (32k).

Regarding the signal bandwidth, it is possible to choose either the normal mode (bandwidth: 5.83 MHz, where the guard band is reduced compared with that for ISDB-T) using 35/36 of the 6 MHz channel bandwidth or a compatible mode (5.57 MHz: the same bandwidth as for ISDB-T).

Table 2.6 Transmission parameters of LTE-based 5G Terrestrial Broadcast

	LTE-based 5G Terrestrial Broadcast	Advanced ISDB-T		
Modulation	Cyclic Prefix-OFDM			
Channel bandwidth	5 MHz	6 MHz		
Signal bandwidth	4.5 MHz	Normal mode: 5.83 MHz Compatible mode: 5.57 MHz		
Number of segments	25 resource blocks	Normal mode: 35 Compatible mode: 33 + adjusting bands		
Bandwidth of segments	180 kHz	167 kHz		
FFT size	41,472	8,192	16,384	32,768
Number of carriers	12,150	7,561	15,121	30,241
Carrier spacing	370.37 Hz	771.60 Hz	385.80 Hz	192.90 Hz
Scattered pilot ratio	1/6, 1/12	1/3, 1/6, 1/12, 1/24, 1/48		
Carrier modulation	QPSK,16QAM, 64QAM, 256QAM (Uniform)	QPSK, 16QAM, 64QAM, 256QAM, 1024QAM, 4096QAM (Non-uniform)		
Number of OFDM symbols per frame	13	224	112	56
Effective OFDM symbol length	2,700 μsec	1,296 μsec	2,592 μsec	5,184 μsec
Guard interval ratio	1/9	1/4, 1/8, 800/8,192	1/4, 1/8, 1/16, 800/16,384	1/8, 1/16, 1/32, 800/32,768
Inner code	Turbo code	LDPC code		
Outer code	N/A	BCH code		
System	SISO	SISO, 2×1 MISO, 2×2 MIMO		

2.2.3. 5G Broadcast System Overview

The numerology of LTE-based 5G Terrestrial Broadcast for HPHT networks being specified in 3GPP Release 16 [80] are listed in Table 2.6. For comparison, the transmission parameters of advanced ISDB-T are also shown in Table 2.6. Note that we focus on a broadcasting system for fixed reception with a 6-MHz bandwidth in this thesis, and the numerology of LTE-based 5G terrestrial broadcasting for fixed reception in HPHT networks with a 5-MHz bandwidth is excerpted for comparison in the table. Guard interval is referred to as the cyclic prefix (CP) in the 3GPP specification.

2.3. Channel Models

During the development of the DVB-T2 specification, different channel models [81] have been used to provide simulated performance results. Although the main objective in this thesis is evaluation and optimization of the fixed reception performance of a dual-polarized MIMO, the channels have been chosen to verify the performance in a wide range of reception conditions including fixed, mobile and SFN.

2.3.1. AWGN channel

In this channel model only AWGN is considered to the signal and there is only one direct path. Given the ideal channel $h[n]$=1 in (2.2), a received signal y at the nth sample is expressed as follows.

$$y[n] = s[n] + w[n] \tag{2.14}$$

Although this model is simple and straightforward, it can be applied to a wide set of communication channels. Shannon-Hartley theorem [82] indicates that the capacity of the AWGN channel, i.e., the maximum rate at which information can be communicated across noisy channel with arbitrary reliability, is:

$$C = \log_2(1 + \mathrm{SNR}) \ \ \mathrm{bits/s/Hz} \tag{2.15}$$

where SNR is the signal-to-noise ratio in linear units, which is expressed as P/σ^2 where P being the variance of the transmitted signal s and σ^2 being the variance of noise w.

For 2×2 MIMO system, the matrix $\widetilde{\mathbf{H}}$ is calculated as:

$$\begin{aligned}\widetilde{\mathbf{H}} &= \mathbf{PX} \odot \mathbf{H} \\ &= \begin{bmatrix}1 & 0\\ 0 & 1\end{bmatrix}\begin{bmatrix}1 & 0\\ 0 & 1\end{bmatrix} \odot \begin{bmatrix}h_{11} & h_{12}\\ h_{21} & h_{22}\end{bmatrix} = \begin{bmatrix}1 & 0\\ 0 & 1\end{bmatrix}\end{aligned} \tag{2.16}$$

where PI parameter p is set to 0 [dB] in (2.12) and XPD parameter x is set to ∞ [dB] in (2.13). Setting each coefficient h_{11}=h_{22}=1, the matrix $\widetilde{\mathbf{H}}$ can be considered as the identity matrix $\mathbf{I}$, and a received signal $\mathbf{y}$ at the nth sample (2.3) is expressed as follows.

$$\mathbf{y}[\boldsymbol{n}] = \mathbf{s}[\boldsymbol{n}] + \mathbf{w}[\boldsymbol{n}] \tag{2.17}$$

It should be emphasized that the SNR for MIMO in this thesis is defined as $(P_1 + P_2)/\sigma^2$ for ATSC3.0 following the methodologies used in the standardization work, where P_1 and P_2 are the transmitted power of each transmit antenna. On the other hand, the CNR for MIMO is defined as P_{ave}/σ^2 for advanced ISDB-T from a practical

perspective, where P_{ave} is the average received power of all the transmit antennas. The detailed reasons are discussed in Section 2.5. Due to this assumption 2×2 MIMO uses double transmit power than SISO for the same CNR. The definition is constant between the simulations, the laboratory experiments and the field experiments of advanced ISDB-T system.

2.3.2. Power imbalance channel

In this model, PI is introduced with the configuration parameter: p [dB], which adjusts the power ratio of vertical polarization to horizontal polarization. The modified channel matrix $\widetilde{\mathbf{H}}$ is represented as:

$$\widetilde{\mathbf{H}} = \begin{bmatrix} \sqrt{2/\left(1+10^{\frac{p}{10}}\right)} & 0 \\ 0 & \sqrt{\left(2\times 10^{\frac{p}{10}}\right)/\left(1+10^{\frac{p}{10}}\right)} \end{bmatrix} \begin{bmatrix} 1 & 0 \\ 0 & 1 \end{bmatrix} \odot \begin{bmatrix} h_{11} & h_{12} \\ h_{21} & h_{22} \end{bmatrix} \quad (2.18)$$

where XPD parameter x=∞.

For instance, 10 dB higher power for the vertical polarized received signal is configured with p=10, and the matrix $\widetilde{\mathbf{H}}$ is calculated as:

$$\widetilde{\mathbf{H}} = \begin{bmatrix} \sqrt{2/11} & 0 \\ 0 & \sqrt{20/11} \end{bmatrix} \begin{bmatrix} 1 & 0 \\ 0 & 1 \end{bmatrix} \odot \begin{bmatrix} h_{11} & h_{12} \\ h_{21} & h_{22} \end{bmatrix} = \begin{bmatrix} \sqrt{2/11} & 0 \\ 0 & \sqrt{20/11} \end{bmatrix} \quad (2.19)$$

where h_{11}=h_{22}=1.

2.3.3. Cross polarized channel

High/Low coupling between polarizations are introduced with Low/High configuration parameter: x [dB], which adjusts the power ratio of the co-polarized channel component and the cross-polarized channel component. The modified channel matrix $\widetilde{\mathbf{H}}$ is represented as:

$$\widetilde{\mathbf{H}} = \begin{bmatrix} 1 & 0 \\ 0 & 1 \end{bmatrix} \begin{bmatrix} \sqrt{1/\left(1+10^{-\frac{x}{10}}\right)} & \sqrt{10^{-\frac{x}{10}}/\left(1+10^{-\frac{x}{10}}\right)} \\ \sqrt{10^{-\frac{x}{10}}/\left(1+10^{-\frac{x}{10}}\right)} & \sqrt{1/\left(1+10^{-\frac{x}{10}}\right)} \end{bmatrix} \odot \begin{bmatrix} h_{11} & h_{12} \\ h_{21} & h_{22} \end{bmatrix} \quad (2.20)$$

where PI parameter p=0.

For instance, full coupling pure co-polarized channel is modeld with x=0, and the matrix $\widetilde{\mathbf{H}}$ is calculated as:

Table 2.7 Tap values of simple two path channel

Tap number	Excess delay [μs]	h_{11}, h_{12}, h_{21}, h_{22}	
		[linear]	[rad]
1	0	$\sqrt{10^{\frac{d}{10}}/\left(1+10^{\frac{d}{10}}\right)}$	0
2	τ	$\sqrt{1/\left(1+10^{\frac{d}{10}}\right)}$	θ

$$\widetilde{\mathbf{H}} = \begin{bmatrix} 1 & 0 \\ 0 & 1 \end{bmatrix} \begin{bmatrix} \sqrt{1/2} & \sqrt{1/2} \\ \sqrt{1/2} & \sqrt{1/2} \end{bmatrix} \odot \begin{bmatrix} h_{11} & h_{12} \\ h_{21} & h_{22} \end{bmatrix} = \begin{bmatrix} \sqrt{1/2} & \sqrt{1/2} \\ \sqrt{1/2} & \sqrt{1/2} \end{bmatrix} \quad (2.21)$$

where h_{11}= h_{12}= h_{21}=h_{22}=1. Furthermore, in the case of full coupling channel with PI parameter p=10, the channel matrix is modified as follows.

$$\widetilde{\mathbf{H}} = \begin{bmatrix} \sqrt{2/11} & 0 \\ 0 & \sqrt{20/11} \end{bmatrix} \begin{bmatrix} \sqrt{1/2} & \sqrt{1/2} \\ \sqrt{1/2} & \sqrt{1/2} \end{bmatrix} \odot \begin{bmatrix} h_{11} & h_{12} \\ h_{21} & h_{22} \end{bmatrix} = \begin{bmatrix} \sqrt{2/22} & \sqrt{2/22} \\ \sqrt{20/22} & \sqrt{20/22} \end{bmatrix} \quad (2.22)$$

2.3.4. Simple two path channel

This channel includes two paths. Each path is defined by the excess delay, amplitude and phase of the coefficients h_{11}, h_{12}, h_{21} and h_{22}. The first tap models the direct path and the second tap models a multipath echo that causes signal distortion in terrestrial transmission channel. This model also represents SFN channel, i.e., a fixed receiver located between two transmitters. The delay, amplitude and phase are configured to the second tap with the delay time τ [μs], Desired-to-Undesired signal Ratio (DUR) parameter d [dB] and phase parameter θ [rad], respectively. Note that the frequency offset is outside the scope of this study.

2.3.5. NGH mobile outdoor channel

The NGH mobile outdoor channel [62] characterizes a fast-fading mobile reception model composed of eight taps. This model was extracted from a measurement that took place in Helsinki in 2010. This model was used during the DVB-NGH [33] standardization process to evaluate performance of the MIMO schemes in realistic scenarios. The first tap is complete LOS component, and the other taps are non-line of sight (NLOS) with Rayleigh distribution. The time domain channel model for 2×2 MIMO is expressed as:

$$\mathbf{H}(t,\tau) = \begin{bmatrix} h_{11}(t,\tau) & h_{12}(t,\tau) \\ h_{21}(t,\tau) & h_{22}(t,\tau) \end{bmatrix} \quad (2.23)$$

Table 2.8 Tap values of NGH mobile outdoor channel [62]

Tap number n	Excess delay τ_n[μs]	σ_{11}^2, σ_{22}^2 [dB]	σ_{12}^2, σ_{21}^2 [dB]
1 (LOS)	0	-4.0	-10.0
2 (NLOS)	0.1094	-7.5	-13.5
3 (NLOS)	0.2188	-9.5	-15.5
4 (NLOS)	0.6094	-11.0	-17.0
5 (NLOS)	1.109	-15.0	-21.0
6 (NLOS)	2.109	-26.0	-32.0
7 (NLOS)	4.109	-30.0	-36.0
8 (NLOS)	8.109	-30.0	-36.0

where $h_{ij}(t,\tau)$ is the impulse response between the jth transmit antenna and the ith receive antenna, t is the time index, and τ is the delay time. The channel model can be decomposed into LOS and NLOS components in vector form as:

$$\mathrm{vec}\left(\mathbf{H}^T(t,\tau)\right) = \bar{\mathrm{h}}\delta(t) + \sum_{n=1}^{8} \mathbf{R}_n^{1/2}\bar{\bar{\mathbf{h}}}_n \delta\left(t-\tau_n\right) \tag{2.24}$$

where $\mathrm{vec}\left(\mathbf{H}^T(t,\tau)\right) = (h_{11}(t,\tau)\ h_{12}(t,\tau)\ h_{12}(t,\tau)\ h_{22}(t,\tau))^T$, $\bar{\mathbf{h}}$ represents the $N_tN_r\times1$ vectorized LOS term, and the summation over the eight taps is the $N_tN_r\times1$ vectorized NLOS term. For each nth tap, the $N_tN_r\times N_tN_r$ covariance matrix $\mathbf{R}_n$ describes the correlation between the channel paths, a $N_tN_r\times1$ random vector $\bar{\bar{\mathbf{h}}}_n$ is the i.i.d. complex Gaussian components of unit variance, and τ_n is its excess delay defined in Table 2.8. The spatial correlation matrix $\mathbf{R}_n$ for taps n = 2, 3, …, 8 is presented as:

$$\mathbf{R}_n = \sigma_{11}^2(\tau_n)\begin{bmatrix} 1 & 0.06 & 0.06 & 0.05 \\ 0.06 & 0.25 & 0.03 & 0.05 \\ 0.06 & 0.03 & 0.25 & 0.06 \\ 0.05 & 0.05 & 0.06 & 1 \end{bmatrix} \tag{2.25}$$

where $\sigma_{11}^2(\tau_n)$ is the co-polar gain in linear unit defined in Table 2.8. Note that the DVB-NHG mobile outdoor channel assumes XPD = 6 [dB] and K factor =∞ for the first tap, i.e., only LOS component is considered with $\mathbf{R}_1=\mathbf{0}$.

In mobile channels, the time dependent variation of the channel realizations produces frequency shifts, and the Doppler effect introduced needs to be considered. The maximum frequency shift F_d in the received signal due to the Doppler effect is:

$$F_d = \frac{v}{c} f_c \cos\alpha \tag{2.26}$$

where v is the receiver velocity, c is the speed of light, f_c is the RF frequency of the signal, and α is the angle between directions of the receiver velocity and the arriving signal.

Under the assumption that signals propagate between the transmitter and the receiver in horizontal plane, the angles of arrival at the receive antenna are uniformly distributed, and a circular symmetric radiation pattern for the receive antenna, the power spectral distribution follows so-called Jakes power spectral density. The Jakes power spectral density is specified to be used at a particular tap in conjunction with a fixed frequency offset proportional to F_d. The spectrum of each tap is represented as:

$$\begin{cases} S(f - 3F_d/4\,, F_d/4) & \text{for } n = 2, 3 \\ S(f + 3F_d/4\,, F_d/4) & \text{for } n = 4, 5, 6, 7, 8 \end{cases} \tag{2.27}$$

where the tap n=1 is LOS with no Doppler shift.

2.4. Multi-Antenna Receivers

Regarding the signal detection at the receiver, some methods are uniquely determined according to the transmission schemes, and the other methods can be applied to any transmission schemes. Here, the reception methods are briefly outlined according to the classification in Table 2.9.

First, when the number of streams, i.e., the number of signals to be transmitted, is one, the purpose of a MIMO system is to improve the SNR at the receiver. Antenna selection transmit diversity is a method of selecting an optimal antenna for transmitting a stream from multiple transmit antennas. Maximum ratio combining (MRC) transmit diversity is a method of forming a transmit beam using multiple transmit antennas and transmitting one stream [83]. These methods require a part of or all the MIMO channel information at the transmitter side to select an optimal antenna or to form an optimal transmit beam. On the other hand, a STC was proposed that does not require MIMO channel information at the transmitter side, which can be used in systems without feedback, such as broadcasting. STC is one method for transmit diversity, and space-time block coding (STBC) [28] and space-time trellis code (STTC) [84] are used. In the case of STTC, maximum likelihood sequence estimation (MLSE) [85] is applied, so when the number of trellis states is high, a large amount of calculation is required. Since STC does not require channel information at the transmitting side, the complexity of the transmitting side is quite low.

Next, an overview of signal detection schemes for MIMO systems that aim to expand transmission capacity is provided. When the number of transmission streams is two or more, each stream is spatially multiplexed, and this is called SM. An input stream is

Table 2.9 Signal detection in MIMO receiver

Number of streams	Transmit scheme	Receive scheme	Complexity
1	Space Time Coding	Space Time Decoding	Low (STBC) High (STTC)
	Antenna Selection/MRC Transmit diversity	MRC Receive diversity	Low
2 or more	SDM	Spatial filtering	Low (ZF) Mid (MMSE)
		Ordered successive detection (BLAST, SIC)	Mid
		MLD	High
	E-SDM	Spatial filtering	Low (ZF) Mid (MMSE)
		Ordered successive detection (BLAST, SIC)	Mid
		MLD	High
		MRC Receive diversity	Low

generally divided into multiple streams and transmitted simultaneously, and each divided stream is called a substream. In the case of SM, classification similar to the above-mentioned transmission diversity can be made. When channel information is not available at the transmitting side, each substream can be transmitted from each transmit antenna with equal power. In this thesis, this method of SM without beam forming is called as space division multiplexing (SDM) in a precise sense [86]. Since SDM uses all transmit antennas, when the MODCOD of substreams are the same, the transmission capacity can be multiplied by the number of transmit antennas. However, since the spatially multiplexed substreams interfere with each other at the receiver, a separate detection technique is required.

Optimal detection method, known as Maximum Likelihood Detection (MLD) [85], uses channel information to generate replicas of received signals for all possible combinations of transmitted signals, and searches for the closest point among them. Therefore, when the number of possible combinations is high, the complexity increases exponentially with the number of the transmit antennas. In contrast, the simplest and most practical signal detection scheme in SDM is spatial filtering, which is equivalent to forming beam toward desired signals and null points toward unwanted signals at the receiving side. In this thesis, two algorithms, Zero Forcing (ZF) and Minimum Mean Square Error (MMSE), are used to reduce complexity, which are described in following subsections. Note that Eigenbeam SDM (E-SDM) that requires channel information at the transmitter side [87] and ordered successive detection that repeats spatial filtering as many times as the number of substreams [88] are out of the scope of this thesis.

2.4.1. ZF Detection

Linear detectors represent a good alternative to the optimum MIMO detection, since they reduce drastically the complexity while maintaining a good performance. This type of detectors transforms the joint MIMO demapping into independent single-antenna demapping processes. For instance, in a 2×2 MIMO system, a demapper with complexity M^2 is transformed into two independent demappers with complexity M. Here, M denotes the number of signal points in the constellation used for carrier modulation. The ZF detector sets the interferers amplitude to zero, which is simply done by inverting the channel matrix [89]. In case $N_r \geq N_t$, the Moore-Penrose inverse matrix $\mathbf{H}^+$ of the channel matrix $\mathbf{H}$ is represented as:

$$\mathbf{H}^+ = (\mathbf{H}^{\mathrm{H}}\mathbf{H})^{-1}\mathbf{H}^{\mathrm{H}} \tag{2.28}$$

where $\mathbf{H}$ is the channel matrix, and the superscripts $^{-1}$, $^{\mathrm{H}}$ denote matrix inversion and Hermitian transposition. The ZF detection results are given by:

$$\hat{\mathbf{x}} = \mathbf{H}^+\mathbf{y} \tag{2.29}$$

where $\mathbf{y} = \mathbf{H}\mathbf{x} + \mathbf{w}$ is the received vector, $\hat{\mathbf{x}}$ is the estimated transmitted vector. The main drawback of ZF detection is the fact that the algorithm attempts to completely separate signals even if the SNR deteriorates significantly. which enhances the noise. In particular, when the channel matrix ($\mathbf{H}^{\mathrm{H}}\mathbf{H}$) is ill-conditioned, i.e., the determinant is small, the noise power is enhanced.

2.4.2. MMSE Detection

MMSE detection can be used to counteract the noise enhancement problem of the ZF detection. The MMSE detection estimates $\hat{\mathbf{x}}$ minimizing the error caused by the noise and the interference combined, and the results are given by [90]:

$$\hat{\mathbf{x}} = (\mathbf{H}^{\mathrm{H}}\mathbf{H} + \sigma^2\mathbf{I})^{-1}\mathbf{H}^{\mathrm{H}}\mathbf{y} \tag{2.30}$$

where $\mathbf{y} = \mathbf{H}\mathbf{x} + \mathbf{w}$ is the received vector, $\mathbf{H}$ is the channel matrix, $\hat{\mathbf{x}}$ is the estimated transmitted vector, $\mathbf{I}$ is the identity matrix and σ^2 is the noise power.

2.4.3. MLD and Max-Log Demapping

The optimum MLD (also known as ML demapper) computes LLRs λ_k for all coded bits b_k, $k=1, 2, \ldots, U\times N_t$, where U denotes the number of bits per symbol in carrier modulation and N_t denotes the number of transmit antenna. For the LLR calculation, a total number

of M^{N_t} Euclidean distances between the received vector **y** and the transmitted vector **x** is calculated. Here, M denotes the number of signal points in the constellation. A single output λ_k is computed as:

$$\lambda_k = \log \frac{\sum_{\mathbf{x} \in \chi_k^1} \exp\left(-\frac{\|\mathbf{y} - \mathbf{H}\mathbf{x}\|^2}{\sigma^2}\right)}{\sum_{\mathbf{x} \in \chi_k^0} \exp\left(-\frac{\|\mathbf{y} - \mathbf{H}\mathbf{x}\|^2}{\sigma^2}\right)} \tag{2.31}$$

where **H** is the channel matrix, σ^2 is the noise power, χ_k^1 and χ_k^0 are the set of constellation symbols with the corresponding bit label b_k to 1 and 0, respectively. The complexity increases exponentially with the number of bits per symbol U and the number of transmit antenna N_t. For each demapping execution, the complexity order is $\mathcal{O}(M^{N_t})$

To reduce the complexity of MLD, the max-log approximation is introduced. The computation of logarithmic and exponential functions is replaced to a minimum distance problem as following.

$$\log\left(\sum_i \exp(x_i)\right) \approx \max_i(x_i) \tag{2.32}$$

Applying the max-log approximation, the LLR can be computed as:

$$\lambda_k = \min_{\mathbf{x} \in \chi_k^0}\left(\frac{\|\mathbf{y} - \mathbf{H}\mathbf{x}\|^2}{\sigma^2}\right) - \min_{\mathbf{x} \in \chi_k^1}\left(\frac{\|\mathbf{y} - \mathbf{H}\mathbf{x}\|^2}{\sigma^2}\right) \tag{2.33}$$

where the complexity of each execution has still order $\mathcal{O}(M^{N_t})$.

2.5. Simulations

The methodology to evaluate the potential capacity improvement that can be achieved with MIMO techniques in DTT systems is summarized as follows:

A set of physical layer simulations are conducted in order to validate the MIMO performance with different types of channel estimation schemes, channel interpolation methods, MODCOD combinations, demapping algorithms and MIMO precoding schemes for different channel models using the physical layer simulator developed. In order to obtain the performance of 2×2 SM MIMO or combined with other technologies, a physical layer simulator was developed. The simulated performance was evaluated in terms of Bit Error Rate (BER) for a given SNR or CNR.

For ATSC 3.0 system evaluation in this thesis, SNR was used to maintain consistency with the standardization work. For MIMO transmission, the SNR was defined as the ratio of the total transmit power for two polarized signals (antenna #1 and #2) to the AWGN power at each receiver (either antenna #1 or #2) in this thesis. With the definition, the transmitting power of SISO and MIMO is equal, and a fair comparison can be made from the perspective of power consumption efficiency [54]. In this thesis, the required SNR was defined as the SNR to achieve BER =1×10^{-4} for ATSC 3.0.

Alternatively for advanced ISDB-T system evaluation, CNR was used from a practical perspective for the following laboratory and field experiments. For MIMO transmission, the CNR was defined as the ratio of the average received power for two polarized signals to the AWGN power at each receiver. More specifically the transmit power of each transmit antenna is constrained as equal and the CNR is defined as $\mathrm{CNR} = P_{ave}/\sigma^2$, where P_{ave} is the average received power of all the receive antennas. For instance, in 1×1 SISO system, the average received power $P_{ave}= P_1=1$. In 2×2 MIMO system, with the received power of each antenna $P_1 = P_2 = 1$, the average is calculated as $P_{ave} = (P_1 + P_2)/2 = 1$. Note that according to this assumption 2×2 MIMO uses double transmit power than SISO for the same CNR value. The transmitting power constraint in this thesis is expressed as follows.

$$\sum_{j}^{N_t} P_j = N_t \tag{2.34}$$

Here, P_j denotes the transmit power of jth antenna and the number of transmit antenna $N_t= 2$. In this thesis, the required CNR was defined as the CNR to achieve BER = 1×10^{-7} [91] for advanced ISDB-T.

In the literature multiple definitions are used for SNR or CNR and most MIMO studies assume that the total transmit power is kept constant between MIMO and SISO for fair comparison especially for theoretical analysis [54]. However, since this thesis focuses on the performance comparison between MIMO and SISO in practical deployment scenarios, we decided to use the CNR definition based on the average received power P_{ave}. This is because when MIMO is deployed, there is a high possibility that a new transmitter will be added to support 2×2 MIMO transmission to the existing SISO transmitter. As a practical rollout scenario, the total transmission power would be doubled to improve transmission capacity and services, when it is permitted by radio regulations. In the field

experiments, MIMO signals were emitted with two transmitters under the condition of twice the transmission power compared with SISO.

We measured the BER characteristics and found the required SNR or CNR for a given BER threshold. The SISO performance was evaluated with the channel frequency response (CFR) from the horizontal transmit antenna to the horizontal receive antenna. To evaluate the MIMO performance, four CFRs were used to reproduce the MIMO channel in the channel simulator.

In an OFDM system the CNR can be defined with respect to the SNR. In practical use, some of the outer end carriers of an OFDM signal are unused (null carriers) to reduce the potential interfere to adjacent RF channels due to the spectrum roll-off. The number of null carriers depend on the FFT size, the larger the FFT size the quicker the spectrum roll-off and therefore more carriers can be used for data transmission [81]. In the CNR definition used in this thesis the carrier power refers to effective carrier power. Since the noise added at the receiver in time domain affects all the carriers, i.e., effective and null carriers, the signal to noise ratio at the input of the OFDM demodulator in time domain (SNR) and the signal to noise ratio at the baseband signal for each carrier (CNR) has the following relationship in dB.

$$\mathrm{CNR} = \mathrm{SNR} + 10 \cdot \log_{10}\left(\frac{N_{\mathrm{FFT}}}{N_{\text{Number of carriers}}}\right) \tag{2.35}$$

2.5.1. Channel Estimation

The performance of MIMO scattered pilot is evaluated by physical layer simulations. The transmitter chain complies with the ATSC 3.0 specification. MIMO channel estimation algorithms are described in Section 3.1.

The two MIMO pilot encoding schemes are compared in terms of BER after BCH decoding. Moreover the MSE between the estimated channel and the real channel is also evaluated. MSE is defined as:

$$MSE = E_{l,k}\left\{\frac{1}{N_t N_r}\sum_{j=1}^{N_t}\sum_{i=1}^{N_r}\left\|h_{ij}[l,k] - \hat{h}_{ij}[l,k]\right\|^2\right\} \tag{2.36}$$

Table 2.10 Basic parameters for channel estimation evaluation in ATSC 3.0

FFT size	8k
Number of carriers	6913
Signal bandwidth	5.83 MHz
Modulation and code rate	QPSK 5/15 64 NUC 12/15
GI pattern	GI5_1024 (GI ratio: 1/8, GI length: 148 μs)
MIMO scattered pilot encoding	Walsh-Hadamard Null Pilot
Frequency Interpolation	DFT Linear

where $h_{ij}[l,k]$ and $\hat{h}_{ij}[l,k]$ denote the real and estimated CFR of *i*th receive antenna and *j*th transmit antenna for carrier k of the OFDM symbol number l, respectively. $E_{l,k}\{\cdot\}$ refers to the expectation calculation over l and k.

Both mobile and fixed reception scenarios have been considered with the NGH mobile outdoor channel [62] and the simple two path SFN channel, respectively. In the channel estimation evaluation shown in Chapter 3, the DUR parameter d=3 [dB], the delay time τ=0.5 GI duration and the phase parameter $\theta=\pi/2$ are configured to the simple two path channel as a typical fixed reception environment in an SFN.

The basic transmission parameters for simulations are shown in Table 2.10. In the simulation parameters, FFT size, modulation and GI ratio are selected to be the same as the operational parameters in current DTT system ISDB-T in Japan [70]. The required SNR of the current service for SISO rooftop reception is about 20 dB [92]. Using 64NUC 12/15, the SNR for MIMO would be about the same threshold with the same total transmit power as SISO, i.e. half power in each antenna. The mobile reception service known as One-Seg, which targets at handheld terminals and launched on April 1st, 2006, in Japan, has been provided with QPSK 2/3 with SISO [70], and the QPSK 5/15 is selected as the parameters to provide the same capacity with MIMO. It is assumed that the XPD parameter x is infinite as an ideal case (AWGN), 18 dB as a practical fixed reception scenario (SFN) [93] and 6 dB for the mobile reception scenario (Rice, NGH outdoor) [62]. The performance is evaluated with a MMSE detector. Long LDPC codes (64k) and NUCs standardized in ATSC 3.0 are used [94]. Convolutional Time Interleaver (CTI) with the parameter N_{rows}=724 (time interleaving depth of approximately 100 ms) is adopted and FIL is also applied.

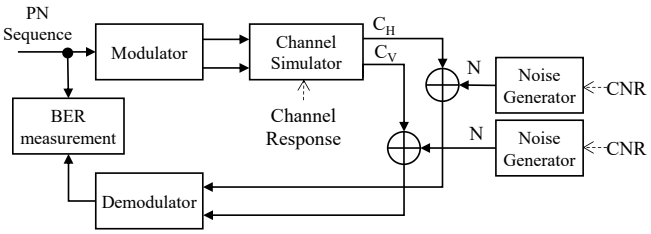

Figure 2.9 Block diagram of simulation.

2.5.2. System Performance Evaluation

The transmission performance of each configuration is evaluated by physical layer simulations. The block diagram of the simulations is shown in Figure 2.9. The performance measure is BER, which is generally used for evaluating DTTB systems. The BER is measured after BCH decoding for ATSC 3.0, and we specified the required SNR to be the smallest SNR at which a BER lower than 1×10^{-4} can be obtained. Alternately the BER is measured before BCH decoding for advanced ISDB-T, and the required CNR is measured at which a BER lower than 1×10^{-7}, where the value assumes that data transmission is unidirectional, and data cannot be retransmitted. Note that Quasi Error Free (QEF) is obtained at the required CNR after decoding the BCH code in advanced ISDB-T, but QEF is not achieved in 5G Broadcast because CRC code allows for only error detection.

For the evaluation of broadcast MIMO practical gain, we evaluated the required CNR of several parameter sets in an ideal channel (AWGN) for the SISO/MIMO configurations with advanced ISDB-T system. The output signals of the modulator were input to a channel simulator, and two independent AWGNs with equal power were added to the signals. The channel responses were configured in the channel simulator shown in Figure 2.9, and the actual reception environments were reproduced for follow-up verification. Note that the CNR definition in advanced ISDB-T simulations is consistent with that in laboratory and field experiments.

2.6. Laboratory Experiments

This section describes the performance evaluation methodologies and the experimental setup for laboratory experiments. We evaluated the required CNR of several parameter sets in an ideal channel (AWGN) for the SISO/MIMO configuration in laboratory experiments. Figure 2.10 shows a block diagram of the experiments. The output signals

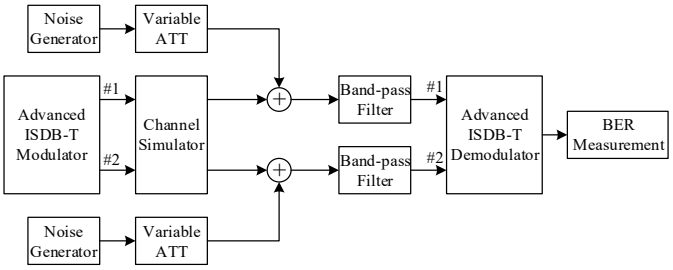

Figure 2.10 Block diagram of laboratory experiments.

of the modulator were input to a channel simulator, and two independent AWGNs were added to the signals.

The MIMO channel snapshots were configured in the channel simulator shown in Figure 2.10, and the actual reception environments were reproduced for follow-up verification. The SISO performance was evaluated with the CFR from the horizontal transmit antenna to the horizontal receive antenna. To evaluate the MIMO performance, four CFRs were used to reproduce the MIMO channel in the channel simulator. For MIMO, the required CNR was defined as the average value of the required CNRs between input signals #1 and #2 to the demodulator. The required CNR is defined as the minimum CNR at which the BER before BCH decoding is below 1×10^{-7}.

2.7. Field Experiments

Figure 2.11 shows a block diagram of the transmission and reception for the field experiments. A single pseudo random bit sequence was generated, coded with BCH codes and LDPC codes, and then modulated in a prototype advanced ISDB-T modulator. The modulated SISO/MIMO signals were converted into RF signals at the same frequency and amplified to the desired power level. After that, the signals were transmitted from the dual-polarized antenna installed at an experimental test station. At the receiver site, the transmitted signals were received by the dual-polarized Yagi antenna. Each received signal was filtered by a band-pass filter and attenuated by a variable attenuator (ATT). The required received power is measured while setting the input point of a low noise amplifier (LNA) as the specified point for the received power. In a prototype demodulator, the received signals were demodulated with ZF detection, and the BER was measured on a measurement vehicle. The required received power is defined as the minimum received power at which the BER before BCH decoding is below 1×10^{-7}.

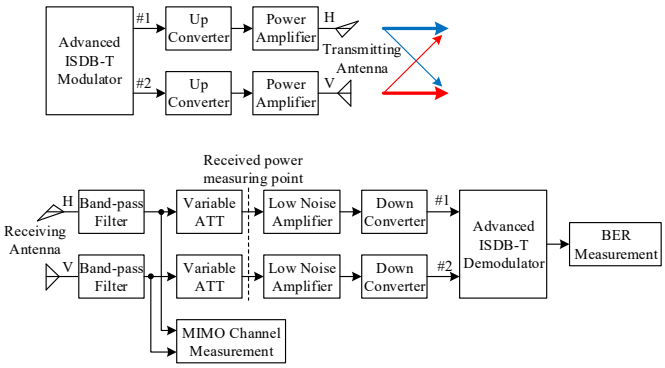

Figure 2.11 Block diagram of transmission and reception equipment for field experiments.

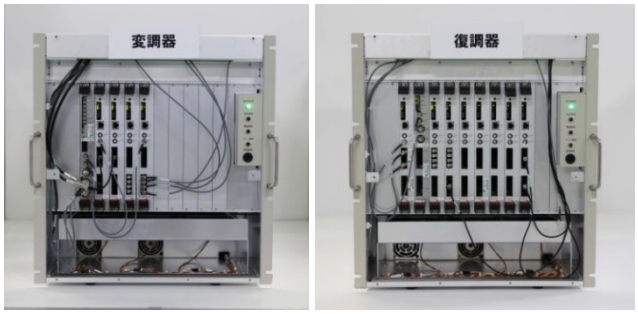

Figure 2.12 Modulator (left) and demodulator (right) used for experiments.

In the field experiments, SISO performance was evaluated by transmitting a horizontally polarized radio wave with the experimental test station. The required received power was specified at the input point of the LNA for horizontal wave with the horizontal element of the receiving antenna. For MIMO parameters, radio waves were transmitted with horizontal and vertical polarization, and the required received power was specified as the average received power of the horizontally and vertically polarized waves. The required received power was measured by inserting the same amounts of attenuations into both received signals of the horizontally and vertically polarized waves, decreasing the received power, and when a BER of 1×10^{-7} or less was achieved, the average value was calculated as the required received power. Assuming fixed rooftop reception in an HPHT network, the receiving antenna height was set 10 m above ground level. The required received power in an ideal AWGN channel with the experimental equipment was measured, and the degradation in the required received power from the ideal channel was evaluated in the field experiments.

Figure 2.12 shows a prototype FPGA-based modulator and demodulator used for the experiments. Figure 2.13 shows the transmit and receive antennas for the UHF channel 46 used for STC-SFN field experiments in Hitoyoshi city shown in Section 4.3.

1) Dual-polarized transmission antenna

Antenna type	Dual-polarized dipole antenna
Frequency	671 MHz (UHF Ch 46)
Gain	Over 10 dBd
Cross-polarization discrimination	Over 15 dB (in half power angle)
VSWR	Under 1.20

VSWR: voltage standing wave ratio

2) Dual-polarized reception antenna

Antenna type	8 element dual-polarized Yagi antenna
Receiving frequency range	597 - 674 MHz (UHF Ch 33 - Ch 46)
Gain	9.0 dBd
Front to back ratio	Over 13 dB
Cross-polarization discrimination	Over 25 dB (Boresight)

Figure 2.13 Transmit antenna (left) and receive antenna (right) used for field experiments in Section 4.3.

Figure 2.14 Transmit antenna (left) and receive antenna (right) used for field experiments in Section 5.1.

Figure 2.15 Transmit antenna (left) and receive antenna (right) used for field experiments in Section 5.2.

Figure 2.14 shows the transmit antenna installed at Tokyo Tower and the receive antenna that was used for the measurements. The transmit/receive antennas are developed for the UHF channel 28 and used for practical gain evaluation in Tokyo shown in Section 5.1. Figure 2.15 depicts the transmit antenna installed at the test station on the hillside of Mt. Ikoma and the receive antenna used for the field measurements in Osaka shown in Section 5.2. The transmit/receive antennas are designed for the UHF channel 19.

Table 2.11 lists details on the experimental test stations used for the field experiments. We installed a cross-polarized (horizontal and vertical) transmit antenna shared by SISO/MIMO at each transmitter site. Two transmitters were installed at the stations to handle the MIMO transmission.

Table 2.11 Specifications of experimental test stations

Transmitter site	Kumamoto				Tokyo		Osaka	
	Hitoyoshi City		Mizukami Village		Tokyo Tower (Shiba, Minato-ku)		Mt. Ikoma (Higashiosaka City)	
Transmission frequency	671.143 MHz (UHF Ch 46 in Japan)				563.143 MHz (UHF Ch 28 in Japan)		509. 143 MHz (UHF Ch 19 in Japan)	
Polarization	Horizontal	Vertical	Horizontal	Vertical	Horizontal	Vertical	Horizontal	Vertical
Transmission power	10 W	10 W	3 W	3 W	1 kW	1 kW	1 kW	1 kW
E.R.P	140 W	135 W	25 W	25 W	2.1 kW	2.1 kW	4.6 kW	4.6 kW
Transmitting antenna type and configuration	Dual-polarized multi-stage dipole antenna one-stage one-sided		Dual-polarized multi-stage dipole antenna one-stage one-sided		Dual-polarized multi-stage dipole antenna two-stage three-sided		Dual-polarized multi-stage dipole antenna two-stage two-sided	
Transmitting antenna height	632 m above sea level		1080 m above sea level		280 m above sea level		570 m above sea level	

Table 2.12 Specifications of receiving antenna

Antenna type	8-element dual-polarized Yagi antenna
Gain	9.0 dBd
Front-to-back ratio	Over 13 dB
Cross-polarization discrimination	Over 25 dB (Boresight)

Table 2.12 shows specifications of the receive antenna used. A dual-polarized Yagi antenna was equipped on a measurement vehicle to receive SISO/MIMO signals. The receiving antenna was mounted on a pole so that the orthogonal antenna elements were horizontal and vertical.

Chapter 3 Broadcast MIMO Channel Estimation

Regarding the MIMO pilot configuration in ATSC 3.0, five different boosting values are available per 16 different pilot patterns for each pilot encoding algorithm. This chapter focuses on the performance and optimization on the pilot boosting, pilot pattern and the MIMO pilot encoding algorithms considering the channel interpolation method at the receiver. It should be noted that the analysis on the optimum pilot boosting for both MIMO pilot encoding algorithms for ATSC 3.0 is novel because the performance has not been evaluated in literature. The study greatly contributes to the selecting the pilot configuration in ATSC3.0, because the newly introduced NP encoding algorithm has not been evaluated and compared with Walsh-Hadamard so far. The performance is evaluated with the plain SM MIMO standardized in ATSC 3.0. The main contribution of this chapter is to provide a guideline on MIMO pilot configuration in ATSC3.0 for broadcasters.

The optimum pilot boosting is theoretically deduced and evaluated by physical layer simulations with an ATSC 3.0 simulator. The evaluations of the pilot pattern and the encoding algorithm are extracted from physical layer simulations in both fixed and mobile reception scenarios.

3.1. Channel Estimation in ATSC 3.0

As the result of pilot encoding process, MIMO pilots are divided into two subsets (one per antenna). The two subsets are designed to be orthogonal in phase or amplitude to observe the channel separately. The details of the channel estimation parameters are described as follows.

3.1.1. Pilot Encoding

Figure 3.1 illustrates the MIMO scattered pilot MP3_2, i.e., $D_X = 3$, $D_Y = 2$, for WH encoding and NP encoding. The differences between the two MIMO pilot encoding algorithms are described next.

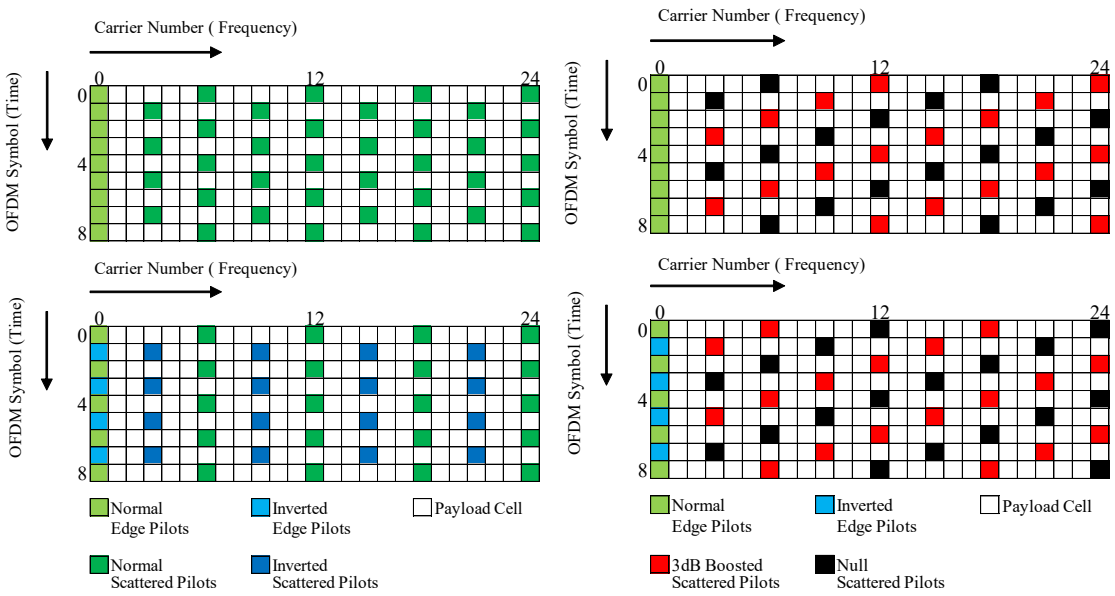

Figure 3.1 MIMO pilots for Walsh-Hadamard encoding (left) and Null Pilot encoding (right). For Antenna #1 (top) and #2 (bottom).

A. Walsh-Hadamard Encoding

With WH encoding, the phases of all pilots transmitted from antenna #1 are not modified. Regarding the signal transmitted from antenna #2, the pilots can be partitioned into two subsets, and the phases of the scattered pilots are inverted every second pilot bearing carrier. That results that the half of scattered pilots transmitted from antenna #2 are not modified and that the other half pilots are inverted. As the result of the phase inversion on every second pilot bearing carrier, the number of carriers between the scattered pilot bearing carriers in each subset is doubled.

B. Null Pilot Encoding

With NP encoding, the amplitudes of the scattered pilots of both subsets are modified in both signals transmitted from antennas #1 and #2. With NP encoding, antenna #1 alternately transmits scattered pilots with 3 dB increased transmit power and scattered pilots with null power (zero amplitude). Scattered pilots of antenna #2 are transmitted with null power and with 3 dB gain in reverse order. The 3 dB boosting keeps the total signal power of the scattered pilot to be the same as SISO.

3.1.2. Pilot Decoding

2×2 MIMO OFDM system can be modeled as:

Table 3.1 Equivalent D_X and D_Y in MIMO pilots

SISO	MIMO	
	Walsh-Hadamard encoding	Null Pilot encoding
D_X	$2D_X$	D_X
D_Y	D_Y	$2D_Y$

$$\begin{bmatrix} y_1 \\ y_2 \end{bmatrix} = \begin{bmatrix} h_{11} & h_{12} \\ h_{21} & h_{22} \end{bmatrix} \begin{bmatrix} x_1 \\ x_2 \end{bmatrix} + \begin{bmatrix} w_1 \\ w_2 \end{bmatrix} \tag{3.1}$$

where y_i is the received symbol for receive antenna #i, x_j the transmitted symbol for transmit antenna #j, w_i the noise for receive antenna #i, h_{ij} the CFR from transmit antenna #j to receive antenna #i. Here, x_j corresponds to the output constellation symbol of a BICM block.

The first channel estimation step is to estimate the CFRs at the scattered pilot positions. A basic technique is the Least Square (LS) estimation, which does not exploit the correlation of the channel across frequency and time [95]. The next step is channel interpolation. In order to reduce the complexity, channel interpolation is performed with a cascade of two 1-dimentional operations. First operation is a linear time interpolation to obtain the CFRs at scattered pilot bearing carriers. Linear interpolation is a common option for time interpolation since it only requires two points to be known. The second is frequency interpolation. Here, two common interpolations are investigated for the frequency interpolation. One option is linear interpolation which is the computationally least expensive but provides poor interpolation in cases where the data to be interpolated is non-linear. The second option is Discrete Fourier Transform (DFT) interpolation [96], [97]. The frequency interpolation is applied to fulfill the CFRs for all data carriers in a single OFDM symbol.

Considering the interpolation operations mentioned above and the characteristics of both MIMO pilot encoding algorithms, the equivalent values of D_X and D_Y after channel interpolation are summarized in Table 3.1. The channel estimation with each pilot encoding algorithm is explained as follows.

A. Walsh-Hadamard Decoding

The resulting CFRs obtained by LS estimation are the sum or the difference of the two subsets, because the phase inversion is applied in WH encoding scheme. k_{sum}, the set of carrier indexes on which normal scattered pilots are transmitted from antenna #2 in Figure 3.1 (left, bottom), is defined as $k_{sum} = 2 \times N \times D_X$. where N is a non-negative

integer (N=1, 2, …). The sum of the two CFRs is estimated from the scattered pilots on the carrier number k_{sum} of the OFDM symbol number l_{sum} as:

$$\tilde{h}_{\text{sum1}}[l_{\text{sum}}, k_{\text{sum}}] = \frac{y_1[l_{\text{sum}}, k_{\text{sum}}]}{x_1[l_{\text{sum}}, k_{\text{sum}}]} = h_{\text{sum1}}[l_{\text{sum}}, k_{\text{sum}}] + \frac{w_1[l_{\text{sum}}, k_{\text{sum}}]}{x_1[l_{\text{sum}}, k_{\text{sum}}]} \quad (3.2)$$

$$\tilde{h}_{\text{sum2}}[l_{\text{sum}}, k_{\text{sum}}] = \frac{y_2[l_{\text{sum}}, k_{\text{sum}}]}{x_1[l_{\text{sum}}, k_{\text{sum}}]} = h_{\text{sum2}}[l_{\text{sum}}, k_{\text{sum}}] + \frac{w_2[l_{\text{sum}}, k_{\text{sum}}]}{x_1[l_{\text{sum}}, k_{\text{sum}}]} \quad (3.3)$$

where x_1=x_2, $h_{\text{sum1}} = h_{11} + h_{12}$, $h_{\text{sum2}} = h_{21} + h_{22}$ [81]. l_{sum} is the OFDM symbol number which satisfies k_{sum} mod $(D_X \times D_Y) = D_X \times (l_{\text{sum}} \text{ mod } D_Y)$. $\tilde{h}_{\text{sum1}}$ and $\tilde{h}_{\text{sum2}}$ are obtained for the scattered pilot cell as the LS estimations of h_{sum1} and h_{sum2}, respectively. On the other hand, the difference between the two channel responses is estimated from the scattered pilots on the carrier number $k_{\text{dif}} = (2 \times N - 1) \times D_X$ of the OFDM symbol number l_{dif} as:

$$\tilde{h}_{\text{dif1}}[l_{\text{dif}}, k_{\text{dif}}] = \frac{y_1[l_{\text{dif}}, k_{\text{dif}}]}{x_1[l_{\text{dif}}, k_{\text{dif}}]} = h_{\text{dif1}}[l_{\text{dif}}, k_{\text{dif}}] + \frac{w_1[l_{\text{dif}}, k_{\text{dif}}]}{x_1[l_{\text{dif}}, k_{\text{dif}}]} \quad (3.4)$$

$$\tilde{h}_{\text{dif2}}[l_{\text{dif}}, k_{\text{dif}}] = \frac{y_2[l_{\text{dif}}, k_{\text{dif}}]}{x_1[l_{\text{dif}}, k_{\text{dif}}]} = h_{\text{dif2}}[l_{\text{dif}}, k_{\text{dif}}] + \frac{w_2[l_{\text{dif}}, k_{\text{dif}}]}{x_1[l_{\text{dif}}, k_{\text{dif}}]} \quad (3.5)$$

where x_1=x_2, $h_{\text{dif1}} = h_{11} - h_{12}$, $h_{\text{dif2}} = h_{21} - h_{22}$. l_{dif} is the OFDM symbol number which satisfies k_{dif} mod $(D_X \times D_Y) = D_X \times (l_{\text{dif}} \text{ mod } D_Y)$. $\tilde{h}_{\text{dif1}}$ and $\tilde{h}_{\text{dif2}}$ are obtained for the scattered pilot cell as the LS estimations of h_{dif1} and h_{dif2}, respectively. In order to obtain the estimates of the sum and difference of the CFR on all cells, time interpolation is performed first on every pilot bearing carrier. Next, frequency interpolation is performed separately on each subset, i.e., sum and difference estimates. After the 2-dimentional interpolation, the sum and difference estimates $\hat{h}_{\text{sum1}}$, $\hat{h}_{\text{sum2}}$, $\hat{h}_{\text{dif1}}$ and $\hat{h}_{\text{dif2}}$ are obtained for each cell, and the estimated CFR matrix, i.e., $\hat{h}_{11}$, $\hat{h}_{12}$, $\hat{h}_{21}$ and $\hat{h}_{22}$, can be obtained for each cell as below.

$$\begin{bmatrix} \hat{h}_{11} & \hat{h}_{12} \\ \hat{h}_{21} & \hat{h}_{22} \end{bmatrix} = \frac{1}{2} \begin{bmatrix} \hat{h}_{\text{sum1}} + \hat{h}_{\text{dif1}} & \hat{h}_{\text{sum1}} - \hat{h}_{\text{dif1}} \\ \hat{h}_{\text{sum2}} + \hat{h}_{\text{dif2}} & \hat{h}_{\text{sum2}} - \hat{h}_{\text{dif2}} \end{bmatrix} \quad (3.6)$$

Consequently, the Nyquist limit of the channel estimation in frequency falls to half compared to the uncoded scattered pilot in SISO as shown in Table 3.1.

B. Null Pilot Decoding

The CFRs from transmit antenna #1 to receive antenna #1 and #2 (h_{11} and h_{21}) are estimated on the 3 dB boosted scattered pilots transmitted by antenna #1 as:

$$\tilde{h}_{11}[l_1, k_1] = \frac{y_1[l_1, k_1]}{x_1[l_1, k_1]} = h_{11}[l_1, k_1] + \frac{w_1[l_1, k_1]}{x_1[l_1, k_1]} \tag{3.7}$$

$$\tilde{h}_{21}[l_1, k_1] = \frac{y_2[l_1, k_1]}{x_1[l_1, k_1]} = h_{21}[l_1, k_1] + \frac{w_2[l_1, k_1]}{x_1[l_1, k_1]} \tag{3.8}$$

where $[l_1, k_1]$ indicates the location of the scattered pilots colored in red in Figure 3.1 (right, top). $\tilde{h}_{11}$and $\tilde{h}_{21}$ are obtained for the 3 dB boosted scattered pilot cell as the LS estimations of h_{11} and h_{21}, respectively. The CFRs from transmit antenna #2 (h_{12} and h_{22}) are estimated in the same manner on the 3 dB boosted scattered pilots transmitted by antenna #2 as:

$$\tilde{h}_{12}[l_2, k_2] = \frac{y_1[l_2, k_2]}{x_2[l_2, k_2]} = h_{12}[l_2, k_2] + \frac{w_1[l_2, k_2]}{x_2[l_2, k_2]} \tag{3.9}$$

$$\tilde{h}_{22}[l_2, k_2] = \frac{y_2[l_2, k_2]}{x_2[l_2, k_2]} = h_{22}[l_2, k_2] + \frac{w_2[l_2, k_2]}{x_2[l_2, k_2]} \tag{3.10}$$

where, $[l_2, k_2]$ indicates the location of the scattered pilots colored in red in Figure 3.1 (right, bottom). $\tilde{h}_{12}$ and $\tilde{h}_{22}$ are obtained for the 3 dB boosted scattered pilot cell as the LS estimations of h_{12} and h_{22}, respectively. Note that the locations of the CFRs estimated for transmit antenna #1 in (3.7), (3.8) are different from that for transmit antenna #2 in (3.9), (3.10).

In order to obtain the estimated CFR matrix, i.e., $\hat{h}_{11}$, $\hat{h}_{12}$, $\hat{h}_{21}$ and $\hat{h}_{22}$, time and frequency interpolation are performed separately on the values of (3.7), (3.8), (3.9) and (3.10). As the result of the nulling for the scattered pilot, the Doppler limit of channel estimation in time equivalently falls to half compared to SISO as shown in Table 3.1. On the other hand, 3 dB higher SNR is obtained in the channel estimation results compared to SISO as the result of the 3 dB boosting.

3.1.3. Pilot Boosting

The pilot boosting defines the boosted power level of the scattered pilot compared with the data carriers. The pilot boosting affects the performance because higher pilot boosting improves channel estimation accuracy. Meanwhile the higher pilot boosting also

Table 3.2 ATSC 3.0 MIMO Scattered Pilot Boosting Power

SP Pattern	Boosting Power *b* [dB]				
	0	**1**	**2**	**3**	**4**
MP3_2	0	0	1.40	2.20	2.90
MP3_4	0	1.40	2.90	3.80	4.40
MP4_2	0	0.60	2.10	3.00	3.60
MP4_4	0	2.10	3.60	4.40	5.10
MP6_2	0	1.60	3.10	4.00	4.60
MP6_4	0	3.00	4.50	5.40	6.00
MP8_2	0	2.20	3.80	4.60	5.30
MP8_4	0	3.60	5.10	6.00	6.60
MP12_2	0	3.20	4.70	5.60	6.20
MP12_4	0	4.50	6.00	6.90	7.50
MP16_2	0	3.80	5.30	6.20	6.80
MP16_4	0	5.20	6.70	7.60	8.20
MP24_2	0	4.70	6.20	7.10	7.70
MP24_4	0	6.10	7.60	8.50	9.10
MP32_2	0	5.40	6.90	7.70	8.40
MP32_4	0	6.70	8.20	9.10	9.70

Table 3.3 ATSC 3.0 Data Carrier Power Reduction

SP Pattern	Power Reduction [dB]				
	0	**1**	**2**	**3**	**4**
MP3_2	0	0	0.27	0.45	0.64
MP3_4	0	0.14	0.33	0.48	0.59
MP4_2	0	0.08	0.33	0.51	0.65
MP4_4	0	0.17	0.34	0.45	0.57
MP6_2	0	0.16	0.36	0.52	0.63
MP6_4	0	0.18	0.32	0.42	0.51
MP8_2	0	0.18	0.36	0.48	0.60
MP8_4	0	0.17	0.29	0.39	0.46
MP12_2	0	0.19	0.34	0.45	0.54
MP12_4	0	0.16	0.26	0.34	0.40
MP16_2	0	0.19	0.31	0.41	0.49
MP16_4	0	0.15	0.24	0.31	0.36
MP24_2	0	0.17	0.28	0.36	0.42
MP24_4	0	0.14	0.21	0.27	0.31
MP32_2	0	0.16	0.26	0.32	0.38
MP32_4	0	0.12	0.19	0.24	0.27

decreases the power of the data carriers, thus the choice of the pilot boosting is not straightforward. The pilot boosting values for each MIMO SP pattern in ATSC 3.0, which is completely the same as SISO, are listed in Table 3.2. The corresponding power reduction of the data carriers for each SP pattern and pilot boosting is listed in Table 3.3. The continual and edge pilots are considered to be data carriers to calculate the power reduction values in Table 3.3.

3.2. MIMO Pilot Boosting Analysis

In the ATSC 3.0 standardization process, the equalized data signal-to-noise ratio (SNR_{EQ}) was the metric used for obtaining the best overall performance taking into account the pilot boosting value and the channel interpolation method for SISO [55]. SNR_{EQ} was used to design the pilot boosting values for SISO in the standardization process. SNR_{EQ} is estimated as:

$$SNR_{EQ} = \frac{\sigma_S^2 \times a}{\sigma_N^2 + \sigma_N^2 \times f_{\text{int}}/b} = SNR \times \frac{a}{1 + f_{\text{int}}/b} \tag{3.11}$$

where σ_S^2 is the data signal power, σ_N^2 the noise power, b the scattered pilot boosting power compared with the data signal power in linear unit, a the power normalization $a = (D_X \times D_Y)/(D_X \times D_Y - 1 + b)$, and $f_{\text{int}} = f_{\text{int,time}} \times f_{\text{int,freq}}$ is the noise reduction factor by time and frequency interpolation. The value of $f_{\text{int,time}}$ was set to {0.750, 0.688} for SISO with D_Y = {2, 4}, which can be calculated from the distance between the two symbols to be linear interpolated [81]. The values of $f_{\text{int,freq}}$ varies depending on the receiver design, and the five different boosting values of ATSC 3.0 are standardized so that the boosting values are optimum for $f_{\text{int,freq}}$ = {0, 0.25, 0.5, 0.75, 1}. It should be noted that the pilot boosting value for MIMO is directly adopted as the same value for SISO.

The equalized data signal-to-noise ratio for 2×2 MIMO (SNR_{EQ_MIMO}) is considered as:

$$SNR_{EQ\_MIMO} = \frac{\sigma_S^2 \times a}{\sigma_N^2 + 2 \times \sigma_N^2 \times e \times f_{\text{int}}/b} = SNR \times \frac{a}{1 + 2 \times e \times f_{\text{int}}/b} \tag{3.12}$$

where e is the noise reduction factor of pilot encoding/decoding process. Note that the noise power caused by the channel estimation error is doubled compared with SISO in (3.11) because the result of MIMO detection is affected by the channel estimation errors from transmit antenna #1 and #2, hence the factor 2 is introduced. With WH encoding the value of e is set to 0.5, because the channel estimation error is reduced to half by the averaging process following the adding/subtracting the sum and difference of the CFR in (3.6). With NP encoding, although the value of e is 1, the scattered pilot power b is doubled compared with SISO because of 3 dB boosting. Consequently, SNR_{EQ_MIMO} is equivalent to SNR_{EQ} with both pilot encoding algorithms in ATSC 3.0.

The value of f_{int} for MIMO pilot can be different from SISO. The value of $f_{\text{int,time}}$ remains to {0.750, 0.688} for D_Y = {2, 4} with WH encoding, but {0.688, 0.672} for D_Y

Table 3.4 Noise Reduction Factor with $f_{int,time}$ = {0.750, 0.688} for D_Y= {2, 4}

MIMO Pilot Pattern	Walsh-Hadamard				Null Pilot			
	$f_{int,freq}$		f_{int}		$f_{int,freq}$		f_{int}	
	linear	DFT	linear	DFT	linear	DFT	linear	DFT
MP3_2	0.676	1	0.507	0.750	0.704	1	0.484	0.688
MP3_4	0.676	1	0.465	0.688	0.704	1	0.473	0.672
MP4_2	0.672	1	0.504	0.750	0.688	1	0.473	0.688
MP4_4	0.672	1	0.462	0.688	0.688	1	0.462	0.672
MP6_2	0.669	1	0.502	0.750	0.676	1	0.465	0.688
MP6_4	0.669	1	0.460	0.688	0.676	1	0.454	0.672
MP8_2	0.668	1	0.501	0.750	0.672	1	0.462	0.688
MP8_4	0.668	1	0.459	0.688	0.672	1	0.451	0.672
MP12_2	0.667	1	0.500	0.750	0.669	1	0.460	0.688
MP12_4	0.667	1	0.459	0.688	0.669	1	0.449	0.672
MP16_2	0.667	1	0.500	0.750	0.668	1	0.459	0.688
MP16_4	0.667	1	0.459	0.688	0.668	1	0.449	0.672
MP24_2	0.667	1	0.500	0.750	0.667	1	0.459	0.688
MP24_4	0.667	1	0.458	0.688	0.667	1	0.448	0.672
MP32_2	0.667	1	0.500	0.750	0.667	1	0.459	0.688
MP32_4	0.667	1	0.458	0.688	0.667	1	0.448	0.672

= {2, 4} with NP encoding because the equivalent D_Y is doubled. The values of $f_{int,freq}$ and the consequent f_{int} for WH and NP encodings are numerically calculated and summarized in Table 3.4. Whereas the larger D_X offers the smaller $f_{int,freq}$ with linear interpolation, it remains constant with DFT interpolation when it takes into account the Nyquist bandwidth in the interpolation process.

Figure 3.2 presents the SNR_{EQ} divided by SNR for D_Y=2 with WH encoding and DFT interpolation (top), and linear interpolation (bottom) under the noise reduction factors in Table 3.4. The higher SNR_{EQ}/SNR corresponds to the lower degradation due to the channel estimation. As to the selectable five different boosting in Figure 3.2 (top), boost4 corresponds exactly to the optimum boosting, because the boosting value of boost4 is designed to be optimum for the receiver with $f_{int,freq}$ = 1 and the value of $f_{int,freq}$ corresponds to 1 for DFT interpolation. With the higher D_X, the higher optimum amplitude is obtained. Note that the gain in SNR_{EQ}/SNR obtained by the optimum pilot boosting from boost0 is at most 0.4 dB in MP3_2, and over 1.5 dB with MP32_2 in Figure 3.2 (top).

Figure 3.2 (bottom) presents SNR_{EQ}/SNR with frequency linear interpolation. The optimum boosting becomes smaller than that of DFT interpolation depicted in Figure 3.2 (top), because $f_{int,freq}$ of linear interpolation is smaller than DFT interpolation. Figure 3.2 (bottom) indicates that boost2 or boost3 are optimum in this configuration and that the optimization on SP boosting power yields less gain compared with DFT interpolation. It is considered that the smaller $f_{int,freq}$ reduces the noise power in the channel estimation result, hence the smaller boosting is enough to obtain the best performance. SNR_{EQ}/SNR

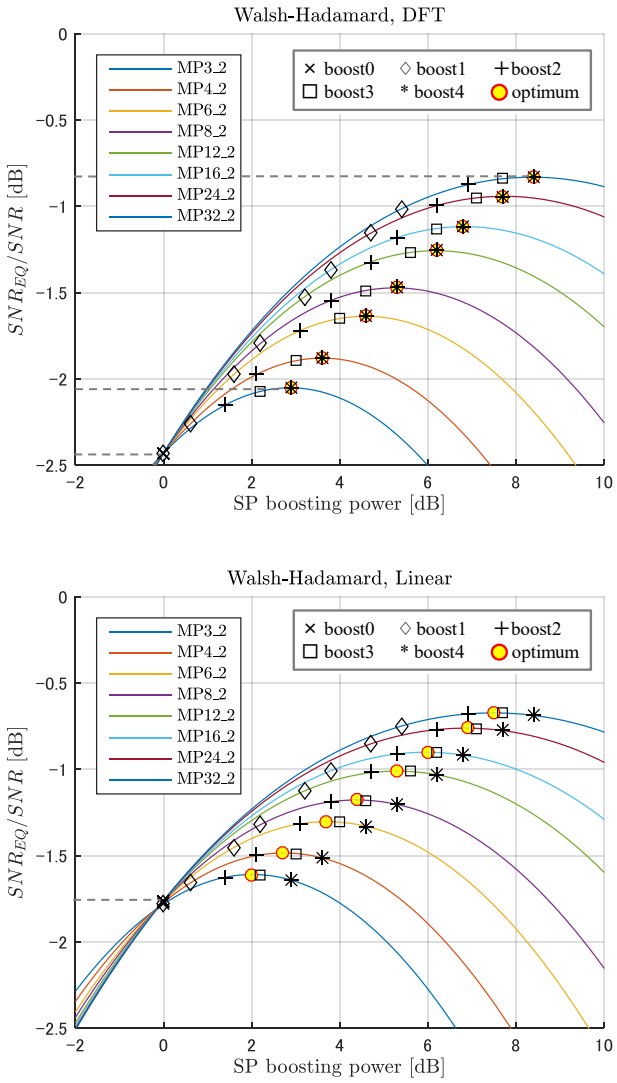

Figure 3.2 Equalized SNR performance for D_Y=2 with WH encoding and DFT interpolation (top). With WH encoding and linear interpolation (bottom).

for boost0 with linear interpolation is better by 0.7 dB than that with DFT interpolation, i.e., SNR_{EQ}/SNR = -2.45 dB for DFT interpolation and -1.75 dB for linear interpolation in Figure 3.2 (top) and Figure 3.2 (bottom) all SP patterns, respectively.

Figure 3.3 (top) shows SNR_{EQ}/SNR for D_Y=2 with NP encoding and DFT interpolation. The optimum boosting for NP becomes slightly smaller than that of WH encoding in Figure 3.2 (top), because the noise reduction factor $f_{\text{int,time}}$ is smaller than WH encoding. The value of boost4 was standardized to be optimum for SISO only with $f_{\text{int,time}}$ = {0.750, 0.668} for D_Y = {2, 4}. Hence for NP encoding boost4 does not correspond perfectly to the optimum boosting value. Figure 3.3 (top) shows that boost3 or boost4 are optimum in

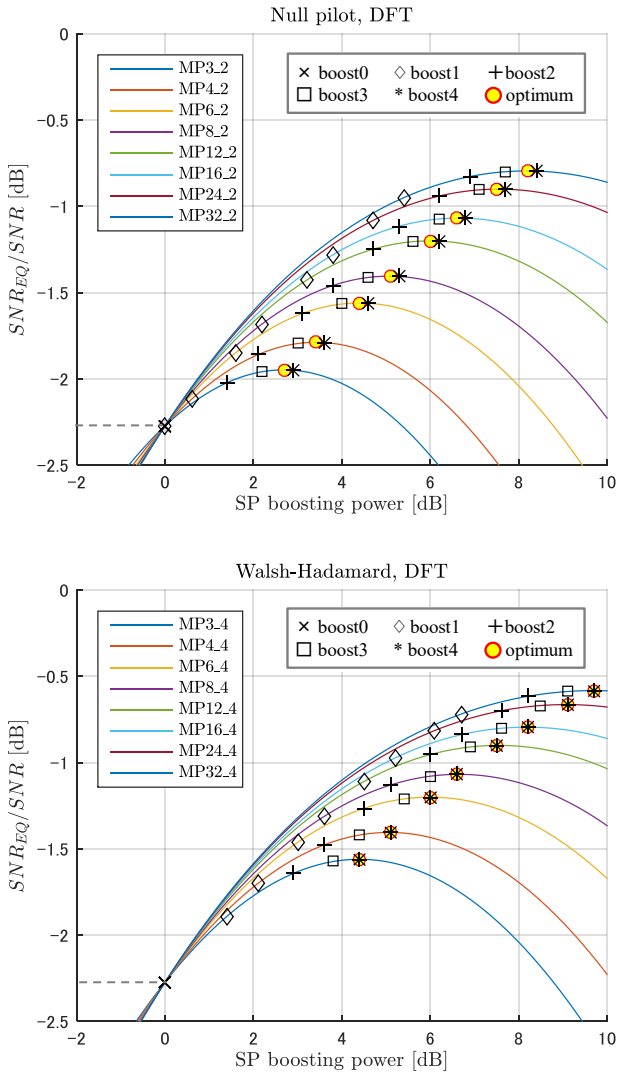

Figure 3.3 Equalized SNR performance for D_Y=2 with NP encoding and DFT interpolation (top). D_Y=4 with WH encoding and DFT interpolation (bottom).

this configuration. Note that SNR_{EQ}/SNR for boost0 is better by 0.2 dB with NP encoding than WH encoding, i.e. SNR_{EQ}/SNR = -2.45 dB for WH and -2.25 dB for NP. This gain is considered to be introduced by the 3 dB boosting in SP power.

Figure 3.3 (bottom) presents SNR_{EQ}/SNR for D_Y =4 with WH encoding and DFT interpolation. Boost4 corresponds to the optimum boosting. The gain obtained by the optimization on pilot boosting power with D_Y = 4 becomes greater than D_Y = 2. SNR_{EQ}/SNR for boost0 is better by 0.2 dB with D_Y = 4 than D_Y = 2, i.e. SNR_{EQ}/SNR = -2.25 dB for D_Y = 4 and -2.45 dB for D_Y = 2 in Figure 3.3 (bottom) and Figure 3.2 (top), respectively. This gain is introduced by the noise reduction factor $f_{\text{int,time}}$.

3.3. Channel Estimation Evaluation

3.3.1. Pilot Boosting

We evaluated the optimum pilot boosting with the densest pilot pattern MP3_2 as an example with the parameters in Table 2.10. The BER performance comparison for SP boosting with WH encoding and DFT interpolation is shown in Figure 3.4. Here, XPD parameter x is set to be infinite and AWGN channel is used to evaluate the ideal condition. The result showed that the best performance is achieved with pilot boost4 or boost3, and the gain compared to boost1 is 0.3 dB at BER $=1\times10^{-4}$. It is assumed that the gain can be larger for a stricter BER criterion. Therefore, the analysis of the equalized SNR (Figure 3.2, top) has a consistency with the BER evaluation results.

Figure 3.5 shows the required SNR for several SP patterns with WH encoding and DFT interpolation. The transmission parameters in Table 2.10 are used. The result showed that the best performance is achieved with boost4 or boost3 for all SP patterns. The gain of MP3_4 from MP3_2 with boost0 is 0.2 dB and the gain becomes the same value theoretically calculated from Figure 3.2 (top) and Figure 3.3 (bottom). The gain of boost4 from boost0 becomes over 1 dB with MP16_2 and MP16_4. These results conclude that the boosting value should be selected carefully with higher D_X and D_Y, but the best boosting is boost4 or boost3 regardless of pilot pattern.

Figure 3.6 shows the required SNR comparison for several SP configurations with MP3_2. The transmission parameters in Table 2.10 are used. Compared with DFT interpolation, linear interpolation shows better performance by about 0.7 dB for WH encoding with boost0 as described in Figure 3.2 (top) and (bottom). It can be also observed that NP-DFT shows 0.2 dB better result than WH-DFT with boost0 as mentioned in Figure 3.2 (top) and Figure 3.3 (top), because of the smaller $f_{\mathrm{int,freq}}$. We confirmed that the best boosting value varies depending on the configuration, e.g. the best boosting is boost4 or boost3 for DFT interpolation but boost3 or boost2 for linear interpolation.

Figure 3.7 shows the required SNR comparison for AWGN, SFN, Rice (K factor = 10) and NGH outdoor (maximum Doppler frequency: F_d =33.3 Hz) with MP3_2 and WH-DFT. The transmission parameters in Table 2.10 are used with QPSK 5/15. This result indicates that the best boosting value is boost4 for all channels, which keeps a consistency with the equalized SNR analysis shown in Figure 3.2 (top). Additionally, the gain

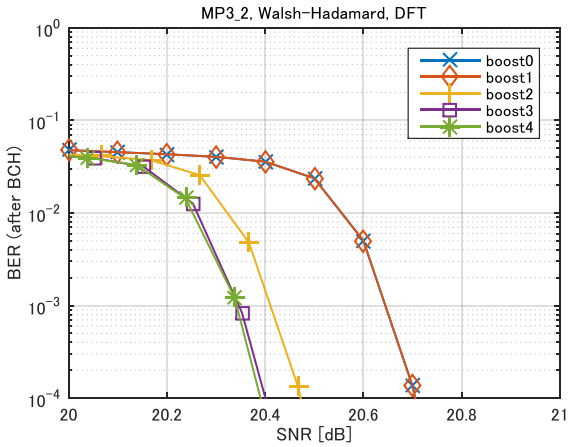

Figure 3.4 BER comparison for pilot boosting with MP3_2, Walsh-Hadamard encoding and DFT interpolation in AWGN channel.

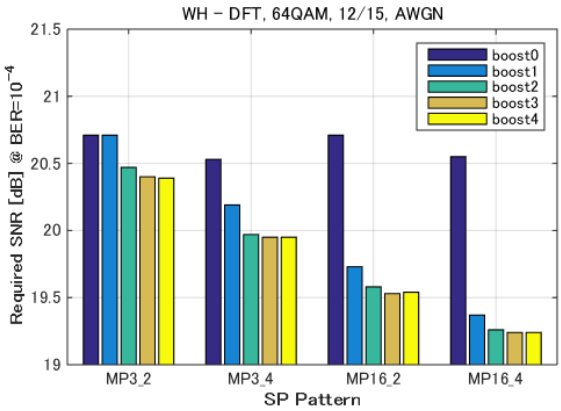

Figure 3.5 Required SNR comparison for MIMO pilot pattern with Walsh-Hadamard encoding and DFT interpolation in AWGN channel.

introduced by the pilot boosting is constant regardless of the channel. It is confirmed that the gain obtained by the pilot boosting optimization with QPSK 5/15 in AWGN is almost the same as 64NUC 12/15 (WH-DFT in Figure 3.6). From these results, the optimum boosting value is considered as an independent parameter from the modulation and code rate.

The simulation results concluded that boost3 is practically the best pilot boosting for all configurations evaluated in this subsection. In the following subsections, we conducted the performance evaluation with boost3.

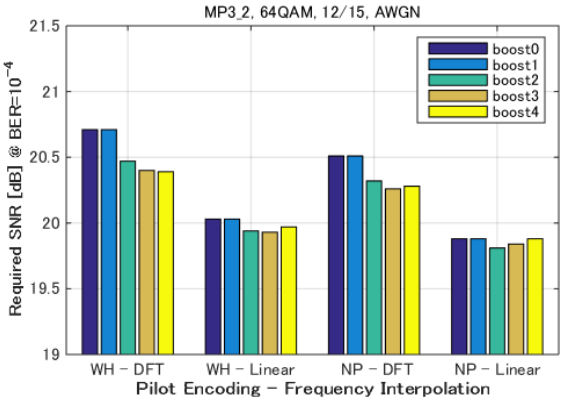

Figure 3.6 Required SNR comparison for MIMO pilot encoding and frequency interpolation with MP3_2 in AWGN channel.

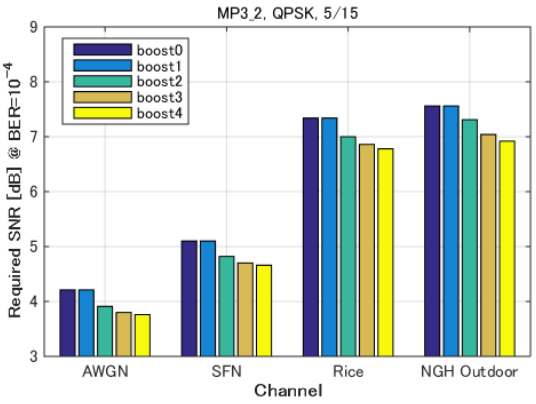

Figure 3.7 Required SNR comparison for different channel models with MP3_2, Walsh-Hadamard and DFT interpolation.

3.3.2. Frequency Interpolation

We compared two common interpolation algorithms, i.e. DFT and linear interpolation, for the frequency interpolation with both MIMO pilot encoding schemes. Figure 3.8 shows MSE comparison with both MIMO pilot encoding schemes in the SFN channel. The other parameters are the same described in Table 2.10. This result showed that MSE of linear interpolation converges on a value even with a high SNR, and the estimation error is caused by the frequency interpolation.

Figure 3.9 shows MSE comparison in the SFN channel with SNR = 20 dB and different delays. This result showed that the error increases gradually as the delay time increases. In this result, linear interpolation achieved slightly lower MSE than DFT interpolation because of the smaller $f_{\text{int,freq}}$ with short delay echoes. However, linear interpolation is

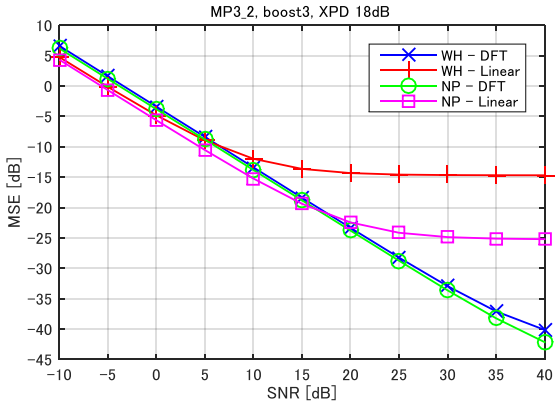

Figure 3.8 MSE comparison with MP3_2 in SFN channel (*d* = 3dB, τ =0.5 GI).

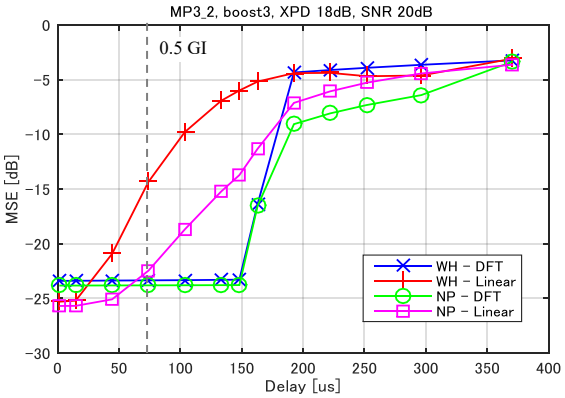

Figure 3.9 MSE comparison with MP3_2 in SFN channel (*d* = 3dB, SNR = 20 dB).

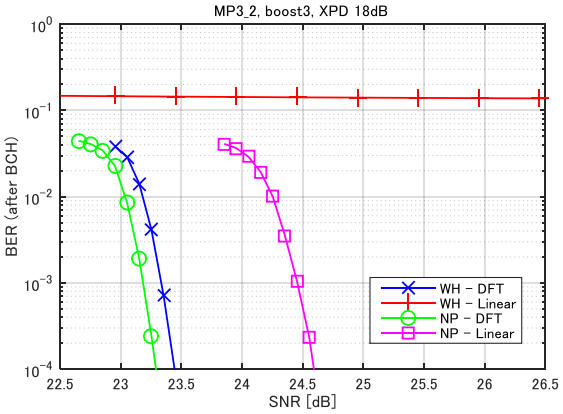

Figure 3.10 BER comparison with MP3_2 in SFN channel (*d* = 3dB, τ =0.5 GI) with 64NUC 12/15.

gradually degraded as the delay time increases because of the frequency interpolation error. It is confirmed that MSE of WH-Linear is rapidly increased with long echoes due to the virtually double D_X. DFT interpolation showed lower MSE than linear interpolation with long delay echoes up to GI (148 μs) regardless of the MIMO pilot encoding.

Comparing WH and NP, NP showed slightly better MSE because of the 3dB pilot boosting and the smaller $f_{\text{int,time}}$.

The BER performance in the SFN channel is shown in Figure 3.10. This result shows a consistency with MSE evaluation in Figure 3.8, i.e. NP-DFT shows the best performance in BER and also the lowest MSE at around SNR = 23 dB. In addition, it is confirmed that QEF is not achieved with WH-Linear configuration in the SFN channel, because the MSE is higher than the required SNR.

Figure 3.11 shows MSE comparison for different MIMO pilot encoding with MP3_2 in NGH outdoor channel (F_d = 33.3 Hz). This result shows that MSE of all configurations converges on a value around -25 dB that is the tracking error for the time varying channel. Note that the MSEs in Figure 3.11 become straight lines in the low SNR region (below 10 dB), because the SNR is dominant compared with the tracking error.

Figure 3.12 shows MSE comparison in the NGH outdoor channel with SNR = 5 dB for different maximum Doppler frequency. This result shows that the error increases gradually as the maximum Doppler frequency increases. In low F_d region, NP showed slightly better MSE than WP because of the 3dB pilot boosting and the smaller $f_{\text{int,time}}$. However, MSE of NP is rapidly increased in high Doppler frequency channel because the tracking error is increased due to the virtually doubled D_{Y}. In this result, linear interpolation showed better performance than DFT interpolation for all F_d spans with both MIMO pilot encoding schemes. It is considered that the noise reduction factor for the channel estimation is dominant in such a low SNR region.

The BER performance with QPSK 5/15 in NGH outdoor channel is shown in Figure 3.13. It is confirmed that NP-Linear is the best performance in BER. This result shows a consistency with MSE evaluation, i.e. the lowest MSE is obtained with NP-Linear at around SNR = 6 dB in Figure 3.11. It is considered that the channel is composed of some short echoes (up to 8.1 μs delay in time), thus linear frequency interpolation works well.

The simulation results concluded that DFT interpolation is better for the SFN channel to cope with long echoes. On the other hand, linear interpolation works well in a mobile channel in which only short delay echoes exist. Especially, since the tracking error is much smaller than the SNR, linear interpolation is better than DFT because of the smaller noise reduction factor. It should be noted that the DFT interpolator is defined as

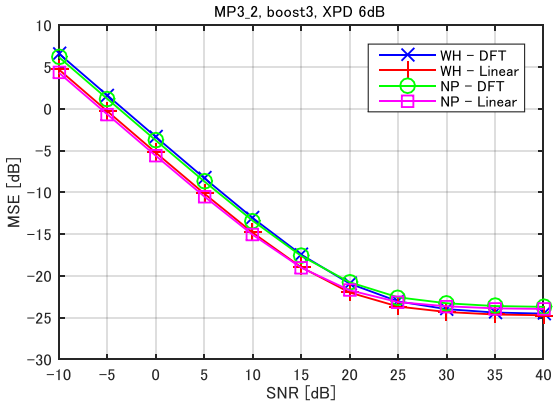

Figure 3.11 MSE comparison with MP3_2 in NGH Outdoor channel (F_d = 33.3Hz).

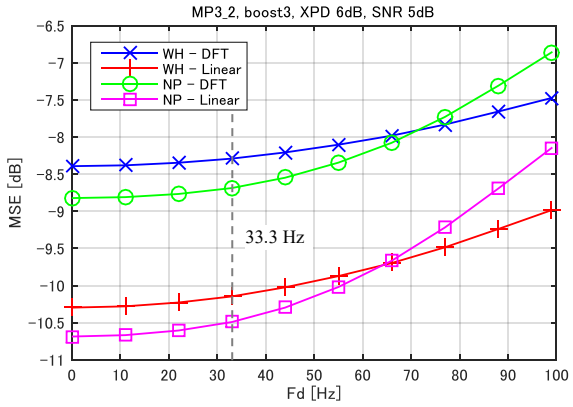

Figure 3.12 MSE comparison with MP3_2 in NGH Outdoor channel (SNR = 5 dB).

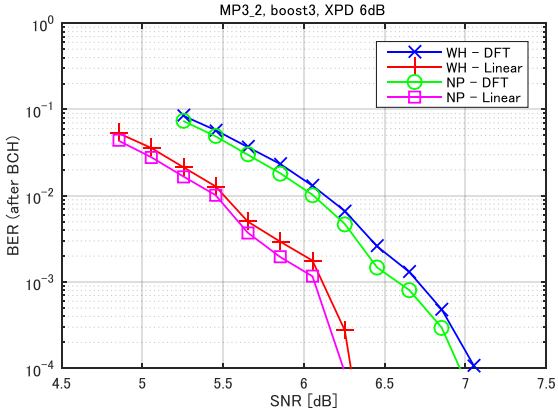

Figure 3.13 BER comparison with MP3_2 in NGH Outdoor channel (F_d = 33.3Hz) with QPSK 5/15.

$f_{\text{int,freq}}$ = 1 in this thesis. The conclusion that linear interpolation is better in a mobile channel can vary if the DFT interpolator is implemented with the smaller $f_{\text{int,freq}}$.

Table 3.5 Transmission parameters for MIMO pilot recommendation

FFT size	8k	16k	32k
Number of carriers	6913	13285	27649
Signal bandwidth	5.83 MHz		
Modulation and code rate	64 NUC 12/15 for SFN channel QPSK 5/15 for NGH Outdoor		
MIMO scattered pilot encoding	Null Pilot Walsh-Hadamard		
Frequency Interpolation	DFT for SFN channel Linear for NGH Outdoor		
Pilot boosting	boost3		

3.3.3. MIMO Scattered Pilot Recommendation

We evaluated the optimum MIMO scattered pilot configuration for fixed/mobile reception scenario with several GI/FFT combinations. The GI length is a parameter selected by broadcasters depending on the required coverage, i.e. network configuration, geographical condition and the required distance between the SFN transmitters. First, we evaluated the required SNR in three SFN scenarios, i.e. with short GI (GI1_192: 28 μs), middle GI (GI5_1024: 148 μs) and long GI (GI7_2048: 296 μs) for all the FFT size. The simulation parameters are summarized in Table 3.5.

Figure 3.14 shows the required SNR for GI5_1024 with all the allowed SP configurations for each FFT size. The results of WH and NP encoding are shown in solid and dashed line, respectively. The results are grouped according to D_X, e.g. 8k-D$_X$3-WH presents the results for MP3_2 and MP3_4 with 8k FFT and WH encoding. The values of SP overhead, 16.7 % and 8.3 %, correspond to MP3_2 and MP3_4 in 8k-D$_X$3-WH. The result shows that NP encoding provides slightly better performance than WH with the same SP overhead. It is considered that 3 dB pilot boosting and the smaller $f_{\text{int,time}}$ introduces this gain. From the point of FFT size, larger FFT achieves the same Nyquist limit with the sparser SP patterns and better performance with the smaller $f_{\text{int,freq}}$.

Figure 3.15 and Figure 3.16 describe the results with GI1_192 and GI7_2048. Note that the allowed SP patterns are different for each GI length as shown in Table 2.2 and Table 2.3. NP encoding showed better performance than WH regardless of GI duration. With short GI case, the required SNR becomes the lowest with the sparsest SP because of the smallest $f_{\text{int,freq}}$. We conclude that NP encoding with larger FFT size and larger D_X SP pattern is the best configuration for fixed reception scenario, such as the time invariant SFN channel.

Next, we evaluated the required SNR in two NGH outdoor scenarios with a middle speed and a high-speed reception. GI5_1024 and the parameters in Table 3.5 are used.

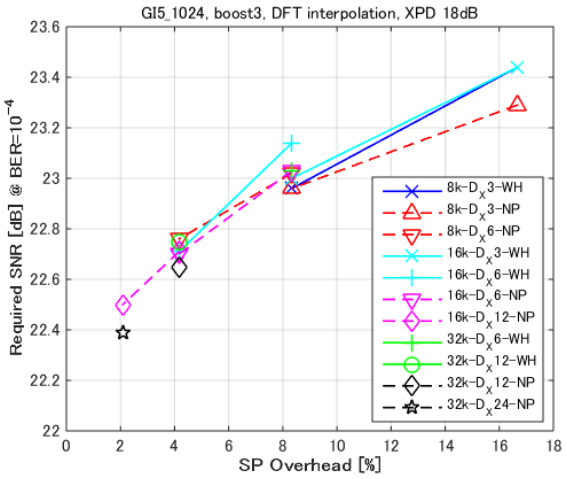

Figure 3.14 Required SNR comparison in SFN channel (d = 3dB, τ =0.5 GI) with GI5_1024 and 64NUC 12/15.

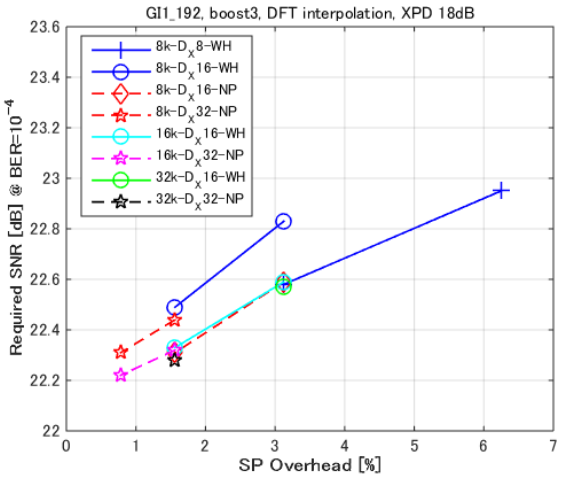

Figure 3.15 Required SNR comparison in SFN channel (d = 3dB, τ =0.5 GI) with GI1_192 and 64NUC 12/15.

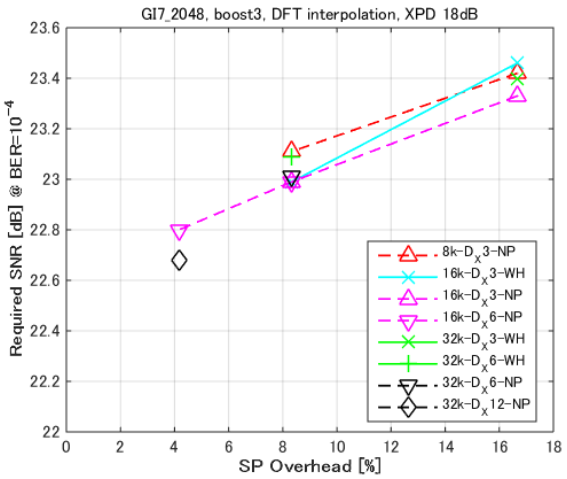

Figure 3.16 Required SNR comparison in SFN channel (d = 3dB, τ =0.5GI) with GI7_2048 and 64NUC 12/15.

Figure 3.17 shows the result in a middle speed reception (F_d = 33.3 Hz, 60 km/h@600

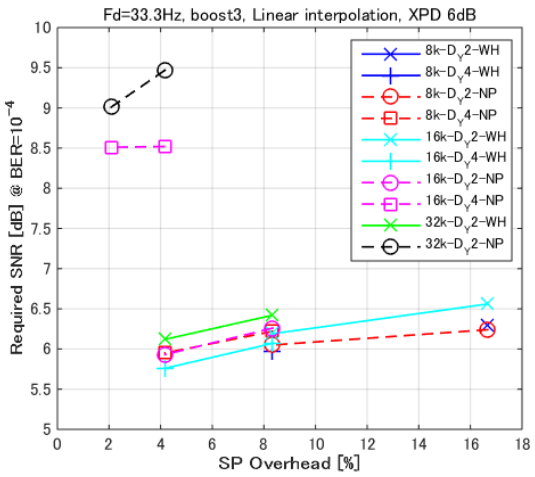

Figure 3.17 Required CNR comparison in NGH Outdoor channel (F_d = 33.3 Hz) with GI5_1024 and QPSK 5/15.

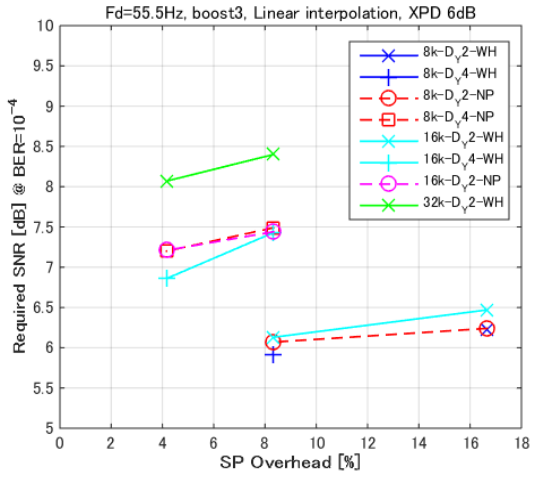

Figure 3.18 Required SNR comparison in NGH Outdoor channel (F_d = 55.5 Hz) with GI5_1024 and QPSK 5/15.

MHz) with all the allowed SP configurations for GI5_1024. The results are grouped according to D_Y. The result showed that the performance of NP encoding with 16k-D$_Y$4 and 32k-D$_Y$2 are degraded to a large extent compared with the other configurations. It is considered that the equivalent D_Y is doubled in NP encoding scheme, thus the performance in the time varying channel is severely degraded especially with larger FFT and larger D_Y.

Figure 3.18 shows the result in a high-speed reception (F_d = 55.5 Hz, 100 km/h@600 MHz) with GI5_1024. The worst configurations, 16k-D$_Y$4-NP and 32k-D$_Y$2-NP are excluded here. The simulation indicated that WH shows slightly better performance than NP with the same SP overhead. Comparing 16k-D$_Y$4-WH and 32k-D$_Y$2-WH, it is confirmed that the performance with 32k FFT is degraded in such a high-speed time

varying channel even with $D_Y = 2$. We conclude that WH encoding with smaller FFT size and smaller D_Y is the best configuration for mobile reception scenario.

3.4. Conclusions

This chapter evaluates the two MIMO pilot encoding algorithms adopted in ATSC 3.0, known as Walsh-Hadamard and Null Pilot encoding. Regarding the pilot boosting evaluation, a theoretical analysis and a physical layer simulation considering two channel interpolation algorithms, namely DFT interpolation and linear interpolation for frequency interpolation, conclude that boost3 is a practical option as the optimum pilot boosting for both pilot encoding algorithms. The pilot boosting values were standardized for SISO, but the five different boosting values cover the optimum boosting values for MIMO. It is confirmed that the optimum pilot boosting greatly improves the performance especially with higher D_X and D_Y and that the maximum gain in required SNR reaches over 1.5 dB.

Based on the optimization of the pilot boosting described above, the optimum MIMO pilot configuration including pilot pattern and pilot encoding algorithm for fixed/mobile reception scenario is evaluated by physical layer simulations. The studies were conducted with different channels, a SFN channel for fixed reception and DVB-NGH outdoor channel for mobile reception.

From the simulation results in a fixed SFN channel, it can be observed that Null Pilot encoding provides better performance than Walsh-Hadamard encoding and that larger D_X SP pattern is the best configuration. The simulation results confirmed that larger FFT size can reduce the pilot overhead and achieve lower required SNR in a fixed-time invariant SFN channel. In long echo SFN channel, DFT interpolation provides better performance than linear interpolation in terms of the frequency interpolation at the receiver. In contrast, it was confirmed that Walsh-Hadamard encoding with smaller D_Y SP pattern is the best configuration in a high Doppler time varying mobile channel. From the simulation results in DVB-NGH outdoor channel, it can be observed that smaller FFT size and linear interpolation at the receiver can achieve the lowest required SNR. It should be noted that Null Pilot encoding is rapidly degraded especially with (16k FFT, D_Y=4) or (32k FFT D_Y=2) in time varying channel because of the virtually doubled D_Y and that Walsh-Hadamard encoding with linear frequency interpolation can be severely degraded in frequency selective fading channel because of the virtually doubled D_X.

Chapter 4 Broadcast MIMO Signal Processing

This chapter presents signal processing technologies for complexity reduction and transmission robustness improvement in a cross-polarized 2×2 MIMO transmission model. The transmission performance is evaluated in fixed reception scenario using MIMO channel response captured in an urban area by physical layer simulations. To evaluate DTTB network for 2×2 cross-polarized MIMO, two experimental stations were set up and STC based 4×2 MIMO SFN scheme was evaluated in laboratory and field experiments.

4.1. Low-Complexity Demapping

NUCs have been developed in recent digital broadcasting systems [98] to close the gap to the Shannon limit. NUCs improve the transmission performance, especially for high-order constellations. Maximum likelihood (ML) demapping is known to be an optimal algorithm, but the implementation cost of the ML demapper greatly increases in high-order constellations such as 4096 NUCs at the receiver.

To solve the demapping complexity, some demapping algorithms have been investigated for two-dimensional (2D) NUCs [99], [100], [101]. We focused on one-dimensional (1D) NUCs (called NUQAMs in this thesis) and conducted computer simulations to examine the degradation in the transmission performance by applying a decision threshold (DT) demapping algorithm [102] to reduce the complexity in the LLR calculation. We assessed the degradation in the transmission performance caused by the DT demapper in several MIMO transmission channels captured in an actual environment.

4.1.1. Demapping Algorithm

The receiver first applies a linear MIMO signal detection such as ZF or MMSE, followed by per stream demapping. In the LLR calculation, the 2D ML demapper generally requires the calculations of a total number of *M* Euclidean distances between the received symbol and all the candidate symbols, where *M* indicates the number of signal points in a constellation. The LLR calculation can be expressed as:

$$\lambda(b_k|y) = ln\frac{P(b_k=1|y)}{P(b_k=0|y)} = ln\frac{\sum_{x\in X_k^1} exp\left[-\frac{(y-x)^2}{2\sigma^2}\right]}{\sum_{x\in X_k^0} exp\left[-\frac{(y-x)^2}{2\sigma^2}\right]} \quad (4.1)$$

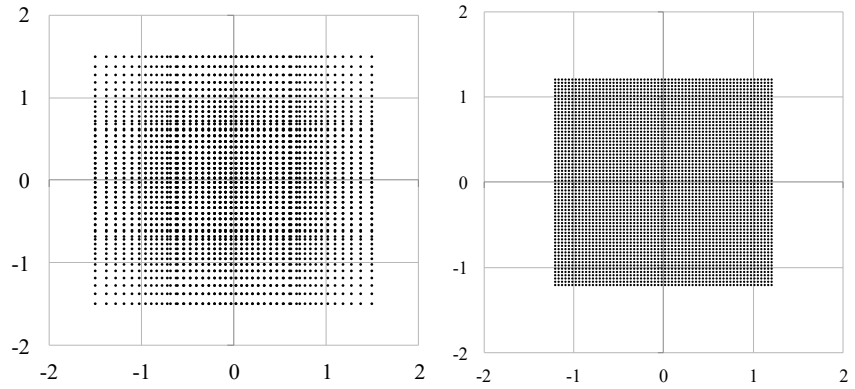

(a) 4096 NUQAM **(b) 4096 QAM**

Figure 4.1 Constellations used in demapping algorithm verification.

where λ denotes the value of LLR, b_k denotes the bit value in bit position k transmitted by a symbol, σ^2 denotes the noise power, y denotes the received symbol after equalization, X denotes all the transmitting symbols, and X_k^0 and X_k^1 denote the subsets of X in which $b_k = 0$ and $b_k = 1$, respectively. For example, the 2D ML demapper calculates 4096 Euclidean distances in the in-phase (I) and the quadrature (Q) components in both 4096 NUQAM and 4096 QAM. Figure 4.1 illustrates the signal point arrangements of a 4096 NUQAM we designed and a conventional 4096 QAM. Because the shapes are squares, NUQAMs and QAMs are thought of as two Pulse Amplitude Modulation (PAM) signals in the I/Q components [103]. The 1D ML demapper for PAM signals, such as the I component, can be represented as:

$$\lambda(b_k|y_I) = ln\frac{P(b_k = 1|y_I)}{P(b_k = 0|y_I)} = ln\frac{\sum_{x_I \in X_k^1} exp\left[-\frac{(y_I - x_I)^2}{2\sigma_I^2}\right]}{\sum_{x_I \in X_k^0} exp\left[-\frac{(y_I - x_I)^2}{2\sigma_I^2}\right]} \quad (4.2)$$

where λ denotes the value of LLR, b_k denotes the bit value in bit position k transmitted by the I component of a symbol, σ_I^2 denotes the noise variance in the I component axis, y_I denotes the I component of the received symbol after equalization, X denotes the candidate value of the I component given by all the transmitting symbols. In this case, the 1D ML demapper calculates $\sqrt{M} = \sqrt{4096} = 64$ Euclidean distances in the I component for each bit in both 4096 NUQAM and 4096 QAM. The process needs to be also done for Q component.

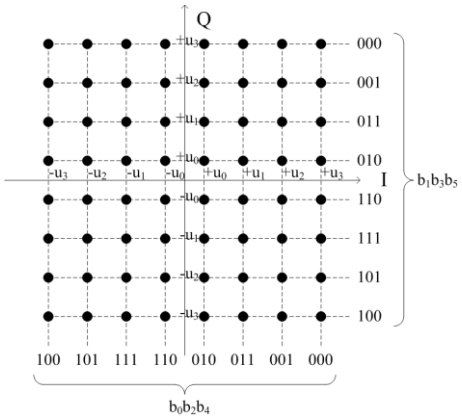

Figure 4.2 Bit allocation of gray-labeled QAM.

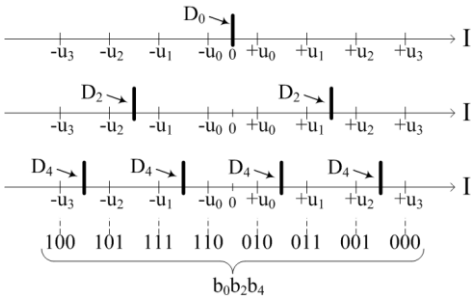

Figure 4.3 Decision threshold for 64 QAM

The DT demapper in [102] is a way of reducing the computational complexity for gray-labeled QAMs. Figure 4.2 shows an example of gray-labeled 64 QAM used in conventional digital terrestrial television broadcasting [104]. The three bits "$b_0b_2b_4$" and the rest "$b_1b_3b_5$" are transmitted by a single symbol on the I and Q components, respectively. The PAM amplitude of the constellation is denoted by u_j. Here, j is incremented by one with increasing amplitude, and the maximum j corresponds to $(2^{(U\text{-}2)/2}\text{-}1)$. U denotes the number of bits transmitted by a symbol, e.g. U = 12 for 4096 NUQAM and 4096 QAM.

The DT algorithm in [102] requires only one Euclidean distance in the I (Q) component to calculate the LLR for each bit regardless of the number of signal points in the constellation. Therefore, the computational complexity is greatly decreased especially in high-order modulation. These approximations correspond to calculating the LLR as the distance of the received equalized signal y_I from the nearest partition boundary. In the case of 64 QAM, the decision thresholds D_k are shown in Figure 4.3. The nearest D_k from the received symbol y_I is chosen as the reference boundary for the distance calculation.

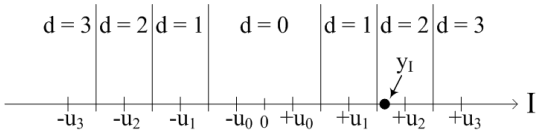

Figure 4.4 Index *d* of nearest PAM amplitude.

In a conventional QAM, the amplitudes $\{u_0, u_1, u_2, \text{and } u_3\}$ are equally spaced, and the values {1, 3, 5, and 7} are specified for the amplitudes before normalization [104]. In this case, the LLRs for the I component can be described as below.

$$\lambda(b_0|y_I) = -\frac{2}{\sigma_I^2}[y_I] \tag{4.3}$$

$$\lambda(b_2|y_I) = -\frac{2}{\sigma_I^2}[|y_I| - 4] \tag{4.4}$$

$$\lambda(b_4|y_I) = -\frac{2}{\sigma_I^2}\left[\left||y_I| - 4\right| - 2\right] \tag{4.5}$$

In this thesis we generalized the formula of the DT algorithm for NUQAMs as:

$$\begin{aligned}
\lambda'(b_k|y_I) &= -\frac{(u_a - u_b)}{\sigma_I^2}\left\{|y_I| - \frac{(u_a + u_b)}{2}\right\}(-1)^c, \\
&\text{for } k = 0,2,4,6,8,\cdots \\
&\quad a = (c-1) * 2^{\frac{U-k}{2}} + 2^{\frac{(U-2)-k}{2}} \\
&\quad b = a - 1 \\
&\quad c = \left(d \text{ div } 2^{\frac{U-k}{2}}\right) + 1 \\
&\quad d = \arg\min_n |y_I - u_n|
\end{aligned} \tag{4.6}$$

where λ' denotes the value of LLR calculated by DT demapper, *d* denotes the index of the nearest PAM amplitude from y_I, and "div" denotes the operation of calculating the quotient. Equation (4.7) shows example of the formula for k=0 and 2. Figure 4.4 illustrates an example of the index *d*, in which d = 2, indicating that u_2 is the nearest amplitude from the received symbol y_I.

Table 4.1 Transmission parameters for demapping evaluation.

FFT size	32 k
Number of radiated carriers	22465
Signal bandwidth	5.57 MHz
Carrier modulation scheme	16 QAM/NUQAM 64 QAM/NUQAM 256 QAM/NUQAM 1024 QAM/NUQAM 4096 QAM/NUQAM
Guard interval duration	126 μs (Guard interval ratio: 1/32)
FEC	LDPC Code - code length: 64800 - code rate R: 3/4
MIMO detection	Zero forcing
Pilot signal ratio	SP/CP: 4.2% TMCC/LLch: 1.0%

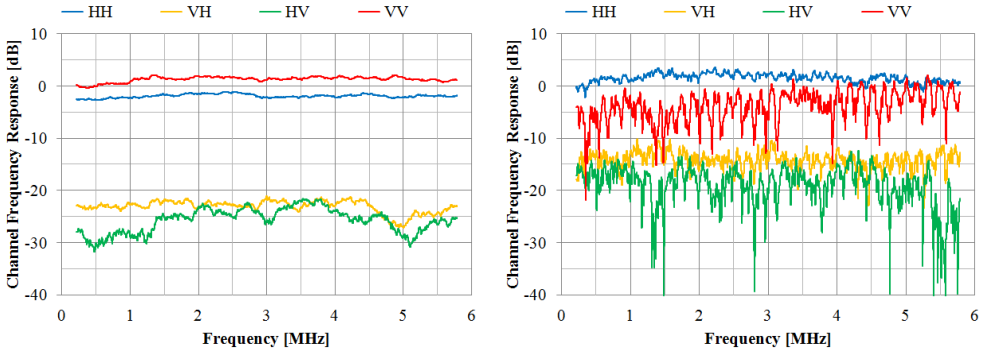

(a) Line-of-sight (MIMO channel index 2) **(b) Non-line-of-sight (MIMO channel index 10)**

Figure 4.5 MIMO channel snapshots captured in urban area.

$$\lambda'(b_0|y_I) = -\frac{2u_0}{\sigma_I^2}[y_I]$$

$$\lambda'(b_2|y_I) = -\frac{(u_a - u_b)}{\sigma_I^2}\left\{|y_I| - \frac{(u_a + u_b)}{2}\right\}$$

$$a = \left(2^{\frac{U-4}{2}}\right) \text{ div } 2$$

$$b = a - 1 \qquad (4.7)$$

4.1.2. Demapping Evaluation

By using the 1D ML and DT demappers described before, we conducted computer simulations with 15 MIMO channel snapshots captured in an urban area [105]. The block diagram of the simulations is illustrated in Figure 2.9. The transmission parameters are shown in Table 4.1. We used the NUQAMs and QAMs in a dual-polarized MIMO-OFDM scheme and evaluated the transmission performances. We measured the BER characteristics and evaluated the required CNR. The BER was measured before BCH decoding.

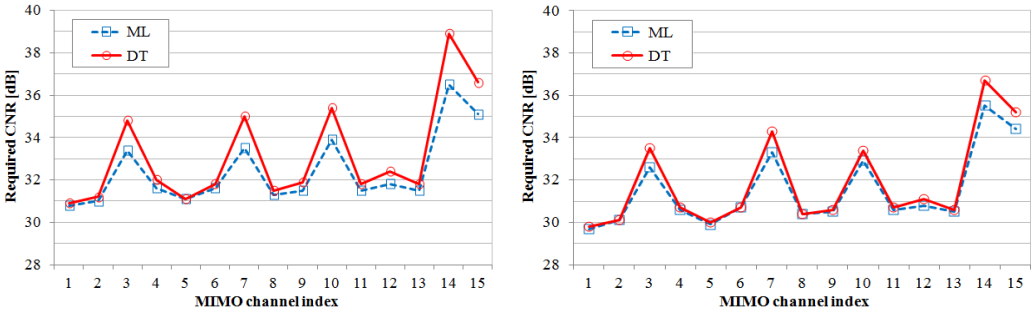

(a) 4096 QAM (b) 4096 NUQAM

Figure 4.6 Required CNR for ML and DT demappers with 15 MIMO channel snapshots.

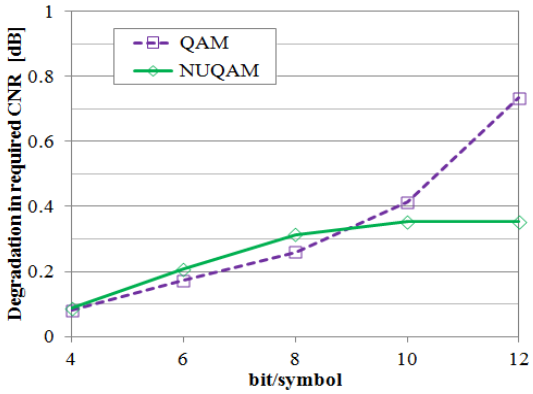

Figure 4.7 Degradation in required CNR in DT demapper from ML demapper for each bit/symbol

Figure 4.5 shows examples of MIMO channels used in the simulations captured at LOS and NLOS reception points. In this figure, "VH" means the channel frequency response from the vertically polarized (V) transmit antenna to the horizontally polarized (H) receive antenna. Three snapshots were captured at the LOS receiving point, and the remaining 12 were captured at the NLOS receiving point which was shadowed by buildings.

Figure 4.6 (a) shows the required CNRs of 4096 QAM using 1D ML and DT demappers by simulations. The required CNRs averaging the performance of 15 MIMO channels were 32.41 dB and 33.14 dB on average for ML and DT demappers, respectively. The degradation in the DT demapper from the ML demapper was 0.73 dB. Figure 4.6 (b) shows the results of 4096 NUQAM. The average required CNRs were 31.50 dB and 31.85 dB for ML and DT demappers, respectively; thus, the degradation was 0.35 dB. The simulation results confirm that the DT demapper slightly deteriorated the required CNR from the ML demapper in both QAM and NUQAM in all MIMO channels.

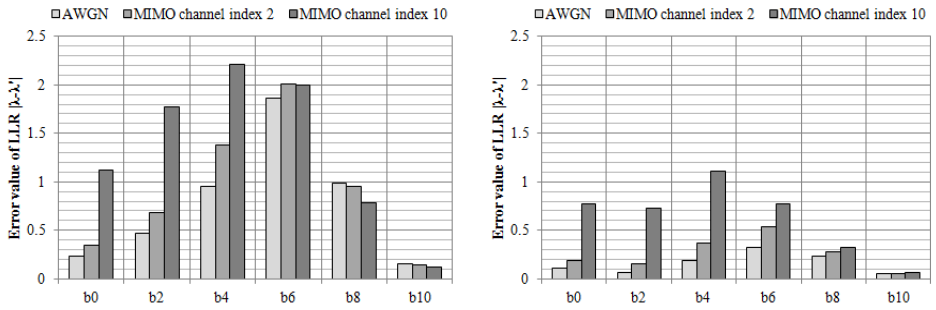

(a) 4096 QAM **(b) 4096 NUQAM**

Figure 4.8 Error values of LLRs in DT demapper from ML demapper for each bit

Figure 4.7 shows the degradation in the DT demapper from the ML demapper for each bit/symbol based on the average of the 15 MIMO channels by simulations. This result shows that the degradation in the required CNR of NUQAM became smaller than that of QAM for the number of signal points M=4096.

We clipped the absolute value of LLR, λ and λ', to 10 considering hardware implementation and examined the error values of LLRs from the ML demapper. Figure 4.8 shows the average error value |λ-λ'| of each bit transmitted on a single OFDM symbol in an AWGN channel, in MIMO channel index 2 (LOS), and in index 10 (NLOS) with the CNR being 30 dB. These graphs indicate that the errors tended to increase according to the channel distortion in both NUQAM and QAM, but the error value became smaller in NUQAM compared with QAM. We considered that the errors in LLRs caused by approximation became smaller in NUQAMs; consequently, the degradation in the required CNR also became smaller for 4096 NUQAM in Figure 4.8.

4.2. MIMO Precoding

This section focuses on the performance evaluation of the MIMO precoding in ATSC 3.0 using physical layer simulations considering cross-polarized 2×2 MIMO reception conditions, e.g. PI in horizontal and vertical polarization and XPD of the reception antennas.

The MIMO precoding performance is evaluated with physical layer simulations in three steps; the PI in horizontal and vertical polarization, the XPD of the reception antennas, and realistic channel conditions using MIMO channel responses captured in field measurements in an urban area.

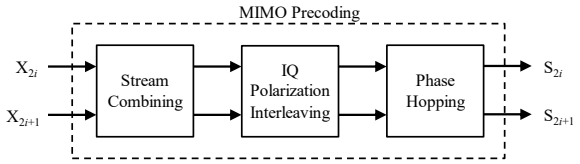

Figure 4.9 MIMO precoding block diagram in ATSC 3.0

4.2.1. Precoding Schemes

The MIMO precoding scheme in ATSC 3.0 is depicted in Figure 4.9. MIMO precoding acts on a pair of input constellation symbols (X_{2i}, X_{2i+1}) and creates a pair of output constellation symbols (S_{2i}, S_{2i+1}), where i is the index of the cell pair within the FEC Block. Each precoding block can be activated independently and it is possible to configure more than one precoding blocks together.

A. Stream Combining

The SC consists of a combination of the pair of input constellation symbols based on a rotation matrix with angle ψ. The SC is available only for lower modulation order with higher code rate, i.e. QPSK with 6/15 to 13/15 and 16QAM with 11/15 to 13/15 in ATSC3.0 specification.

B. IQ Polarization Interleaving

The IQPI is simply a switching interleaving operation, such that the output cells consist of the real (In-phase) component of one input symbol and the imaginary (Quadrature) component of the other input symbol.

C. Phase Hopping

The PH consists of a phase rotation of the symbols of the second transmit antenna. The PH is the same process as that in DVB-NGH [31], i.e. the phase rotation is initialized to 0 radians at the beginning of each FEC Block and is incremented by $2\pi/9$ for every cell pair.

4.2.2. Precoding Evaluation

The performance of MIMO precoding is evaluated by physical layer simulations in which the transmitter complies with the ATSC 3.0 specification. Ideal channel estimation and ideal noise estimation are assumed at the receiver. The different MIMO precoding configurations are compared in terms of BER after BCH decoding. This thesis focuses on the performance evaluation of each MIMO precoding block separately to analyze fundamental characteristics of each precoding scheme considering cross-polarized 2×2

Table 4.2 Power imbalance measured in 15 MIMO channel snapshots

Measurement Number	1	2	3	4	5	6	7	8	9	10	11	12	13	14	15
Power Imbalance [dB]	1.3	3.2	1.4	3.3	0.2	2.4	4.8	1.0	3.3	4.6	0.6	0.8	1.1	0.2	0.5

Table 4.3 Transmission parameters for precoding evaluation

FFT size	16 k
Number of carriers	13825
Signal bandwidth	5.832 MHz
GI pattern	GI5_1024 (GI ratio: 1/16, GI length: 148 μs)

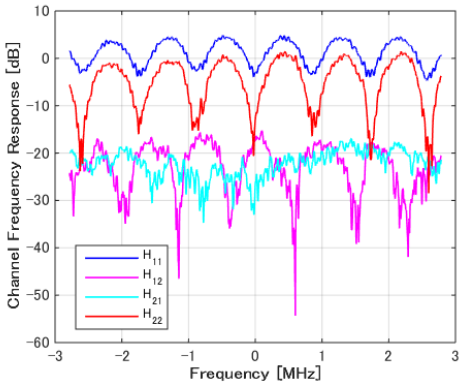

Figure 4.10 MIMO channel snapshots captured in urban area (MIMO channel index 7).

MIMO reception conditions. Several modulation and coding schemes have been evaluated with each MIMO precoding scheme. In the selection of simulation parameters, lower modulation and higher code rate were selected to be available for SC, IQPI and PH. The transmission parameters for simulations are shown in Table 4.3. The performance is evaluated with MLD with long LDPC codes (64k) standardized in ATSC 3.0 [20]. Note that the SNR is defined as the ratio of the total carrier power (antenna #1 and #2) to the noise power at each receiver (either antenna #1 or #2) in Section 4.2 due to the simulator constraints, and the SNR is not consistent with the SNR definition shown in 2.3.1. The required SNR is defined as the SNR to achieve BER $=1\times10^{-4}$ in this Section. The precoding gain is evaluated in three steps as follows.

A. Power Imbalance

The influence of received PI in horizontal and vertical polarization in fixed reception scenario has been considered. The PI channel is modeled using one configuration parameter *p*, which gives the difference between the received signal powers in dB for

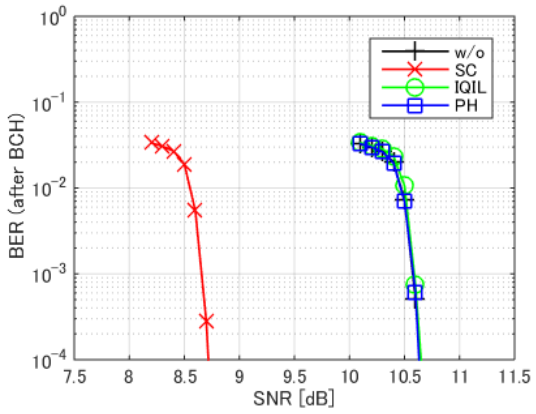

Figure 4.11 BER performance in PI channel p = 6 dB. (QPSK, R=13/15)

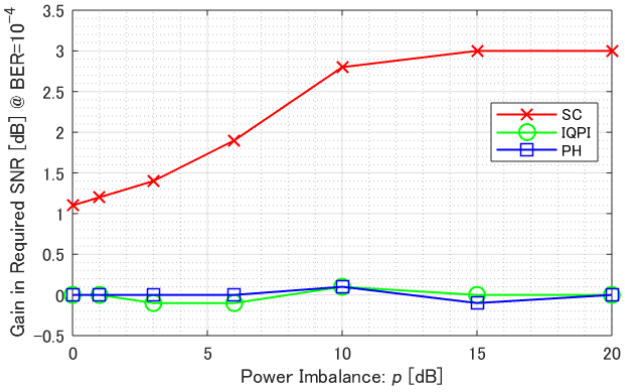

Figure 4.12 MIMO precoding gain in PI channel (QPSK, R=13/15).

horizontal and vertical polarization as explained in 2.3.2. It is assumed that the XPD is infinite as an ideal case.

Figure 4.11 shows BER performance for each MIMO precoding in an PI channel of p = 6 dB with QPSK and code rate R = 13/15. The BER performance is evaluated activating only one precoding block to confirm each precoding gain. The rotation angles standardized in ATSC 3.0 are used for the evaluation. This result shows that only SC introduces gain in the PI channel. It is considered that SC is beneficial in PI channel by spreading the information of the input symbols into the output symbols. This result is aligned with an evaluation result in a power imbalanced mobile channels as shown in a previous study [105].

The MIMO precoding gain in the required SNR obtained for the PI parameter p was evaluated with QPSK and code rate R = 13/15. The simulation result is shown in Figure

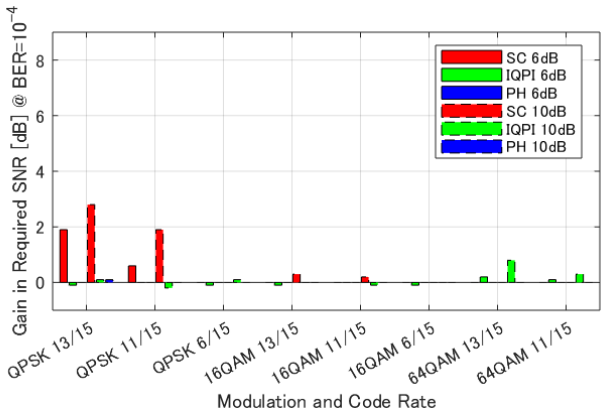

Figure 4.13 MIMO precoding gain in PI channel (p = 6 and 10 dB).

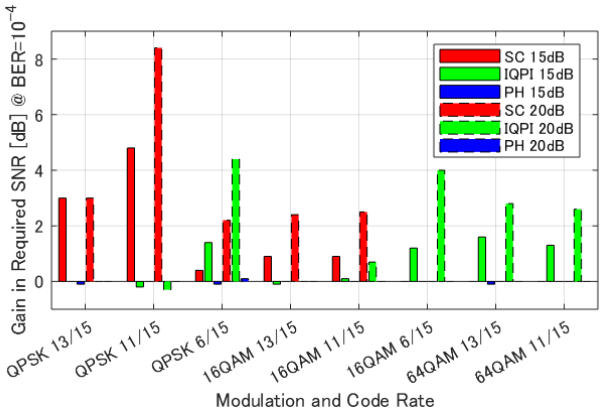

Figure 4.14 MIMO precoding gain in PI channel (p = 15 and 20 dB).

4.12. This result showed that the gain obtained by SC increases as the PI increases and that IQPI and PH provide no gain with QPSK and code rate R = 13/15 in PI channel.

The MIMO precoding gains with other modulation and code rate for p = 6 and 10 dB are shown in Figure 4.13. As extremely high PI scenarios, the gains for p = 15 and 20 dB are also evaluated in Figure 4.14. These results showed that SC provides a significant gain for lower modulation with higher code rate. It was confirmed that IQPI introduces some gains with lower code rate especially in extreme PI conditions. The higher PI values enhance the SNR gains for both SC and IQPI.

B. Cross Polarization Discrimination

The influence of XPD of the receiving antennas in fixed reception scenario was evaluated in the cross polarized channel 2.3.3. The XPD defines a crosstalk between horizontally and vertically polarized antenna at the receiver using one configuration parameter x, which is the ratio of the co-polar component of the specified polarization

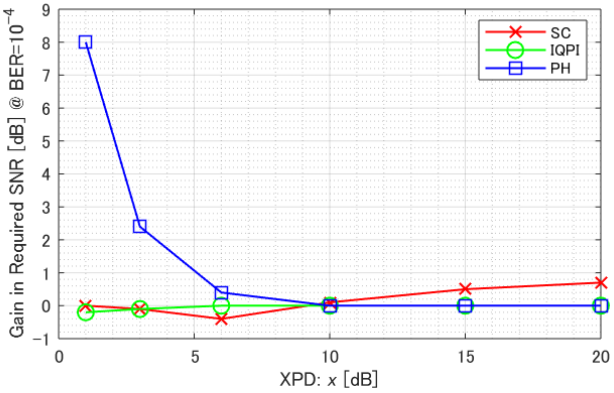

Figure 4.15 MIMO precoding gain for XPD (QPSK, R=13/15).

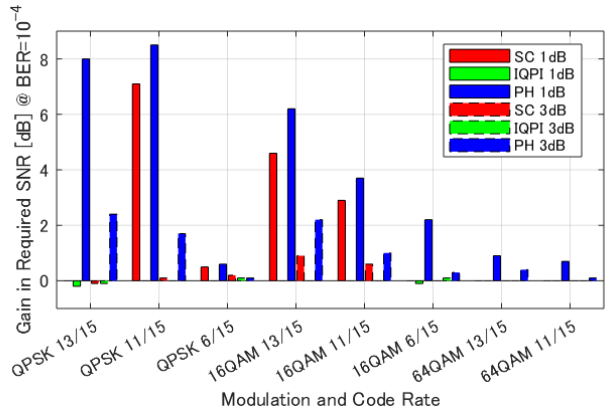

Figure 4.16 MIMO precoding gain for XPD (x =1 and 3 dB).

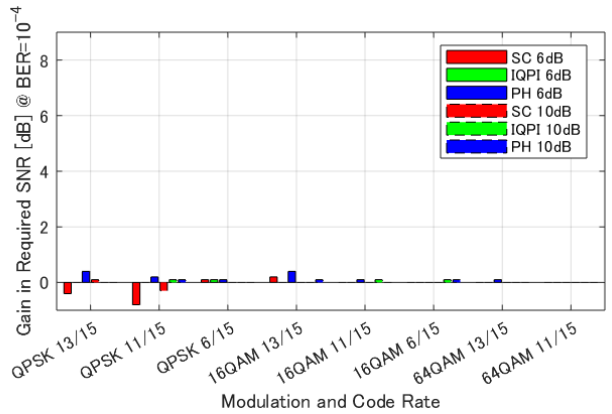

Figure 4.17 MIMO precoding gain for XPD (x = 6 and 10 dB).

compared to the orthogonal cross-polar component between both received signal powers in dB as shown in 2.3.3.

The MIMO precoding gain obtained for the XPD parameter x with QPSK and code rate R = 13/15 is shown in Figure 4.15. This result showed that the gain obtained by PH increases as the XPD decreases and that SC and IQPI provide almost no gain with QPSK

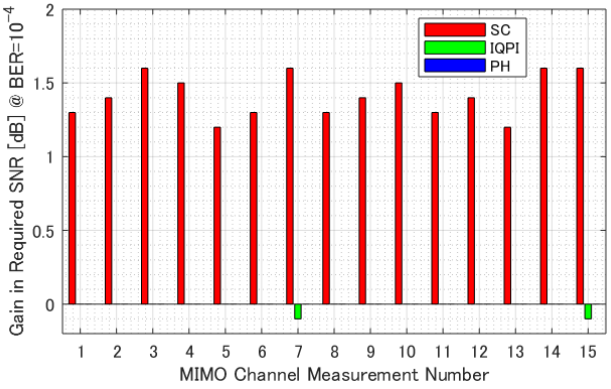

Figure 4.18 MIMO precoding gain for snapshots (QPSK, R=13/15).

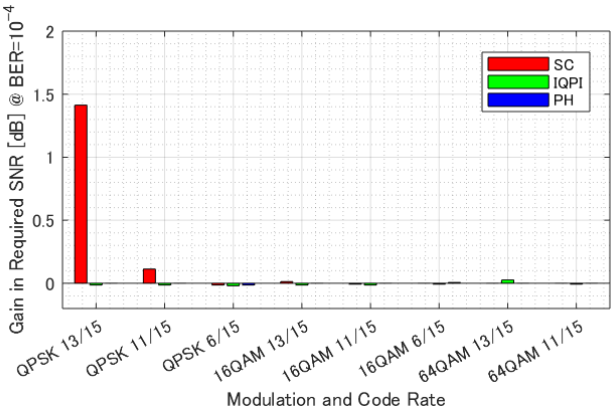

Figure 4.19 MIMO precoding gain for snapshots (average gain for 15 snapshots).

and code rate R = 13/15. It is considered that PH is beneficial with lower XPD receiving antennas by reducing the correlation of the transmission paths in the CFR matrix.

The MIMO precoding gains with other modulation and code rate for x = 1 and 3 dB as extremely low XPD scenarios are shown in Figure 4.16. This result showed that PH provides some gains especially for lower modulations and higher code rates. It was confirmed that SC introduced some gains for some modulations and code rates and that IQPI provides no gain. The lower XPD values enhance the SNR gains for both PH and SC. It should be noted that the gains become negligible with practical XPD values for fixed reception such as x = 6 and 10 dB as shown in Figure 4.17.

C. MIMO Channel Snapshots

The potential gain introduced by the MIMO precoding in a practical reception scenario has been evaluated. The MIMO precoding gain was evaluated using 15 MIMO channel samples captured in a field experiment in Tokyo [106]. The PI measured at the 15 reception points is listed in Table 4.2. One example of CFR matrix of measurement

number 7 is depicted in Figure 4.10. The MIMO channel snapshots were captured using a cross-polar receive antenna whose XPD is greater than 20 dB.

Figure 4.18 shows the precoding gain obtained in a practical evaluation using the MIMO channel snapshots with QPSK and code rate R = 13/15. The result shows that the gain is obtained only with SC and that IQPI and PH provide no gain.

Figure 4.19 shows the average gains obtained for 15 snapshots with other modulation and code rate. The average value in dB is calculated as a mean of 15 gains in dB. The results showed that SC provided gains for QPSK with higher code rate. IQPI and PH introduced no gain. It is considered that the maximum PI measured in the snapshots was 4.8 dB, thus the gain obtained with IQPI was negligibly small. Additionally, the XPD value of the receiving antenna used in the MIMO channel measurements was greater than 20 dB, therefore no gain was obtained by PH.

4.3. Space Time Coding based SFN

To ensure an adequate link budget for a next-generation terrestrial network especially when using MIMO, two experimental stations were installed in the Hitoyoshi area of Kumamoto, Japan. We carried out 8K terrestrial transmission (91 Mbps) over a distance of 27 km on a single UHF band channel (6 MHz bandwidth) with a 2×2 MIMO system [36]. We conducted 8K-UHDTV SFN field experiments using two transmission stations. The conventional SFN is defined as two geographically distributed stations sending the same signals synchronously using the same frequency. When the two signals are received at about the same strength in the conventional SFN, deep nulls would occur on the received spectrum, and the reception quality would be deteriorated. This problem is caused by an erasure effect, the so-called 0-dB echo effect. The study of the erasure effect in the single polar system has been verified by the previous works [107],[108],[109].

To prevent deterioration of the transmission performance in 2×2 MIMO transmission, we investigated a 2×2 MIMO STC-SFN system. In field experiment, the STC method was employed to improve the reliability of high data rate transmission. In this section, the results of the 2×2 MIMO field test using advanced SFN technology is reported.

4.3.1. Space Time Coding Schemes

Figure 4.20 shows the outline of a 2 × 2 MIMO STC-SFN system formed by two experimental stations, namely, the Hitoyoshi and Mizukami stations. The distance

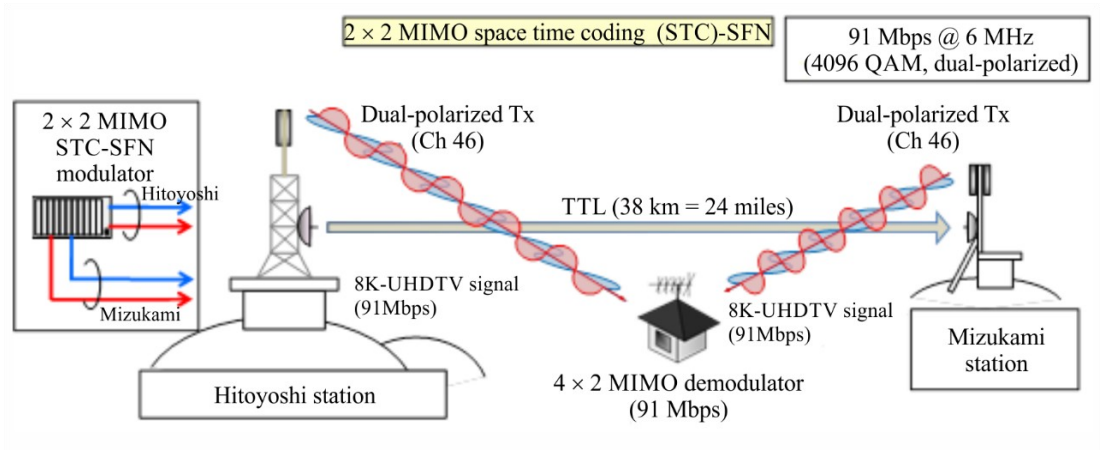

Figure 4.20 Outline of 2×2 MIMO STC-SFN transmission system

between the two stations is 38 km. Both stations use dual-polarized SM MIMO. The Mizukami station was connected to the Hitoyoshi station by a transmitter-to-transmitter link (TTL) in the super high frequency (SHF) band.

In this field experiment, the intermediate frequency TTL (IF-TTL) method was used to transmit an OFDM signal from the Hitoyoshi station to the Mizukami station. The transmission frequencies of the two stations were precisely synchronized by rubidium (Rb) oscillator with a global positioning system (GPS) as a backup.

The 2×2 MIMO STC-SFN system used in this SFN field experiment employed STC technology as a new feature. The Hitoyoshi station transmitted a 91 Mbit/s 8K-UHDTV signal in a 6 MHz bandwidth UHF channel (channel number 46 in Japan), and the Mizukami station also transmitted using the same channel.

The 2×2 MIMO STC-SFN system was developed for this experiment as shown in Figure 4.21. The transmission system can be modeled as

$$\begin{bmatrix} y_1 \\ y_2 \end{bmatrix} = \begin{bmatrix} h_{11} & h_{12} & h_{13} & h_{14} \\ h_{21} & h_{22} & h_{23} & h_{24} \end{bmatrix} \begin{bmatrix} x_1 \\ x_2 \\ x_3 \\ x_4 \end{bmatrix} + \begin{bmatrix} w_1 \\ w_2 \end{bmatrix} \tag{4.8}$$

where the transmitting carrier symbols are denoted as x_1, x_2, x_3 and x_4, and the receiving carrier symbols as y_1 and y_2. h is the channel frequency response estimated by pilot symbols, and h_{ij} is the component corresponding to the ith receive antenna and jth transmit antenna. Here, x_1 and x_2 are the transmitted symbols from main station, and x_3 and x_4 the

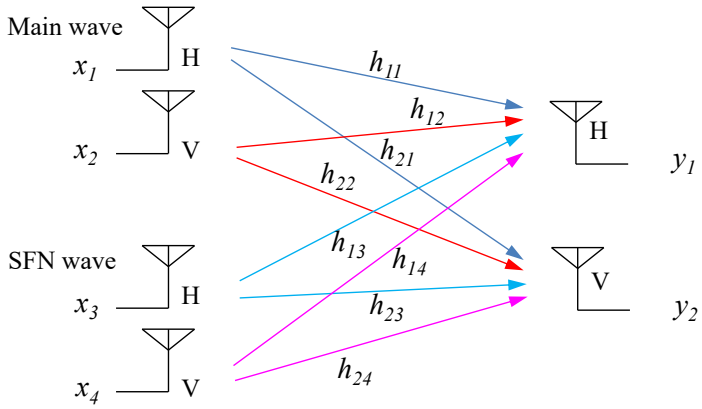

Figure 4.21 Space Time Coding scheme

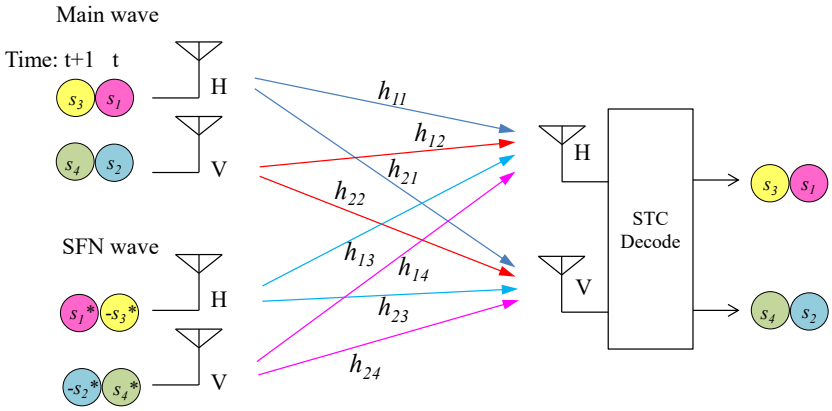

Figure 4.22 Transmission model of 2×2 MIMO STC-SFN

transmitted symbols from SFN station. STC is a method of encoding carrier symbols. An STBC [28] is applied for the carrier symbols by pairing transmit antennas of the same polarization at the two transmission stations as shown in Figure 4.22. The STC scheme can be described as:

$$\begin{bmatrix} y_1(t) \\ y_2(t) \end{bmatrix} = \begin{bmatrix} h_{11}(t) & h_{12}(t) & h_{13}(t) & h_{14}(t) \\ h_{21}(t) & h_{22}(t) & h_{23}(t) & h_{24}(t) \end{bmatrix} \begin{bmatrix} s_1 \\ s_2 \\ -s_3{}^* \\ s_4{}^* \end{bmatrix} + \begin{bmatrix} w_1(t) \\ w_2(t) \end{bmatrix} \tag{4.9}$$

$$\begin{bmatrix} y_1(t+1) \\ y_2(t+1) \end{bmatrix} = \begin{bmatrix} h_{11}(t+1) & h_{12}(t+1) & h_{13}(t+1) & h_{14}(t+1) \\ h_{21}(t+1) & h_{22}(t+1) & h_{23}(t+1) & h_{24}(t+1) \end{bmatrix} \begin{bmatrix} s_3 \\ s_4 \\ s_1{}^* \\ -s_2{}^* \end{bmatrix} + \begin{bmatrix} w_1(t+1) \\ w_2(t+1) \end{bmatrix} \tag{4.10}$$

$$\begin{bmatrix} y_1(t) \\ y_2(t) \\ y_1{}^*(t+1) \\ y_2{}^*(t+1) \end{bmatrix} = \begin{bmatrix} h_{11}(t) & h_{12}(t) & h_{13}(t) & h_{14}(t) \\ h_{21}(t) & h_{22}(t) & h_{23}(t) & h_{24}(t) \\ h_{13}{}^*(t+1) & -h_{14}{}^*(t+1) & -h_{11}{}^*(t+1) & h_{12}{}^*(t+1) \\ h_{23}{}^*(t+1) & -h_{24}{}^*(t+1) & -h_{21}{}^*(t+1) & h_{22}{}^*(t+1) \end{bmatrix} \begin{bmatrix} s_1 \\ s_2 \\ -s_3{}^* \\ s_4{}^* \end{bmatrix} + \begin{bmatrix} w_1(t) \\ w_2(t) \\ w_1{}^*(t+1) \\ w_2{}^*(t+1) \end{bmatrix} \tag{4.11}$$

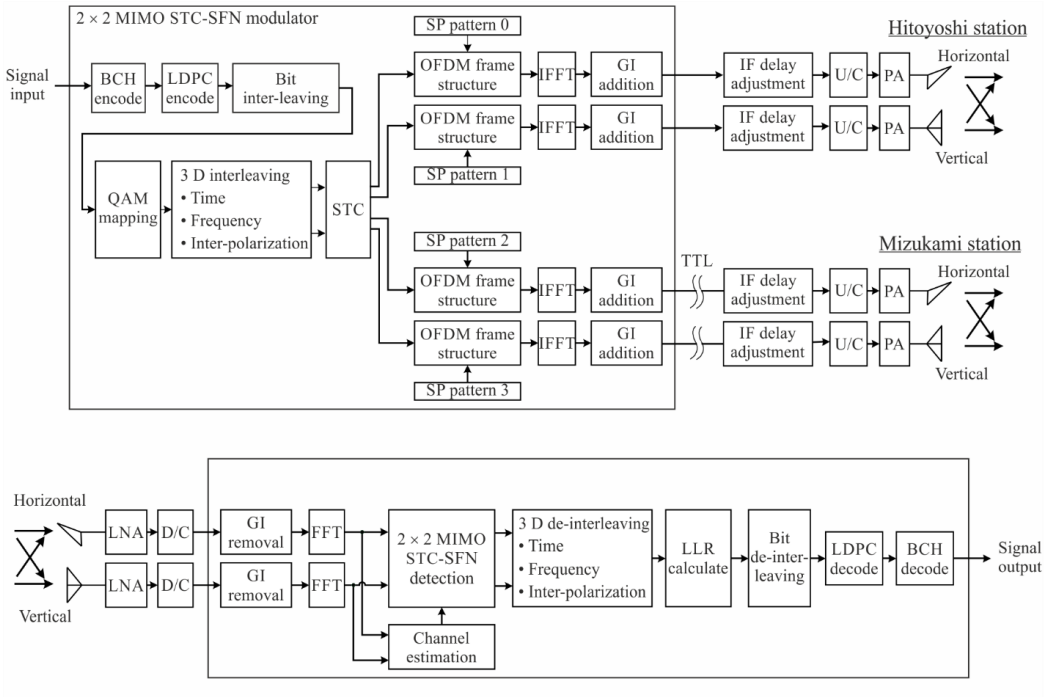

Figure 4.23 Block diagram of 2×2 MIMO STC-SFN system

where s is a carrier symbol of a constellation with a complex value, and * means the complex conjugate. The transmitted symbols s_1, s_2, s_3 and s_4 are encoded, s_1, s_2, $-s_3^*$ and s_4^* are transmitted in time t, and s_3, s_4, s_1^* and $-s_2^*$ are then transmitted in time $t+1$, from each antenna. At the receiver side, the transmitted symbols s_1, s_2, s_3 and s_4 are obtained by decoding the received four symbols $y_1(t)$, $y_2(t)$, $y_1(t+1)$ and $y_2(t+1)$, which are received at two discrete times.

Figure 4.23 shows the block diagram of the 2×2 MIMO STC-SFN system modulator and demodulator used in this field trial. To adjust the time delay between two transmission waves, Intermediate Frequency (IF) delay adjustment equipment with a range of 0.1 μs - 10 ms was installed at both stations as shown in Figure 4.23. In the field tests, the ZF algorithm, which has less complexity than other algorithms (e.g., MMSE or MLD) at MIMO, is applied to (4.11)(4.11) because in the case of using higher-order modulation (e.g., 4096QAM per transmit antenna), the complexity of MLD algorithm is large, and it is difficult to implement on real hardware.

Figure 4.24 shows the SP patterns of the 2×2 MIMO STC-SFN system. To estimate the channel responses from each transmit antenna to each receiving antenna, four orthogonal SP schemes, which are a hybrid of WH and NP encoding schemes [110], were adopted. Note that four orthogonal SP schemes can be designed only with WH encoding

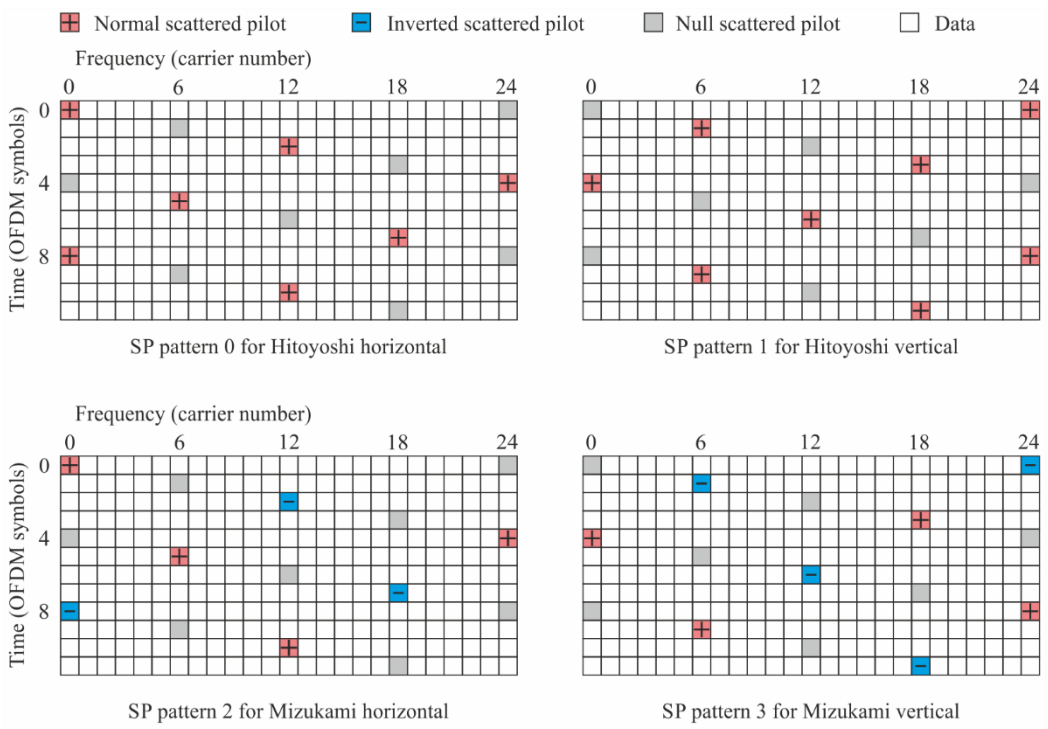

Figure 4.24 Scattered pilot patterns for 2×2 MIMO STC-SFN system

[111], but the accuracy of the channel estimation deteriorates in a doppler channel as shown in 3.3.

4.3.2. Space Time Coding Evaluation

Table 4.4 shows the parameters for MIMO transmission and the specifications of the Hitoyoshi and Mizukami stations are shown in Table 2.11. Figure 4.25 shows the equipment installed in each station. The transmit antennas at Hitoyoshi and Mizukami have the same characteristics.

To compare the differences between 2×2 MIMO STC-SFN system and conventional SFN system, transmission performances were measured at three points (Points A, B, and C in Figure 4.26) within the area of overlap covered by both the Hitoyoshi and the Mizukami stations. Here, LOS stands for line of sight and NLOS stands for non-line of sight. Before measurement, the transmission power and time delay at both stations was adjusted for evaluation under identical conditions. The power ratios of the main and SFN waves were adjusted to 6 dB and the time delay between the main and SFN waves to 2 μs at the receiver inputs at each test point. The power of each wave was defined as the average of the horizontal and vertical waves.

Table 4.4 Transmission parameters for space time coding field test

Modulation scheme	OFDM
Occupied bandwidth	5.57 MHz
Carrier modulation	4096-QAM
FFT size (number of radiated carriers)	32K (22,465)
Guard interval ratio (guard interval duration)	1/32 (126 μs)
Error-correcting code	Inner code: LDPC, coding rate R = 3/4 Outer code: BCH
Transmission capacity	91.8 Mbit/s

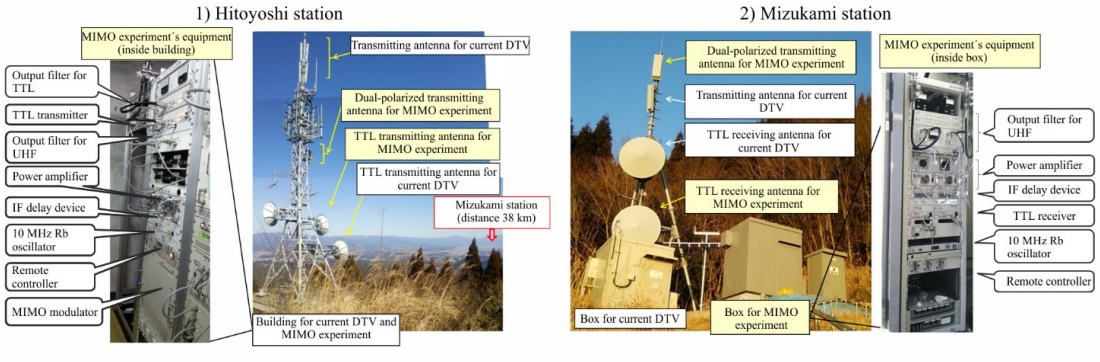

Figure 4.25 Equipment of MIMO experimental stations

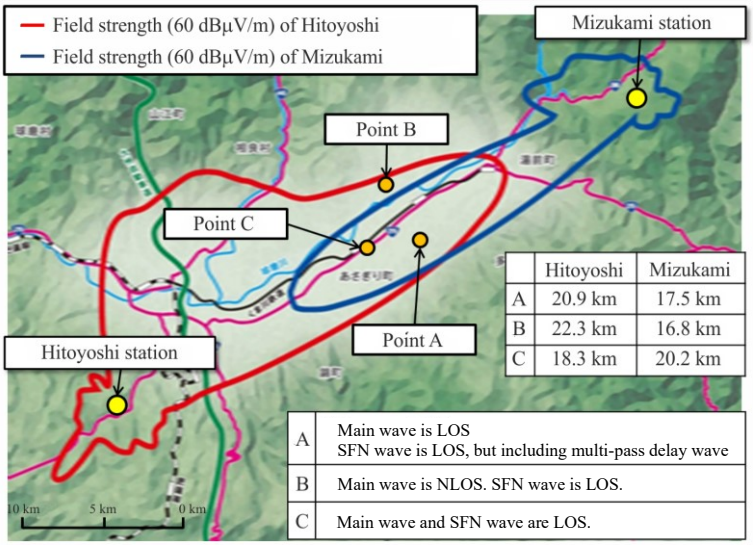

Figure 4.26 Measuring points for Space Time Coding Evaluation

Figure 4.27 plots the reception powers required for both 2×2 MIMO STC-SFN and conventional SFN at all three reception points. The required power in non SFN environment, i.e., single station, is used as a reference. This Figure clearly shows that the null is much shallower in the spectrum of 2×2 MIMO STC-SFN than in conventional SFN. Furthermore, the required power for 2×2 MIMO STC-SFN is 3 dB superior to that

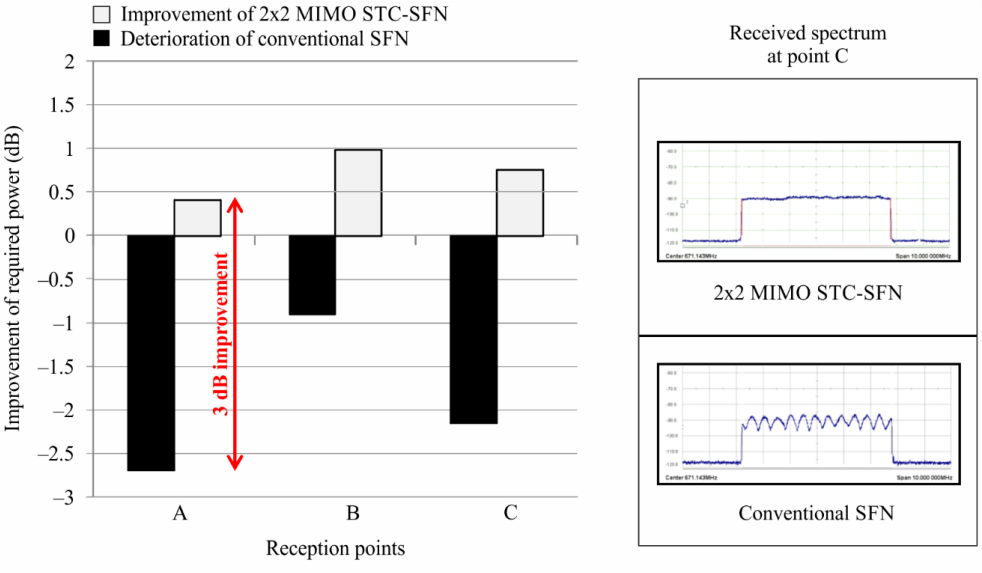

Figure 4.27 Comparison of 2×2 MIMO STC-SFN with conventional SFN in field trial

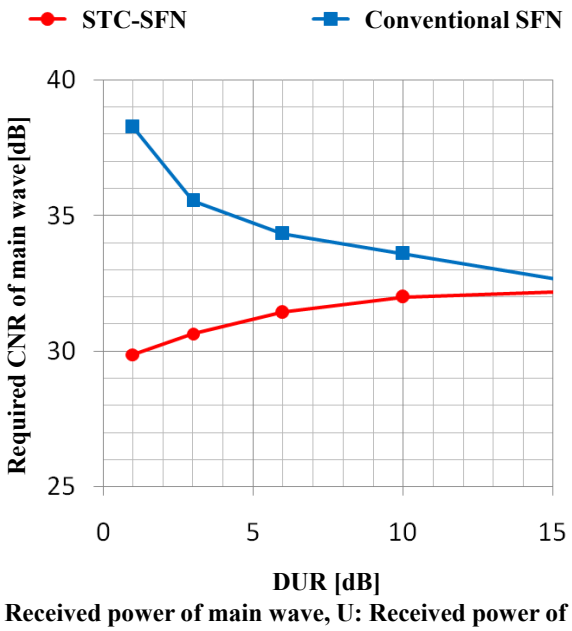

Figure 4.28 Comparison of 2×2 MIMO STC-SFN with conventional SFN in laboratory test

of the conventional SFN. This decreased null in the spectrum and the improvement of required power are clear outcomes of the application of STC technology to SFN.

Figure 4.28 shows the required CNR of main wave measured in laboratory test. When the DUR is 6 dB, STC-SFN improves the required CNR, whereas conventional SFN degrades it. The required CNR difference between STC-SFN and conventional SFN is about 3 dB for DUR=6 dB, which is consistent with the results of the field experiments.

4.4. Conclusions

In Section 4.1, we applied a simplified demapping algorithm to NUQAMs and evaluated the transmission performance in a MIMO-OFDM transmission scheme. We conducted simulations to verify the degradation in the transmission performance using MIMO channel response actually captured in an urban area. The simulation results indicate that the simplified demapping algorithm mitigated the degradation in the required CNR by not more than 0.4 dB when using the 4096 NUQAM, which has the advantage that the simplified demapper greatly reduces the complexity in high-order modulation.

Section 4.2 compares the three MIMO precoding components adopted in ATSC 3.0: Stream Combining, IQ Polarization Interleaving and Phase Hopping. The precoding performances have been compared in terms of power imbalance between horizontal and vertical polarization, cross polarization discrimination and practically captured MIMO channels using physical layer simulations. The results showed that Stream Combining introduced much gain in a practical static reception scenario with lower modulation and higher code rate. However, IQ Polarization Interleaving and Phase Hopping don't provide any gains. It was confirmed that IQ Polarization Interleaving provides gain only in an extremely high power imbalance channel. Phase Hopping is beneficial with extremely lower XPD reception antennas.

In Section 4.3, 4×2 MIMO field tests using two experimental stations composed of an STC-SFN were conducted in Hitoyoshi city, Kumamoto, Japan. We compared two SFN schemes: STC-SFN and conventional SFN without coding. The results confirmed that the required received power of STC-SFN is 3 dB better than that of the conventional SFN when the power ratio of the main wave and the SFN wave is 6 dB.

Chapter 5 Broadcast MIMO Practical Gain and Channel Modeling

In this chapter, the transmission performance was evaluated using a prototype advanced ISDB-T system in laboratory experiments and large-scale field experiments in central Tokyo and Osaka. The required received power improvement when MIMO is introduced to enhance transmission robustness was verified. Alternatively, the transmission capacity enhancement by introducing MIMO for the same robustness as SISO was also evaluated. It is clarified that the amount of degradation in the required received power for MIMO is higher than that for SISO with several MODCOD having different levels of robustness. Simple 8-tap fixed rooftop reception MIMO channel models are generated from 101 snapshots captured in Osaka. With the generated models, we evaluated the MIMO gain over SISO in fixed reception environment by physical layer simulation.

5.1. Evaluation in Tokyo area

This section describes the performance comparison between MIMO and SISO in real reception environment. Measurements were carried out in three steps: advance verification in laboratory, field experiments, and follow-up verification in laboratory. In field experiments, BER measurement results could be affected by several factors, such as fluctuation in the electric field strength, movement of the vehicles passing by the measurement vehicle, and man-made noise occurring at the time of each measurement. To remove those influences on the evaluation results, we evaluated the required CNR in the follow-up verification in laboratory by using the MIMO channel snapshots captured in the field experiments. The detailed methodologies are described in Section 2.6 and Section 2.7.

The experiments were conducted with a single SISO transmission configuration and three MIMO configuration sets for the advanced ISDB-T system, as summarized in Table 5.1. The SISO parameters are a reference and assumed to have the same robustness as the operational parameters of the current DTT system, ISDB-T, for fixed reception in Japan

Table 5.1 Parameter sets for experiments.

	Parameter set			
	SISO (reference)	MIMO		
		No. 1 (scenario 1)	No. 2 (scenario 2)	No. 3 (scenario 3)
Occupied bandwidth	Normal mode: 5.83 MHz			
Number of segments	Normal mode: 35 (31 segments used for fixed reception evaluation)			
FFT size	16,384			
Guard interval ratio (duration)	800/16,384 (126 μsec)			
Scattered pilot ratio	1/12			1/24
Carrier modulation	256QAM Non-uniform	16QAM Non-uniform	256QAM Non-uniform	1024QAM Non-uniform
Inner code rate	12/16			11/16
System	SISO (horizontal)	MIMO (open-loop spatial multiplexing 2×2 cross-polarized)		
Transmission capacity (31 segments)	26.1 Mbps	26.1 Mbps	52.3 Mbps	62.8 Mbps

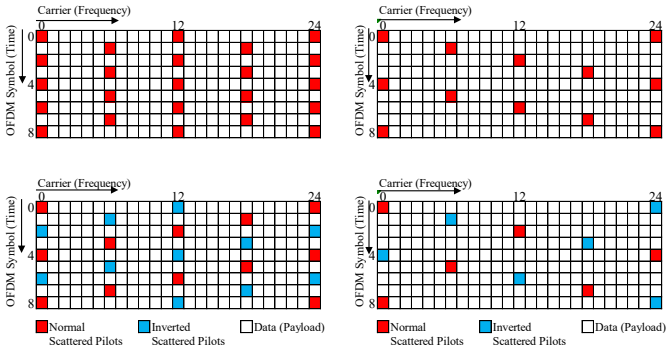

Figure 5.1 Scattered pilots used for experiments. *D*x=6, *D*y=2 (left) and *D*x=6, *D*y=4 (right). For SISO (top) and MIMO (top for signal #1 and bottom for signal #2).

(64 QAM, code rate = 3/4). The required CNR of the operation parameters of ISDB-T is about 20 dB. In the advanced ISDB-T, when 31 out of all 35 segments are used for UHDTV transmission, the transmission capacity reaches 26.1 Mbps. MIMO parameter set No. 1 (scenario 1) introduces MIMO with the same transmission capacity as the reference SISO configuration. We evaluated how the required received power improves compared with SISO. MIMO parameter set No. 2 (scenario 2) introduces MIMO with the same robustness as the reference SISO configuration. We evaluated how the required received power varies when the transmission capacity is doubled compared with SISO. The last parameter set No. 3 (scenario 3) introduces MIMO to greatly increase the capacity to provide 8K program assuming a bit rate of around 60 Mbps with VVC. The required CNR or the required received power was defined as the minimum CNR or the minimum received power at which the value of the BER before error correction of the

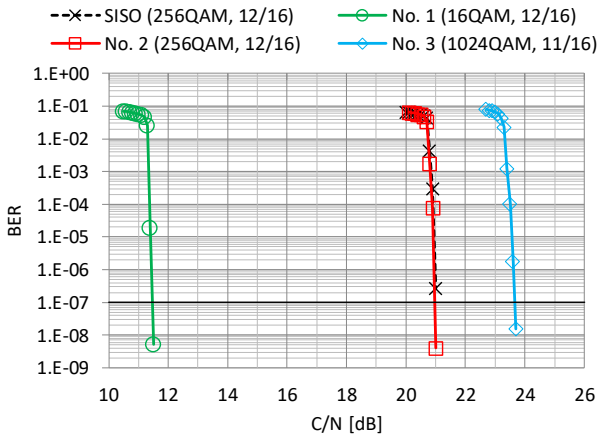

Figure 5.2 BER characteristics in ideal AWGN channel in laboratory experiments.

Table 5.2 Required CNR in advance verification in laboratory experiments.

	Parameter set			
	SISO (reference)	MIMO		
		No. 1 (scenario 1)	No. 2 (scenario 2)	No. 3 (scenario 3)
Required CNR in AWGN channel	21.1 dB	11.5 dB	21.1 dB	23.7 dB

outer code (BCH code) is below 1×10^{-7} [91]. The number of observation bits was set to $1\times10^{+10}$, which corresponds to about 6 minutes in SISO, although the QEF condition of a digital television broadcasting signal means less than one uncorrected error event per hour [112].

Figure 5.1 illustrates the pilot signals used for the experiments. For SISO, the number of carriers between the scattered pilot bearing carriers (Dx) was set to 6, and the number of symbols between the scattered pilots in a single pilot bearing carrier (Dy) was set to 2, which is shown in Figure 5.1 (top, left). MIMO parameter sets No. 1 and 2 were configured to have the same scattered pilots as SISO for output signal #1 and sign inverted scattered pilots for output signal #2, which are shown in Figure 5.1 (top, left) and (bottom, left), respectively. For MIMO parameter set No. 3, Dx = 6 and Dy = 4, shown in Figure 5.1 (right), were selected to increase the transmission capacity.

5.1.1. Advance Verification in Laboratory

We evaluated the required CNR of each parameter set shown in Table 5.1 in an AWGN channel for the SISO/MIMO configuration in laboratory experiments. In preliminary MIMO field trials, a difference in electric field strength between the horizontally and vertically polarized waves was observed [113]. The required CNR with a specific

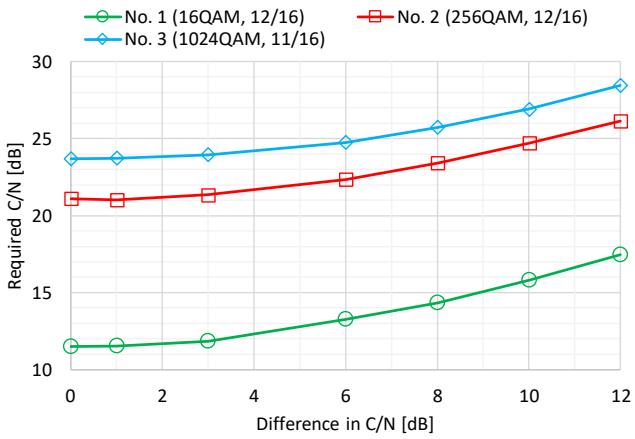

Figure 5.3 Required CNR with difference between CNR values for signals #1 and #2 in laboratory experiments.

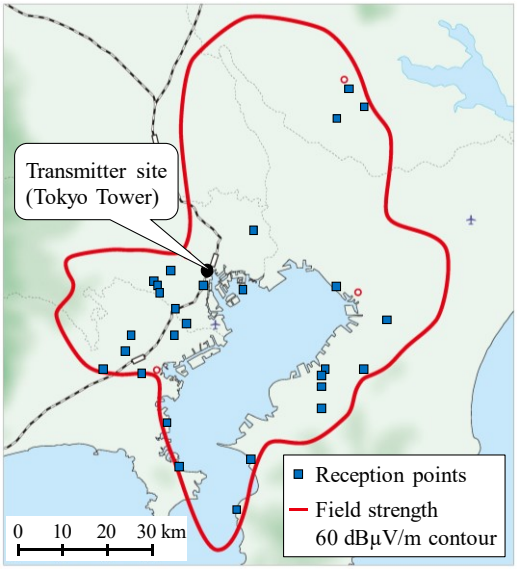

Figure 5.4 Location of experimental test station and reception points in Tokyo

difference between the CNR values for the horizontally and vertically polarized waves was also evaluated for the MIMO parameter sets.

Figure 5.2 shows the BER characteristics for each parameter set in an ideal AWGN channel measured in laboratory. The required CNR values are summarized in Table 5.2. It was confirmed that the difference in the required CNR compared with SISO were -9.6 dB, 0 dB, and +2.6 dB for MIMO parameter sets No. 1, 2, and 3, respectively.

Figure 5.3 shows the average value of the required CNRs between input signals #1 and #2 to the demodulator in Figure 2.11 with a specific difference between the CNR values for signals #1 and #2 for all MIMO parameter sets. The results showed that the required CNRs gradually degraded as the difference between each CNR increased. The

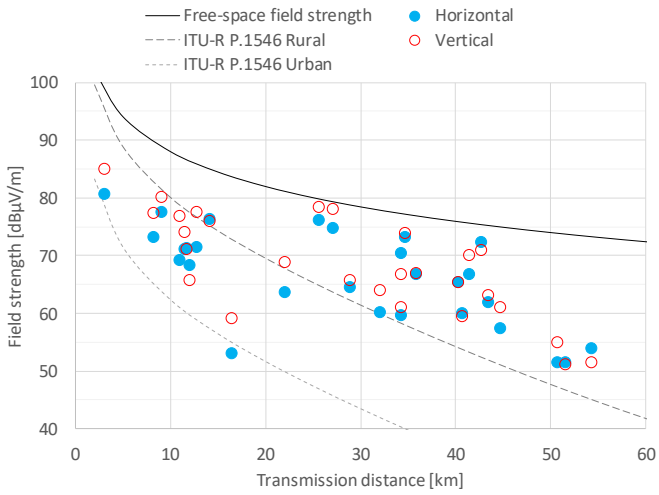

Figure 5.5 Field strength measured in field experiments in Tokyo.

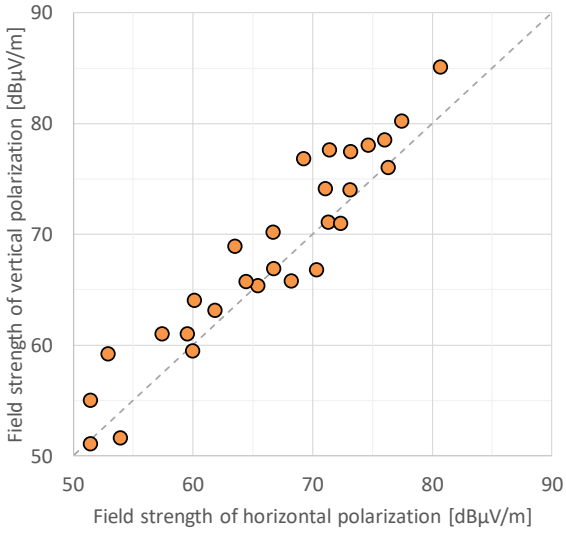

Figure 5.6 Distribution of field strength of horizontal and vertical polarization in field experiments in Tokyo.

degradation was below 1 dB compared with the ideal condition (0 dB difference in CNR) when the difference was less than 3 dB.

5.1.2. Field Experiments

The location of the transmitting station is shown in Figure 5.4. The contour, indicated by a red line, corresponds to the service area for the current DTTB system, ISDB-T, with an electric field strength of 60 dBμV/m. We selected 28 reception points within the contour, and the required received power was measured. For follow-up verification, a MIMO channel snapshot was captured at each point.

A. Field Strength

Figure 5.5 shows the measurement results of the field strength of the horizontally and vertically polarized waves at 28 points. The values of the horizontal wave (solid blue circles in Figure 5.5) were measured with the horizontal element of the receiving antenna while transmitting the radio wave from only Tx 1 (horizontally polarized antenna). Likewise, the values of the vertical wave (red circles in Figure 5.5) were observed by emitting the signal from only Tx 2 (vertically polarized antenna). As shown in Figure 5.5, the results of the field strength measured within 20 km of the transmission distance were lower than the calculated values with a prediction model for rural areas [114], and those closer points were objectively in urban areas. The field strength for the reception points located beyond a 20-km transmission distance were distributed along with or higher than the values predicted for rural areas, and those points were in rural areas.

Figure 5.6 shows the distribution of the field strengths of the horizontally and vertically polarized waves at the 28 points. As shown, the strengths of both waves were almost equally distributed. The transmission facility was designed so that the effective radiation power (E.R.P) of the experimental test station had the same value for both the horizontally and vertically polarized waves.

Figure 5.7 shows the distribution of the difference in field strength obtained by subtracting the field strength of the horizontally polarized wave from that of the vertically polarized wave. That is, when the difference in the field strength is a positive value, it meant that the vertical field strength was high. The maximum difference was 7.5 dB, at which the value of vertical polarization was higher than that of horizontal polarization. The results showed that the difference was independent of the transmission distance, and the field strength of vertical polarization tended to be higher than that of horizontal polarization. The reason the vertically polarized waves were high in the field experiments was due to the difference in the propagation path. It has been mentioned that one advantage of using horizontal polarization is that undesired polarization is not received because of the greater directivity obtainable at the receive antenna at UHF [93], which reduces the effect of reflected waves, particularly in urban areas. The experimental results shown in this subsection align with this description; however, the number of samples (reception points) was limited, so detailed analysis with a higher number of samples is needed to analyze the propagation for each polarization.

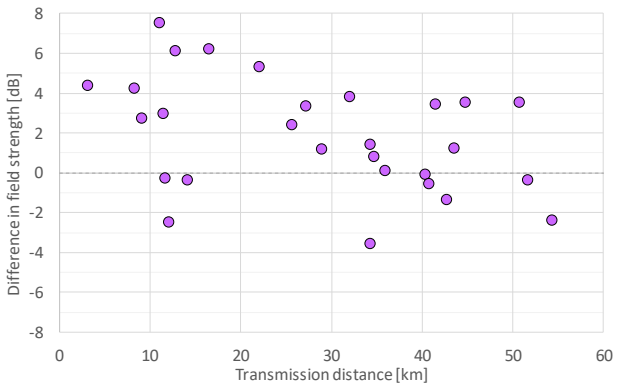

Figure 5.7 Difference in field strength between horizontal and vertical polarization (vertical minus horizontal) in field experiments in Tokyo.

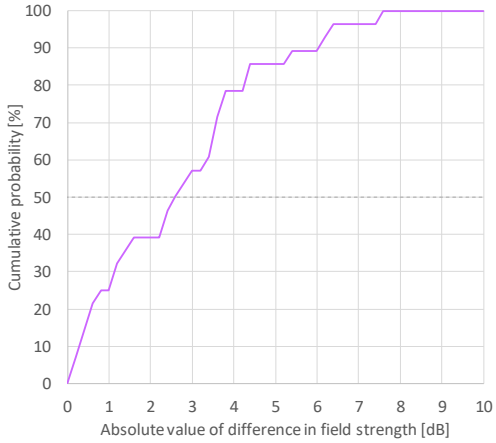

Figure 5.8 Cumulative probability of absolute value of difference in field strength between horizontal and vertical in field experiments in Tokyo.

Figure 5.8 shows the cumulative probability of the absolute value of the difference in field strength between horizontal and vertical polarization. As shown, the 50-percentile absolute difference in the field strength observed was about 2.5 dB. It can be concluded that when introducing dual-polarized MIMO, a difference in received power is unavoidable. The transmitter power can be increased in one of the polarizations to compensate for this difference. However, it is impossible to compensate for the differences for all receivers since the difference in the electric field strength differs depending on the reception environment.

B. Required Received Power for QEF

Next, we compared the required received power of the SISO and MIMO parameter sets. Figure 5.9 shows the results of plotting the required received power of SISO and MIMO at the 28 reception points against the transmission capacity. The results showed that the plots of MIMO were widely distributed compared with SISO.

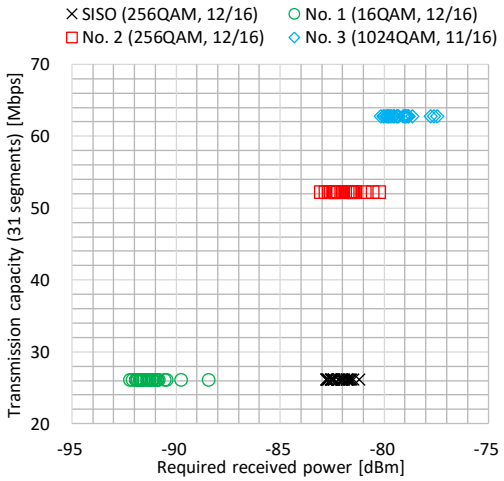

Figure 5.9 Distribution of required received power at 28 reception points.

Table 5.3 summarizes the values of the required received power obtained in the field experiments. The methodologies are described in Section 2.7. Theoretical values were also calculated based on the required CNRs measured in the laboratory test results in Table 5.2 assuming a noise power of -104.5 dBm at the LNAs as based on the noise figure of 1.8 dB specified in the LNA product data sheet. The required received power in an ideal AWGN channel for the experimental equipment measured in the laboratory is shown as a reference. It was considered that the difference of 0.2 dB observed in the laboratory tests between SISO and MIMO parameter set No. 2 was introduced due to an individual difference of the noise figure characteristics at the LNAs used. The minimum, median, and maximum values of the required received power are shown for comparison.

Table 5.4 shows the degradation in the required received power measured in the field experiments compared with the laboratory results. As shown, the median value of the deterioration in SISO was 0.8 dB. In MIMO parameter sets No. 1, 2, and 3, the median values were 1.0, 1.1, and 1.1 dB, confirming that MIMO did not experience a significant increase in required received power at the median compared with SISO. It should be noted that the maximum degradation in SISO was 1.7 dB, while the maximum degradations were 3.9, 2.8, and 3.0 dB for MIMO parameters sets No. 1, 2, and 3. That is, the degradation can increase in MIMO transmission in the worst case. Since it is assumed that there is no difference in urban noise (man-made noise) regarding polarization, the degradation in the MIMO system performance could have been influenced by urban buildings or terrain that caused a difference in reflection characteristics related to polarization.

Table 5.3 Required received power measured in field experiments in Tokyo.

		SISO (256QAM, 12/16)	MIMO		
			No. 1 (64QAM, 12/16)	No. 2 (256QAM, 12/16)	No. 3 (1024QAM, 11/16)
Theoretical [dBm]		-83.4	-93.0	-83.4	-80.8
Laboratory [dBm]		-82.9	-92.4	-83.1	-80.5
Field [dBm]	Minimum	-82.8	-92.2	-83.0	-80.2
	Median	-82.1	-91.4	-82.0	-79.4
	Maximum	-81.2	-88.5	-80.3	-77.5

Table 5.4 Degradation in required received power measured in field experiments in Tokyo compared with laboratory results.

		SISO (256QAM, 12/16)	MIMO		
			No. 1 (64QAM, 12/16)	No. 2 (256QAM, 12/16)	No. 3 (1024QAM, 11/16)
Field [dB]	Minimum	0.1	0.2	0.1	0.3
	Median	0.8	1.0	1.1	1.1
	Maximum	1.7	3.9	2.8	3.0

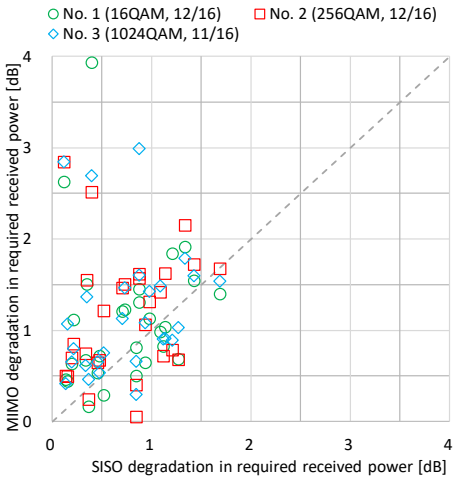

Figure 5.10 Comparison of degradation in required received power between SISO and MIMO in field experiments in Tokyo.

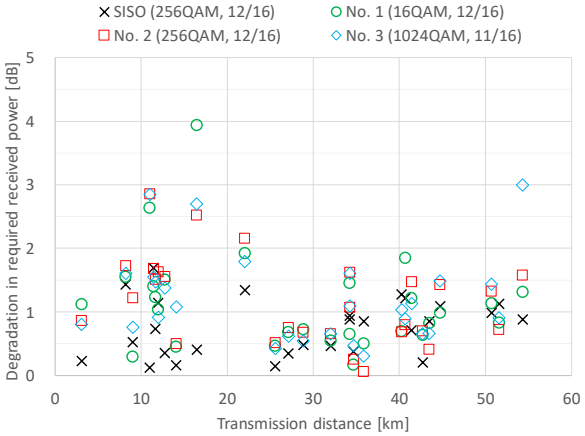

Figure 5.11 Degradation in required received power from viewpoint of transmission distance in field experiments in Tokyo.

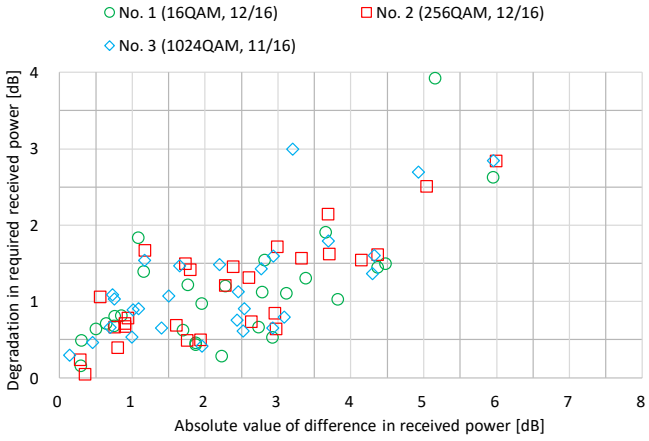

Figure 5.12 Degradation in required received power from viewpoint of absolute value of difference in received power between horizontal and vertical polarization in field experiments in Tokyo.

Figure 5.10 compares the degradation in the required received power of SISO and MIMO in the field experiments. The degradations are calculated with the ideal values

Table 5.5 Difference in required received power compared with SISO in field experiments in Tokyo (positive value means higher received power required)

		MIMO		
		No. 1 (64QAM, 12/16)	**No. 2 (256QAM, 12/16)**	**No. 3 (1024QAM, 11/16)**
Field [dB]	Minimum	-9.4	-0.2	+2.6
	Median	-9.3	+0.1	+2.7
	Maximum	-7.3	+0.9	+3.7

obtained in laboratory experiments as a reference. As we can see, the required received powers were almost the same and distributed on the dotted line, which indicates the same degradation for SISO and MIMOs except for a few reception points. Figure 5.11 shows the degradation compared to the laboratory results in the required received power plotted against the transmission distance. The results showed that the degradation amount was independent of the transmission distance. Figure 5.12 shows the degradation compared to the laboratory results in the required received power versus the absolute value of the difference in received power between horizontal and vertical polarization. The results showed that the degradation in the required received power increased as the difference in the received power increased. Note that the difference in the received power was calculated on the basis of the received power measured for each polarization while transmitting horizontally and vertically polarized waves with Tx 1 and 2 simultaneously in the field experiments.

Table 5.5 summarizes the differences in the required received power in the MIMO parameter sets compared with SISO, which were calculated by subtracting the required received power of SISO from the values of MIMO obtained in the field experiments as shown in Table 5.3. That is, when the difference in the received power was a positive value, it meant that MIMO requires a higher received power compared with SISO. The required power can be improved by at least 7.3 dB with MIMO parameter set No. 1, in which MIMO is introduced with the same transmission capacity as the reference SISO configuration. This demonstrated that by introducing MIMO, we can expect transmission to be robust in a real environment. It was confirmed that the required power is degraded compared to the laboratory results by at most 0.9 dB with MIMO parameter set No. 2, in which MIMO is introduced with the same carrier modulation and code rate as the reference SISO, doubling the transmission capacity. The required power is also deteriorated by at most 3.7 dB with MIMO parameter set No. 3, in which a transmission capacity of 62.8 Mbps is achieved for fixed reception assuming the provision of a VVC

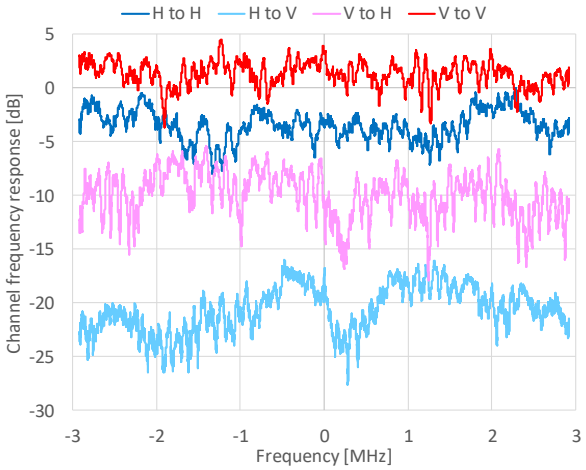

Figure 5.13 Example of MIMO channel frequency responses captured in field experiments in Tokyo

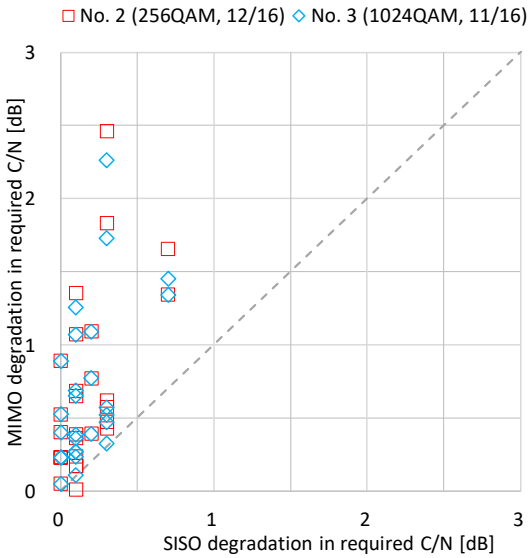

Figure 5.14 Comparison of degradation in required CNR between SISO and MIMO for each MIMO channel snapshot compared with required CNR in AWGN channel in laboratory experiments.

encoded 8K program within a single 6-MHz channel. It is necessary to note that the MIMO gain (7.3 dB in robustness or greatly increased capacity) was obtained on the condition that the transmission power for MIMO is doubled compared with SISO.

5.1.3. Follow-up Verification in Laboratory

Figure 5.13 shows an example of the four CFRs of a snapshot in which we observed the highest difference in field strength between horizontally and vertically polarized waves in the field measurements. The reason for the difference, namely in the average value, was considered to be that the strength varied in the height direction due to the difference in the reflection characteristics. In the experiments, the receiving antenna height was fixed to 10 m above ground level, but it was observed that the values of the

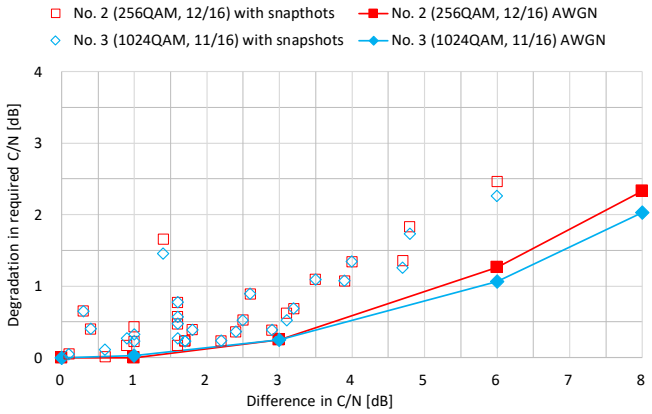

Figure 5.15 Degradation in required CNR from viewpoint of difference in CNR between horizontal and vertical polarization for each MIMO channel snapshot compared with required CNR in AWGN channel in laboratory experiments without difference in CNR.

Table 5.6 Degradation of required CNR measured with MIMO channel snapshots compared with AWGN channel in laboratory experiments

		SISO (256QAM, 12/16)	MIMO	
			No. 2 (256QAM, 12/16)	No. 3 (1024QAM, 11/16)
Field [dB]	Minimum	0	0	0.1
	Median	0.1	0.5	0.5
	Maximum	0.7	2.5	2.3

vertical and horizontal electric field strengths varied independently depending on the reception height.

As the main motivation to introduce MIMO in DTTB is improving the transmission capacity, parameter sets No. 2 and 3 were verified in the laboratory experiments. Figure 5.14 shows the results of plotting the degradation in the required CNR of SISO and MIMO by using the MIMO channel snapshots captured in the field experiments compared with the values measured in the AWGN channel shown in Table 5.2. The results showed that the degradation in the required CNR for SISO was smaller than that for MIMO at all 28 reception points when removing the uncertainties that affected the evaluation results in the field experiments, such as fluctuation in field strength. We observed in the experiments that the received power fluctuated. It was concluded that the fluctuation in the received power during the observation time slot for the $1E^{+10}$ bits would have affected the evaluation results in the field experiments.

Figure 5.15 shows the degradation in the required CNR versus the difference in CNR between horizontal and vertical polarization with the MIMO channel snapshots compared

with the values measured in the AWGN channel in laboratory experiments shown in Table 5.2. It was concluded that the degradation in the required CNR increased along with the increase in the difference in CNR between both polarizations. It was also confirmed that the degradation in required CNR for MIMO parameter sets No. 2 and 3 was almost the same at the 28 reception points.

Table 5.6 summarizes the degradation in required received CNR measured with the MIMO channel snapshots compared with that in the AWGN channel measured in the laboratory. As shown, the median value of the deterioration in SISO was 0.1 dB in Table 5.6. For MIMO parameter sets No. 2 and 3, the median values were 0.5 dB, confirming that MIMO did not experience a significant increase in required CNR compared with SISO when compared with the median values. The maximum degradation in SISO was 0.7 dB in Table 5.6, while the maximum degradations were 2.5 and 2.3 dB for MIMO parameter sets No. 2 and 3. The reason why the values in Table 5.6 were smaller than those in Table 5.4 is considered that the effects of fluctuation in the field strength or/and the effects of a man-made noise were removed. It was concluded that the degradation can increase in MIMO transmission in the worst case even in the reproduced static channel. It should be noted that the required CNR for MIMO was defined as the average value of horizontally and vertically polarized waves and that a difference in CNR can produce a certain level of degradation in MIMO transmission.

5.2. Evaluation in Osaka area

5.2.1. Field Experiments

We obtained MIMO channel snapshots at 101 points in Figure 5.16 using an experimental test station [116] set up in the Osaka area. The measurement points were selected from within the contour where the calculated electric field strength of the experimental test station equals 60 dBμV/m. About 10 of the measurement points were NLOS due to buildings. Details of the field experimental system are shown in Section 2.7. The transmission parameters used for the field experiments are listed in Table 5.7.

Accompanying the MIMO channel capture, the electric field strength of each polarization was measured while transmitting the radio wave either from vertical element or horizontal element. We also measured the cross polarization isolation (XPI), which is defined as the received signal power ratio between co-polarized and cross-polarized transmitting signals.

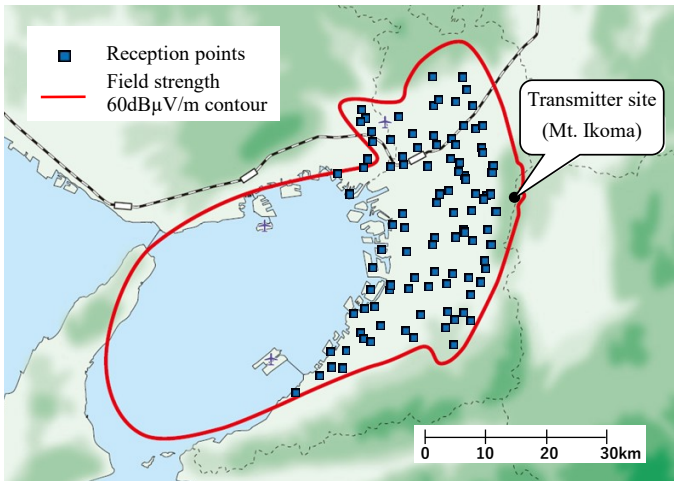

Figure 5.16 Location of experimental test station and reception points in Osaka

Table 5.7 Parameter sets for follow-up verification in simulation

	Parameter set				
	SISO	MIMO			
	(reference)	20 dB	19 dB	18 dB	12 dB
Occupied bandwidth	Normal mode: 5.83 MHz				
Number of segments	Normal mode: 35 (31 segments used for fixed reception evaluation)				
FFT size	16,384				
Guard interval ratio (duration)	800/16,384 (126 μsec)				
Scattered pilot ratio	1/24				
Carrier modulation	1024QAM Non-uniform	1024QAM Non-uniform	256QAM Non-uniform	256QAM Non-uniform	64QAM Non-uniform
Inner code rate	9/16	9/16	11/16	10/16	8/16
System	SISO (horizontal)	MIMO (open-loop spatial multiplexing 2×2 cross-polarized)			
Transmission capacity (31 segments)	25.6 Mbps	51.2 Mbps	50.2 Mbps	45.6 Mbps	27.3 Mbps
Required C/N (AWGN)	20.0 dB	20.4 dB	19.7 dB	18.2 dB	11.8 dB

Figure 5.17 shows the measured electric field strength of the horizontally polarized wave E_H and vertically polarized wave E_V at 101 points. Figure 5.18 shows the cumulative probability of the difference value (E_H - E_V) in the field strength obtained by subtracting the field strength of the horizontally polarized wave from that of the vertically polarized wave. When the difference is a positive value, it meant that the vertical field strength was high. From Figure 5.18, the 50-percentile difference was 0 dB, and no bias was observed in the electric field strength of each polarization. Figure 5.19 shows the cumulative probability of the absolute value of the difference $|E_H - E_V|$ in the field strength between horizontal and vertical polarization. The 50-percentile absolute difference was about 2 dB. This value matches the value of 2.5 dB measured in Tokyo presented in 5.1.2.

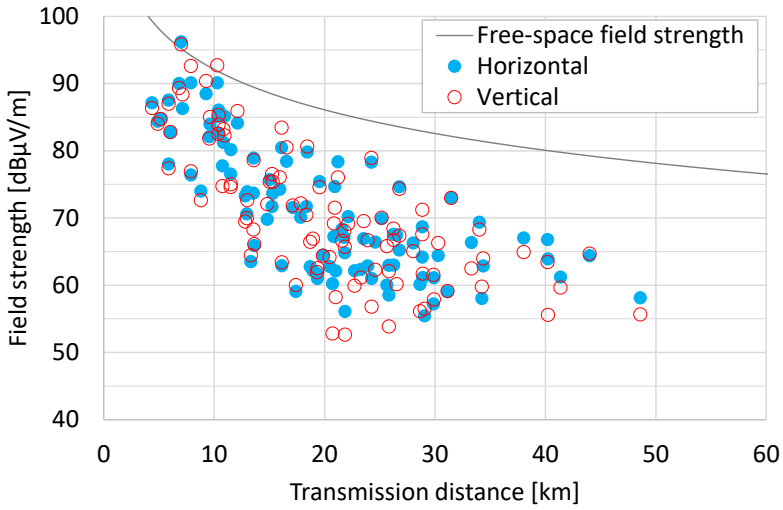

Figure 5.17 Field strength measured in field experiments in Osaka.

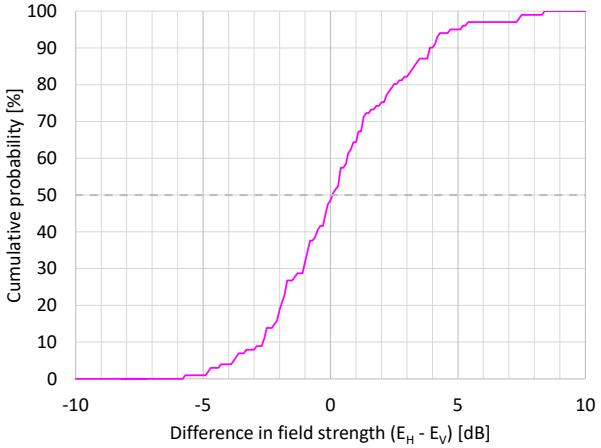

Figure 5.18 Cumulative probability of difference value in field strength between horizontal and vertical in field experiments in Osaka.

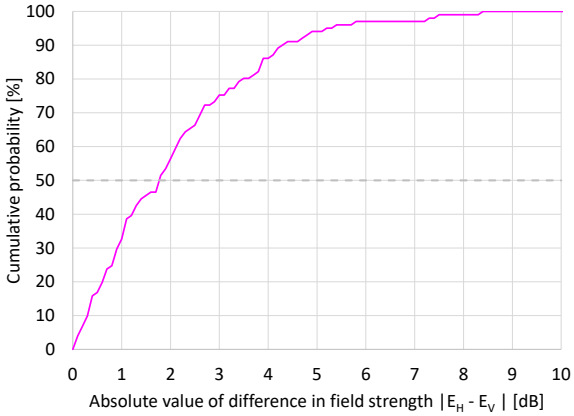

Figure 5.19 Cumulative probability of absolute value of difference in field strength between horizontal and vertical in field experiments in Osaka.

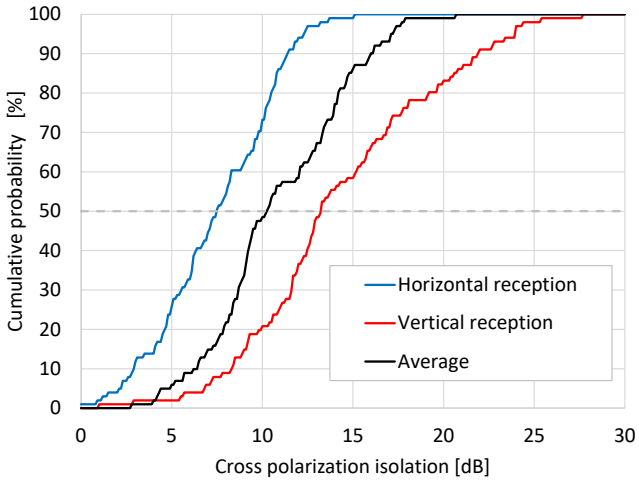

Figure 5.20 Cumulative probability of cross polarization isolation (XPI) in field experiments in Osaka.

Figure 5.20 shows the cumulative probability of measured XPI. The XPI values are calculated as:

$$XPI_H = P_{HH} - P_{VH} \tag{5.1}$$

$$XPI_V = P_{VV} - P_{HV} \tag{5.2}$$

$$XPI_{ave} = (XPI_H + XPI_V)/2 \tag{5.3}$$

where XPI_H and XPI_V are the XPI values in dB for horizontal and vertical reception. XPI_{ave} is calculated at each reception point as the average value of XPI_H and XPI_V. P_{HH} is the received power measured with the horizontal element of the receiving antenna while transmitting the radio wave from horizontal element only. P_{VH} is the received power measured with the horizontal element of the receiving antenna while transmitting the radio wave from vertical element. In the same manner, P_{VV} and P_{HV} are the received power at the vertical element of the receiving antenna while transmitting the radio wave either from vertical or horizontal element, respectively. The received power was measured at the input point of the LNA for each polarization.

According to Figure 5.20, the values of XPI are different between horizontal and vertical polarization. Since there is no difference between the gains of horizontal and vertical polarized transmitting antenna, nor receiving antenna, it is considered that the difference was caused due to the reflection characteristics of each polarized wave in the propagation path. From Figure 5.20, the 50-percentile XPI is approximately 7.5 dB, 13 dB and 10 dB for horizontal, vertical and the average.

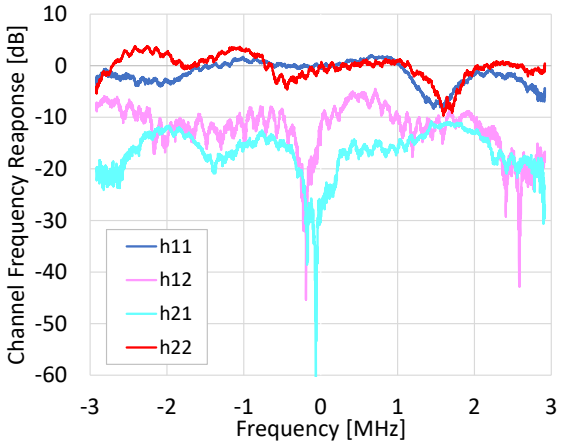

Figure 5.21 Example of MIMO channel frequency responses captured in field experiments in Osaka

While transmitting radio waves from both polarized elements simultaneously, each output signal of the band-pass filter in Figure 2.11 was input to a MIMO channel analyzer to obtain the MIMO channel responses. Figure 5.21 shows an example of the MIMO channel frequency responses captured in the field experiments. The electric field strength at this point were 67.1 and 68.1 dBμV/m for horizontal and vertical polarizations, and the difference in the electric field strength (E_H - E_V) was -1 dB.

5.2.2. Follow-up Verification in Simulation

With the MIMO channel snapshots of 101 points, the required CNR for QEF was evaluated by physical layer simulations. Table 5.7 shows the evaluated transmission parameters for the follow-up verification in simulation. It has been reported that the required CNR of MIMO deteriorates by about 1 dB compared with SISO, when the same carrier modulation and coding rate are configured [117]. In addition, Table 5.6 showed that the maximum degradation in SISO was 0.7 dB for 28 snapshots captured in Tokyo, while the maximum degradations were 2.5 and 2.3 dB for MIMO parameter sets. Based on the previous studies, it is expected that the required CNR of MIMO would degrade by 1 dB or more, and three parameter sets for the required CNR of 20 dB, 19 dB, and 18 dB were selected. As a parameter set that has the same capacity as the reference SISO, MIMO parameters for the required CNR of 12 dB was evaluated. Since MIMO can transmit two stream signals with horizontally and vertically polarized waves, it is possible to use robust carrier modulation/coding rate maintaining the same transmission capacity as SISO.

Figure 5.22 shows the cumulative probability of the required CNR for the parameters for required CNR of 20 dB, 19 dB, and 18 dB. For each snapshot one CNR is calculated in simulation. Although the slopes of SISO and MIMO are different, the 50-percentile

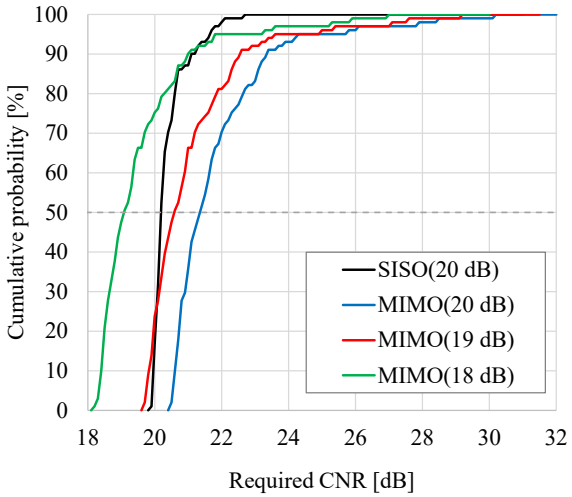

Figure 5.22 Cumulative probability of required CNR in follow-up simulation with 101 snapshots captured in Osaka.

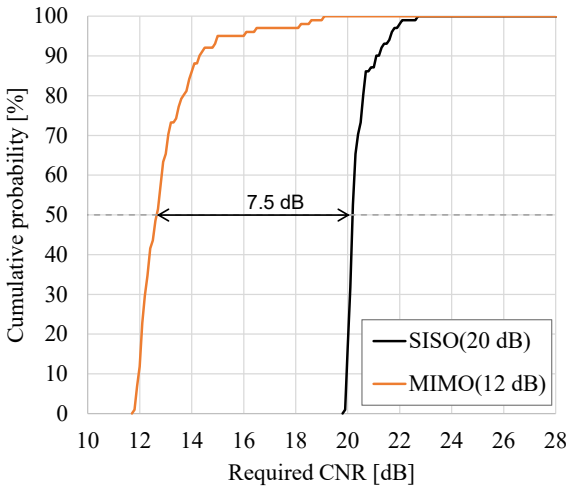

Figure 5.23 Cumulative probability of required CNR in follow-up simulation with 101 snapshots captured in Osaka.

required CNR of SISO (20 dB) was between the values of MIMO (18 dB) and MIMO (19 dB). When comparing the transmission capacity of SISO with that of MIMO (18 dB), the capacity is 25.6 Mbps for SISO and 45.6 Mbps for MIMO, which is about 1.8 times higher than SISO.

Figure 5.23 shows the cumulative probability of the required CNR for the parameter for required CNR of 12 dB. The improvement in the required CNR for MIMO over SISO was 7.5 dB at the 50-percentile value. This result is consistent with the values in Table 5.5, in which an improvement of 7.3 dB was obtained at worst case. Although the required CNR has improved due to the introduction of MIMO, MIMO transmits two signals, and the transmission power is doubled compared to SISO. The amount of improvement decreases by 3 dB when the transmission power is constant for SISO and MIMO.

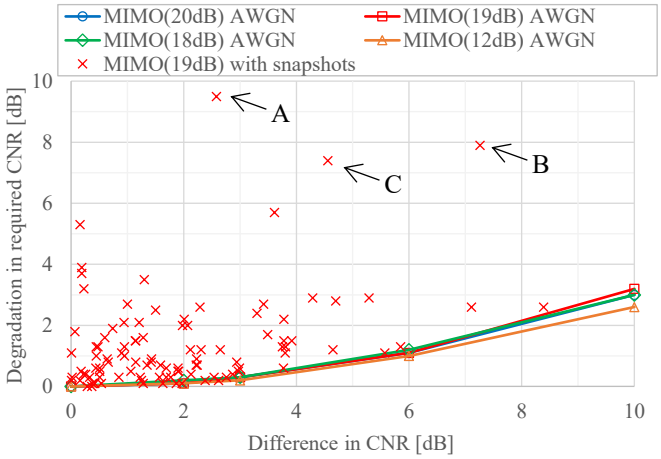

Figure 5.24 Degradation in required CNR from viewpoint of difference in CNR between horizontal and vertical polarization for each MIMO channel snapshot compared with required CNR in AWGN channel without difference in CNR in simulations.

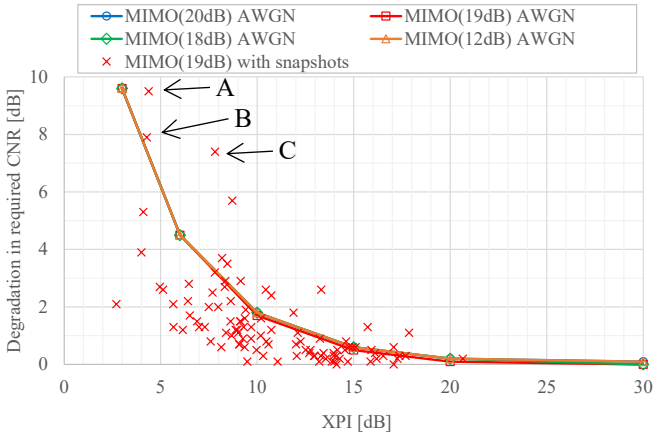

Figure 5.25 Degradation in required CNR from viewpoint of average XPI between horizontal and vertical polarization for each MIMO channel snapshot compared with required CNR in AWGN channel with infinite XPI in simulations.

We evaluated the influence of the difference in CNR between horizontal and vertical polarization as a degrading factor of the transmission performance. Figure 5.24 shows the degradation in the required CNR of MIMO (19 dB) with the MIMO channel snapshots compared with the values measured in the AWGN channel shown in Table 5.7. For reference, the results of MIMO (20 dB), MIMO (19 dB), MIMO (18 dB) and MIMO (12 dB) in the PI channel (2.18) are shown with a solid line in Figure 5.24. It was concluded that the degradation in the required CNR increased along with the increase in the difference in CNR between both polarizations. It was also confirmed that the degradation in required CNR for MIMO parameter sets MIMO (20 dB), MIMO (19 dB), MIMO (18 dB) and MIMO (12 dB) is almost the same for the power imbalance channel. In the results with MIMO channel snapshots, there are some plots where the required CNR is greatly

degraded even though the difference in the CNR is small. This gap seems to be caused by the interference due to the cross-polarized wave and/or multipath echoes.

We verified the influence of the XPI as a degrading factor of the transmission performance. Figure 5.25 shows the degradation in the required CNR of MIMO (19 dB) with the MIMO channel snapshots compared with the values measured in the AWGN channel shown in Table 5.7. Here, the XPI was calculated as the average value of horizontal and vertical polarizations. For reference, the results of MIMO (20 dB), MIMO (19 dB), MIMO (18 dB) and MIMO (12 dB) in the cross-polarized channel (2.20) are shown with a solid line in Figure 5.25. It was observed that the degradation in the required CNR increased along with the decrease in the XPI. The results also showed that the degradation in required CNR for MIMO parameter sets MIMO (20 dB), MIMO (19 dB), MIMO (18 dB) and MIMO (12 dB) is almost the same for the XPD channel. The plots tend to be distributed in a band around the solid line, suggesting that the required CNR varies due to factors other than the XPI. For the points A, B and C in Figure 5.24 in which a large gap was observed in the required CNR, the results in Figure 5.25 indicates that the deterioration in the performance was caused by the low XPI.

5.2.3. Channel Modeling

Simple 8-tap fixed rooftop reception MIMO channel models are generated from 101 snapshots captured in the field experiments. To evaluate MIMO practical gain in broadcasting, we also created 8-tap SISO channel models. With the generated models, we evaluated the gain of MIMO over SISO in fixed reception by physical layer simulation.

The 8-tap deterministic models were generated using the following steps.

a) Calculate the required CNR at 101 points by physical layer simulation and calculate the cumulative probability of the required CNR values obtained.
b) Select the reception points where the cumulative probability corresponds to the required CNR of 50-percentile, 80-percentile, 90-percentile, 95-percentile, 99-percentile values.
c) Extract the top N taps with the highest level from the channel impulse response in time domain and normalize the N taps at each selected point.

Here, in the step c) for SISO, the top N taps were selected in descending order of the value of $|h_{11}|^2$. As for MIMO, the top N taps were chosen in descending order of the total power $|h_{11}|^2+|h_{12}|^2+|h_{21}|^2+|h_{22}|^2$ of the four impulse response components.

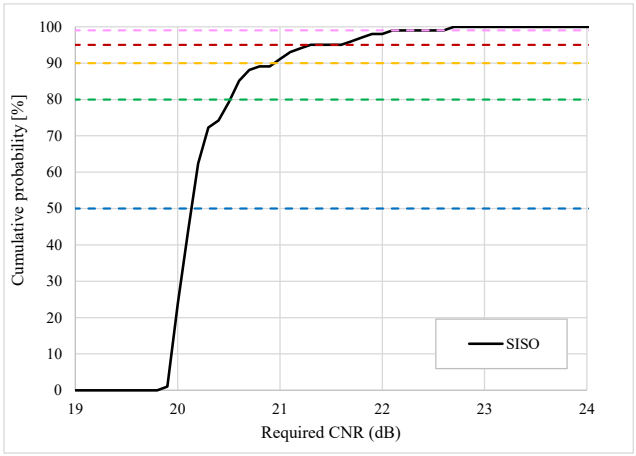

Figure 5.26 Cumulative probability of required CNR for SISO with 101 snapshots captured in Osaka.

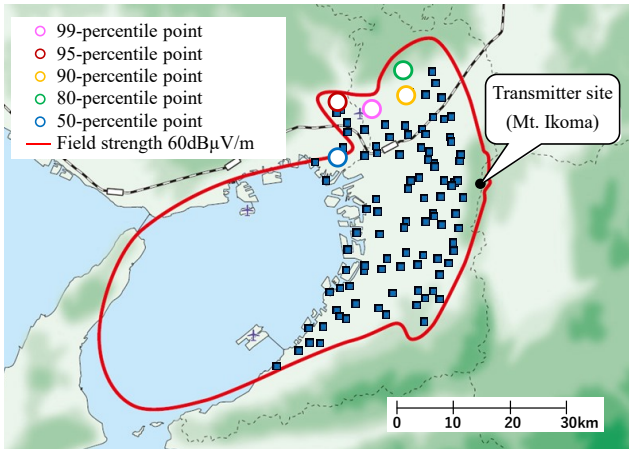

Figure 5.27 Location of 50, 80, 90, 95 and 99-percentile points for SISO.

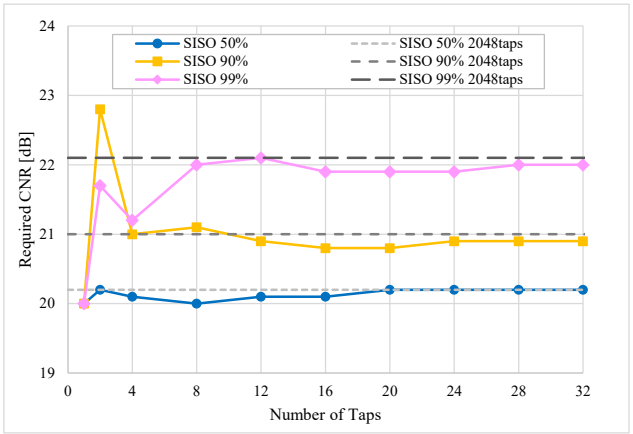

Figure 5.28 Convergence of required CNR due to number of taps of SISO channel model

First, we describe the 8-tap SISO channel models generated. Figure 5.26 shows the cumulative probability of the required CNR evaluated with the SISO parameters in Table 5.7. The 50-percentile, 80-percentile, 90-percentile, 95-percentile, and 99-percentile lines are described with dashed lines in Figure 5.26. The locations of the selected points corresponding to each percentile are shown in Figure 5.27. The simulation result of the

required CNR by changing the number of taps is presented in Figure 5.28 in which the dashed line indicates the value with 2048-taps that corresponds to 324 μsec. Note that the required CNR is converged to 20 dB at 1-tap for all of 50-percentile, 90-percentile and 99-percentile, because the 1-tap channel is equivalent to an ideal AWGN channel. It was observed that by increasing the number of taps, the results approach asymptotically to the dashed lines. Although he required number of taps to converge to the dashed line that is 2048-taps differs depending on the reception point, it can be seen that a larger percentile tends to require a larger number of taps. This trend can be explained because a reception point with a larger percentage is in a difficult reception environment and the channel is distorted by multiple echoes.

The 8-tap fixed roof-top SISO channel models generated are shown in Table 5.8, Table 5.9, Table 5.10, Table 5.11 and Table 5.12, where the amplitude A in dB and the phase φ in rad of each impulse response h_{11} is listed. The tap value h in linear unit is calculated as:

$$h = 10^{\frac{A}{20}} e^{j\varphi} \tag{5.4}$$

where j is the imaginary unit, e is Napier's constant, A in dB is the amplitude and φ in rad is the phase.

Next, we created 8-tap MIMO channel models following the procedure mentioned above. Figure 5.29 shows the cumulative probability of the required CNR evaluated with the MIMO (20 dB) parameters in Table 5.7. The dashed lines indicate 50-percentile, 80-percentile, 90-percentile, 95-percentile, and 99-percentile. The locations of the selected points corresponding to each percentile are depicted in Figure 5.30. The simulation result of the required CNR by changing the number of taps is presented in Figure 5.31 in which the dashed line shows the value with 2048-taps that corresponds to 324 μsec. It should be noted that the required CNR of each percentile does not converge at 1-tap. This is because, unlike the case of SISO, the cross-polar interference degrades the performance even in the 1-tap channel. It can be seen that the results approach asymptotically to the dashed lines by increasing the number of taps in Figure 5.31. It was confirmed that by setting the number of taps to 8 the gap from the dashed line can be suppressed to less than 1 dB.

Table 5.8 Tap values of 50-percentile SISO fixed roof-top channel

Tap number	Excess delay [μs]	h_{11} [dB]	h_{11} [rad]
1	-0.4746	-22.3	-2.56
2	-0.3164	-20.5	-2.52
3	-0.1582	-20.2	-2.37
4	0	-0.4	-2.72
5	0.1582	-16.3	-0.36
6	0.3164	-17	-0.14
7	0.4746	-17.6	0.36
8	0.791	-20.2	0.44

Table 5.9 Tap values of 80-percentile SISO fixed roof-top channel

Tap number	Excess delay [μs]	h_{11} [dB]	h_{11} [rad]
1	-0.6328	-22.7	0.82
2	-0.4746	-21.1	0.82
3	-0.3164	-19	0.84
4	-0.1582	-16.3	0.86
5	0	-2.5	0.89
6	0.1582	-4.6	-1.88
7	0.3164	-15.5	-2.4
8	0.6328	-22.2	-1.47

Table 5.10 Tap values of 90-percentile SISO fixed roof-top channel

Tap number	Excess delay [μs]	h_{11} [dB]	h_{11} [rad]
1	-0.3164	-24.5	0.25
2	-0.1582	-22.2	0.07
3	0	-3.6	0.04
4	0.1582	-4.2	2.82
5	0.3164	-8.9	2.48
6	0.4746	-22	1.23
7	0.6328	-17.4	-2.1
8	0.791	-16.6	-2.2

Table 5.11 Tap values of 95-percentile SISO fixed roof-top channel

Tap number	Excess delay [μs]	h_{11} [dB]	h_{11} [rad]
1	-0.3164	-27.5	-0.85
2	-0.1582	-12.5	-0.82
3	0	-1.2	2.61
4	0.1582	-15.2	1.92
5	0.3164	-8.7	2.19
6	0.4746	-17.3	0.89
7	0.791	-22.9	0.6
8	0.9492	-25.5	-2.72

Table 5.12 Tap values of 99-percentile SISO fixed roof-top channel

Tap number	Excess delay [μs]	h_{11} [dB]	h_{11} [rad]
1	-0.6328	-18.7	-2.55
2	-0.4746	-11.3	-2.55
3	-0.3164	-9.9	0.24
4	-0.1582	-7.1	1.39
5	0	-5.8	-2.82
6	0.1582	-9.6	1.42
7	0.3164	-7	0.92
8	0.4746	-14.2	0.13

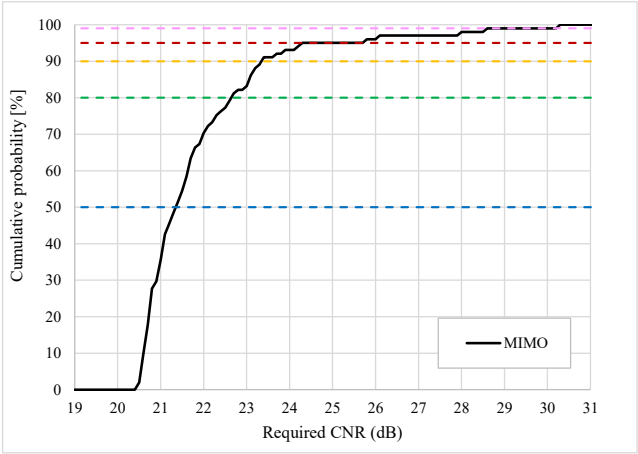

Figure 5.29 Cumulative probability of required CNR for MIMO with 101 snapshots captured in Osaka.

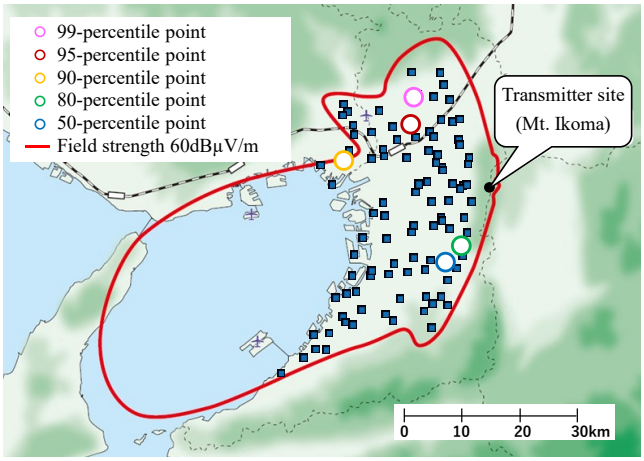

Figure 5.30 Location of 50, 80, 90, 95 and 99-percentile points for MIMO.

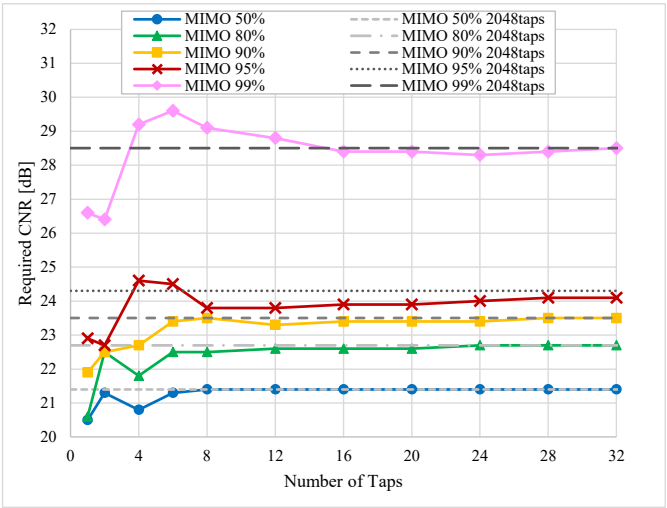

Figure 5.31 Convergence of required CNR due to number of taps of MIMO channel model

Based on the above results, MIMO channel modeling was performed with the number of taps set to 8. The impulse response of each percentile model is shown in Table 5.13, Table 5.14, Table 5.15, Table 5.16 and Table 5.17.

Table 5.13 Tap values of 50-percentile MIMO fixed roof-top channel

Tap number	Excess delay [μs]	h_{11}		h_{12}		h_{21}		h_{22}	
		[dB]	[rad]	[dB]	[rad]	[dB]	[rad]	[dB]	[rad]
1	-0.4746	-48.1	-0.92	-37.8	0.81	-20.7	-2.12	-24	1.25
2	-0.3164	-36.6	-1.13	-38	0.79	-13.4	1.04	-20	1.17
3	-0.1582	-17	-1.05	-37.6	0.78	-27.8	1.49	-6.3	0.94
4	0	-1.3	2.2	-36.1	0.77	-26.9	0.95	-2	-2.38
5	0.1582	-14.7	2.28	-26.3	0.92	-30.5	0.96	-7.4	-2.11
6	0.3164	-33.9	3.05	-13.8	-1.95	-34.2	0.14	-18	-1.82
7	0.4746	-34.8	2.25	-21.4	-1.98	-43.4	1.82	-27.6	-0.88
8	0.6328	-40.2	2.54	-32.7	2.77	-49	2.1	-26.7	-2.38

Table 5.14 Tap values of 80-percentile MIMO fixed roof-top channel

Tap number	Excess delay [μs]	h_{11}		h_{12}		h_{21}		h_{22}	
		[dB]	[rad]	[dB]	[rad]	[dB]	[rad]	[dB]	[rad]
1	-0.4746	-20	-0.48	-30.3	-1.11	-10.6	1.49	-25.9	-0.08
2	-0.3164	-16.7	-0.49	-29.6	-1.11	-15.6	-1.84	-23.7	-0.01
3	-0.1582	-3.4	-0.59	-28.9	-1.1	-19.9	-1.86	-22.8	0.19
4	0	-3.3	2.31	-27.6	-1.09	-22.1	-1.91	-2.2	-0.14
5	0.1582	-9.8	2.82	-25.6	-1.12	-28.8	-1.56	-18.5	-2.7
6	0.3164	-13.7	2.74	-15.1	-1.33	-28.9	-1.45	-22.9	2.83
7	0.4746	-16.2	2.6	-14.2	1.69	-32.7	-1.1	-19	-2.94
8	0.6328	-22.1	2.5	-20.9	1.77	-32	-1.19	-27.7	1.66

Table 5.15 Tap values of 90-percentile MIMO fixed roof-top channel

Tap number	Excess delay [μs]	h_{11}		h_{12}		h_{21}		h_{22}	
		[dB]	[rad]	[dB]	[rad]	[dB]	[rad]	[dB]	[rad]
1	-0.3164	-23.6	-0.47	-34.4	0.9	-16.9	-0.67	-25.6	-2.87
2	-0.1582	-28.1	0.75	-33.1	0.93	-18.4	-0.48	-17	-2.23
3	0	1.6	-0.72	-31.6	1.01	-20.1	-2.5	-5.1	2.11
4	0.1582	-19.9	0.82	-29.9	1.17	-22.3	-2.85	-15.8	1.97
5	0.3164	-24.8	1.21	-16.4	1.02	-33.1	0.43	-13.9	1.51
6	0.4746	-22	2.01	-23.6	-1.14	-35.8	0.57	-25.1	1.24
7	0.6328	-33.9	2.41	-18.9	-2.47	-33.3	2.33	-21.5	-0.51
8	0.791	-22.9	2.21	-34.2	-1.33	-29.1	-2.55	-26.6	0.4

Table 5.16 Tap values of 95-percentile MIMO fixed roof-top channel

Tap number	Excess delay [μs]	h_{11}		h_{12}		h_{21}		h_{22}	
		[dB]	[rad]	[dB]	[rad]	[dB]	[rad]	[dB]	[rad]
1	-0.4746	-21.7	2.82	-25.4	0.36	-12.7	-1.51	-8.8	3.12
2	-0.3164	-19.2	2.8	-24.6	0.26	-8.3	1.18	-20.5	-2.96
3	-0.1582	-14.1	2.56	-19.1	-0.26	-18.8	0.67	-9.1	0.04
4	0	-5.7	-2.83	-10.2	2.58	-17.7	1.65	-3.8	0.55
5	0.1582	-6.4	-0.46	-10.5	0.72	-15.6	1.2	-16.5	-2.92
6	0.3164	-14.4	0.37	-22.7	-0.14	-18.4	2.09	-13.7	-1.8
7	0.4746	-11.1	-0.76	-15.7	-2.46	-22.7	2.46	-24.7	2.92
8	0.6328	-25.6	-1.01	-12.9	-2.72	-23.5	2.15	-26.1	-0.08

Table 5.17 Tap values of 99-percentile MIMO fixed roof-top channel

Tap number	Excess delay [μs]	h_{11}		h_{12}		h_{21}		h_{22}	
		[dB]	[rad]	[dB]	[rad]	[dB]	[rad]	[dB]	[rad]
1	-0.4746	-27.5	1.83	-38.3	-0.55	-13.9	-1.35	-28.3	-0.54
2	-0.3164	-23.7	1.62	-37.7	-0.37	-21.8	2.02	-25.9	-0.5
3	-0.1582	-7.8	1.43	-37.9	-0.2	-25	2.38	-10.9	-0.65
4	0	0.9	-2.08	-36.1	0.04	-9.7	-2.71	-13.1	1.39
5	0.1582	-14.4	-2.38	-21.6	0.73	-33	0.64	-21.4	2.85
6	0.3164	-13.9	0.83	-11.9	-2.37	-30.4	-0.45	-20.5	2.79
7	0.4746	-10.1	-0.74	-16.6	0.65	-26.7	1.3	-31	-1.02
8	0.6328	-24.3	-0.83	-20.7	3.13	-25.4	0.86	-27	2.56

5.2.4. MIMO Practical Gain

MIMO practical gain against SISO was evaluated with the 8-tap channel models described in the previous subsection. The parameters used for evaluation are listed in Table 5.18. With 9 combinations of MODCOD, the MIMO capacity was compared with the SISO capacity in the same percentile, for instance, 50-percentile MIMO channel and 50-percentile SISO channel. Note that the reception points selected for 50-percentile MIMO/SISO channel models are not identical in this study.

The simulation results in 50-percentile MIMO/SISO channels are shown in Figure 5.32. At the required CNR of 20 dB, the SISO capacity is 25.6 Mbps, whereas the MIMO capacity increases to 47.4 Mbps, which is 1.85 times higher than SISO. The MIMO capacity was determined by connecting the points on the graph with a straight line and reading the intersection point with the required CNR. This result shows a consistency with the MIMO gain evaluation in 5.2.2, where the 50-percentile required CNR of SISO (20 dB) was between the values of MIMO (18 dB) and MIMO (19 dB) and the capacity gain achieved was about 1.8 times. As for the required CNR of 10 dB, the capacity of SISO and MIMO are 12.1 Mbps and 21.0 Mbps, and the resulting capacity gain is 1.73 times. With the same procedure, the capacity gain obtained at the required CNR of 30 dB is calculated as 1.85 times, where the SISO capacity is 40.7 Mbps and the MIMO capacity is 75.4 Mbps. In Figure 5.32, the Shannon limit of MIMO/SISO systems are also displayed by dashed lines as the upper limit. The Shannon limit was calculated according to the following formulae as the maximum net data rate in an ideal channel, taking into consideration the signal bandwidth and time duration actually used for data transmission.

$$C_{SISO} = B\left(\frac{N_{seg}}{35}\right)(1-\mathrm{SPR})\left(\frac{1}{1+\mathrm{GIR}}\right)\log_2(1+\mathrm{CNR}) \quad \text{bits/s} \tag{5.5}$$

$$C_{MIMO} = 2B\left(\frac{N_{seg}}{35}\right)(1-\mathrm{SPR})\left(\frac{1}{1+\mathrm{GIR}}\right)\log_2(1+\mathrm{CNR}) \quad \text{bits/s} \tag{5.6}$$

where B is the signal bandwidth, N_{seg} is the number of segments used, SPR is the scattered pilot ratio, GIR is the guard interval ratio, CNR is the signal-to-noise ratio shown in Table 5.18. The receiver uses ZF detection as the most practical implementation.

The results in 80, 90, 95 and 99-percentile channels are shown in Figure 5.33, Figure 5.34, Figure 5.35 and Figure 5.36, respectively. As the percentile of the channel increases, the MIMO capacity curve tends to flatten and the gap from the Shannon limit widens especially at high CNRs. Note that in 95-percentile and 99-percentile channels, QEF is

Table 5.18 Parameter sets for MIMO practical gains evaluation

	Parameter set								
	p1	p2	p3	p4	p5	p6	p7	p8	p9
Signal bandwidth	Normal mode: 5.83 MHz								
Number of segments	Normal mode: 35 (31 segments used for fixed reception evaluation)								
FFT size	16,384								
Guard interval ratio (duration)	800/16,384 (126 μsec)								
Scattered pilot ratio	1/24								
Carrier modulation	QPSK	QPSK	16QAM NUC	64QAM NUC	256QAM NUC	1024QAM NUC	1024QAM NUC	4096QAM NUC	4096QAM NUC
Inner code rate	2/16	5/16	6/16	7/16	9/16	9/16	11/16	11/16	12/16
System	SISO MIMO (Open-loop spatial multiplexing 2×2 cross-polarized)								
Transmission capacity (31 segments)	2.2 Mbps	5.6 Mbps	13.6 Mbps	24.0 Mbps	41.0 Mbps	51.2 Mbps	62.8 Mbps	75.4 Mbps	82.2 Mbps
Required CNR (AWGN)	-2.4 dB	0.9 dB	6.0 dB	10.4 dB	16.7 dB	20.4 dB	24.2 dB	28.4 dB	30.5 dB

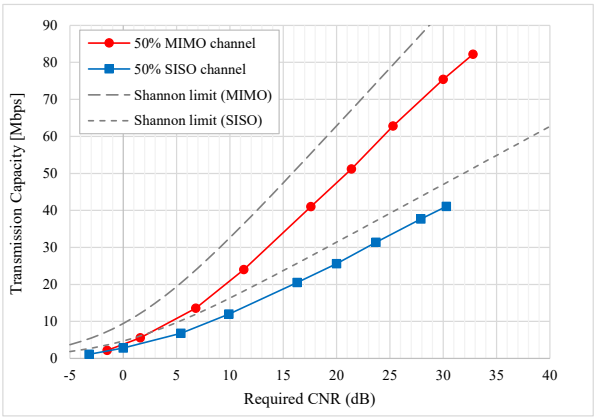

Figure 5.32 Required CNR comparison between MIMO/SISO in 50-percentile channel

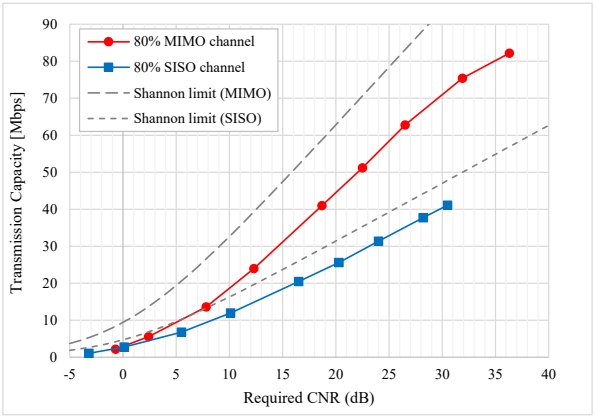

Figure 5.33 Required CNR comparison between MIMO/SISO in 80-percentile channel

not achieved with MIMO parameter p9, therefore only 8 points are plotted for MIMO in

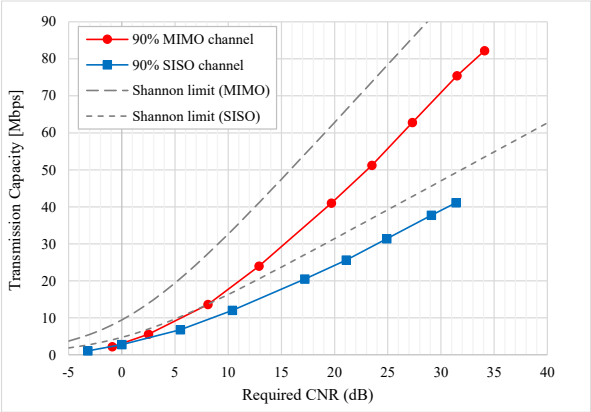

Figure 5.34 Required CNR comparison between MIMO/SISO in 90-percentile channel

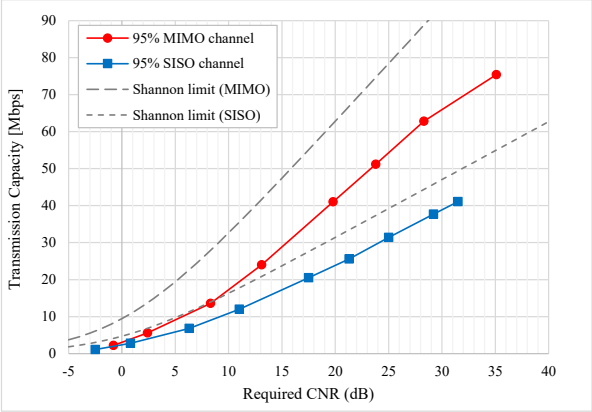

Figure 5.35 Required CNR comparison between MIMO/SISO in 95-percentile channel

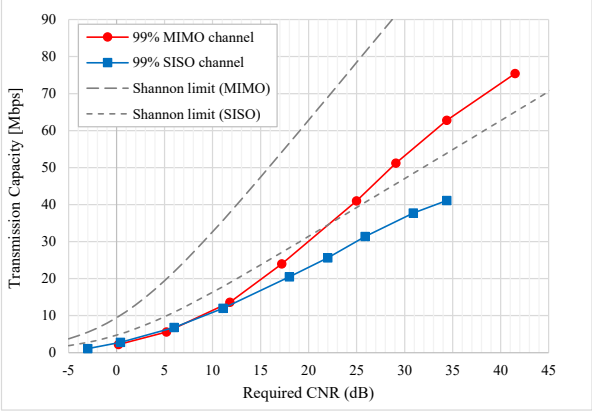

Figure 5.36 Required CNR comparison between MIMO/SISO in 99-percentile channel

Figure 5.35 and Figure 5.36.

Figure 5.37 summarizes the MIMO capacity gain obtained at the required CNR of 10 dB, 20 dB and 30 dB in the created 8-tap channels shown in Table 5.8 to Table 5.17. First, looking at the results at 10 dB CNR, the gain obtained is 1.5 to 1.7 times in 50, 80, 90

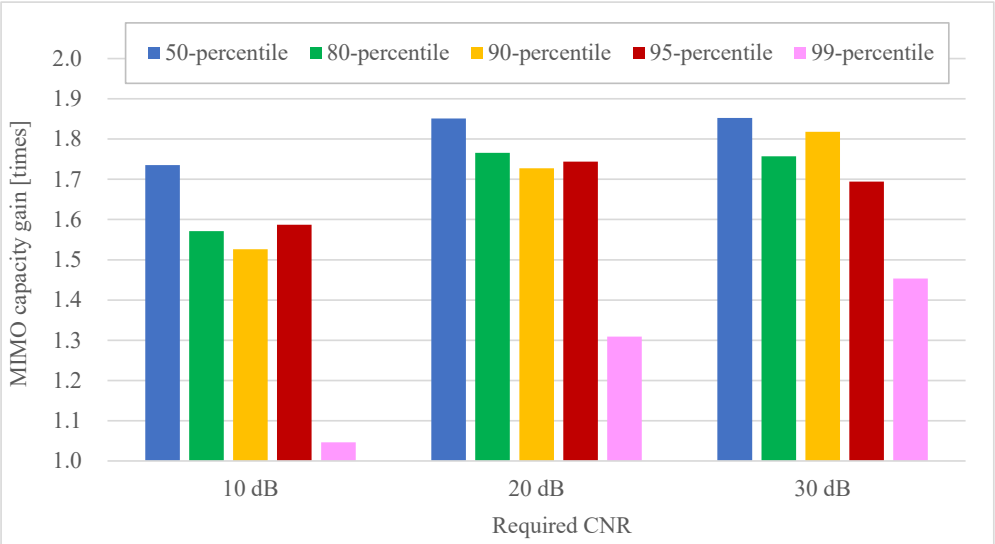

Figure 5.37 MIMO capacity gain against SISO in 8-tap 50, 80, 90, 95 and 99-percentile fixed rooftop channel

and 95-percentile channels, and the gain becomes smaller than that of 20 dB and 30 dB. Furthermore, in the case of 99-percentile, the gain is negligible at 10 dB CNR. It is considered that the decrease in gain is caused by the MIMO detection, i.e., ZF is used as the most practical implementation in this study. The gain can be improved by introducing higher complexity MIMO detection such as MLD. Next, the results obtained at 20 dB and 30 dB showed that the MIMO gain is 1.7 to 1.8 times in 50, 80, 90, 95-percentile channels. The results also concludes that the MIMO practical gain obtained in the current fixed rooftop reception of DTTB assuming a required CNR of 20 dB is about 1.7 times in 95-percentile channels. The 95-percentile is a typical value used for the cell edge reception location probability in DTTB link budget [112][119]. When selecting the parameters for MIMO with the assumption that 95-percentile location probability is guaranteed, it is appropriate to select a MODCOD that is about 1.7 times as large as SISO. We should keep in mind that the MIMO gain decreases in 99-percentile channel even at 20 dB or 30 dB CNRs, the introduction of MIMO requires careful consideration, when 99-percentile location probability should be guaranteed. Note that in broadcasting transmissions, there is a lack of feedback from users to the transmitter. Systems do no permit an adaptative configuration that maximizes the capacity of each individual user, and different channel realizations are obtained at the different reception points. Therefore, systems have to be configured considering the worst channel conditions and signal received.

5.3. Conclusions

Section 5.1 presented the world's first MIMO terrestrial broadcast field measurements in an urban scenario with an HPHT network configuration. The field measurement results were validated with laboratory tests. The results doubling the transmit power for MIMO compared with SISO showed that the required received power can be improved by at least 7.3 dB when improving transmission robustness while maintaining the same transmission capacity as SISO. Moreover, we confirmed that the transmission capacity can be doubled by introducing MIMO with the same modulation scheme and error correction code as SISO, although the required received power increased by 0.9 dB compared with SISO. Regarding the feasibility of the next-generation terrestrial broadcasting system operating at a target bit rate of about 60 Mbps to distribute a VVC-based 8K program within the bandwidth of a single 6-MHz channel, received power increases of 3.7 dB and 2.7 dB were required compared with SISO at the maximum and median values for 28 reception points evaluated in urban areas, respectively.

The electric field strength for horizontal and vertical polarization were also evaluated. It was confirmed that the field strength differed up to 7.5 dB at the maximum and 2.5 dB at the median. The measurement results demonstrated that the field strength of vertical polarization tended to be higher than that of horizontal polarization at the reception points located in urban areas. The results showed no relationship between the transmission distance and the difference in field strength for horizontal and vertical polarization.

In terms of the median value of the degradation in required received power compared to laboratory experiments, the deterioration in MIMO was trivial compared with SISO for the three MIMO deployment scenarios. However, when we evaluated the maximum value of the degradation in received power at 28 locations, MIMO showed a significant deterioration in the worst case. The significant deterioration was confirmed at a few reception points at which the differences in received power between the horizontal and vertical polarization were also significant. There was no relationship between the transmission distance and the amount of deterioration in the required received power.

Additionally, we compared the SISO and MIMO transmission performance by using MIMO channel snapshots excluding uncertainties occurring during field experiments, such as fluctuation in the field strength or the effect of a man-made noise occurring at the time of measurement. From the results of the laboratory experiments with the reproduced

28 channels, it was confirmed that the degradations in the required CNR of MIMO transmission were worse than those of SISO for all locations. The maximum amount of the degradation in the required CNR was 0.7 dB for SISO, while it was 2.5 dB for MIMO with the same modulation and code rate with the reproduced 28 channels. When introducing dual-polarized MIMO, a difference in the received power is unavoidable, and the required received power was considered to have deteriorated due to the difference in the received power.

These experiments were performed by using the signal format for advanced ISDB-T. These results should provide useful knowledge for introducing MIMO for terrestrial broadcasting over HPHT networks in the UHF band. For the next-generation 5G Broadcast system based on the state-of-the-art wireless communication system [115], enhancements with MIMO that utilize multiple reception antennas equipped with receivers can be considered in future releases of 3GPP.

In Section 5.2 the fixed reception performance of MIMO transmission was verified by physical layer simulation with the MIMO channel snapshots of 101 points captured in real environment, which is mainly the LOS environment, to study the link budget in the MIMO broadcasting system. MIMO parameters that provide transmission robustness equivalent to SISO with a required CNR of 20 dB were verified. Note that the total transmit power for MIMO is twice as that for SISO in this study. When compared with MIMO with a required CNR of 18 dB, which provides almost the same robustness as SISO, the transmission capacity increases approximately 1.8 times. It was confirmed that with MIMO parameters that have the same transmission capacity as SISO, the gain in transmission robustness due to the introduction of MIMO is approximately 7 dB. Note that when comparing SISO and MIMO with a constant transmission power, the amount of improvement decreases by 3 dB, and the MIMO gain is reduced to about 4 dB.

The measurements on electric field strength of the horizontally polarized wave and vertically polarized wave at 101 points confirmed that the 50-percentile difference in the field strengths was 0 dB and no bias was observed in the electric field strength of each polarization. The 50-percentile absolute difference in the field strengths was about 2 dB at 101 points. We also measured XPI, which is defined as the received signal power ratio between co-polarized and cross-polarized transmitted signals, in field experiments. The

50-percentile XPI was approximately 7.5 dB, 13 dB and 10 dB for horizontal reception, vertical reception and the average.

Next, We created 8-tap fixed rooftop reception MIMO channel models based on 101 snapshots captured in the field experiments. We also modeled 8-tap SISO channels and evaluated the MIMO practical gain over SISO in broadcasting by simulations. The MIMO capacity gain obtained at the required CNR of 10 dB is 1.5 to 1.7 times in 50, 80, 90 and 95-percentile channels. The gain at 20 dB and 30 dB is 1.7 to 1.8 times in 50, 80, 90, 95-percentile channels. The results concludes that the MIMO practical gain obtained in the current fixed rooftop reception of DTTB assuming a required CNR of 20 dB is about 1.7 times in 95-percentile channels. The MIMO capacity gain decreases to 1.3 to 1.5 times in 99-percentile channel at 20 dB or 30 dB CNRs, respectively. The introduction of MIMO requires careful consideration, when 99-percentile location probability should be covered.

Chapter 6 Conclusions and Future Work

6.1. Conclusions

The author investigated and assessed 2×2 cross-polarized spatial multiplexing (SM) multiple-input multiple-output (MIMO) for digital terrestrial television broadcasting (DTTB) by simulations, laboratory and field experiments focusing on the MIMO gain over single-input single-output (SISO) in practical scenarios, i.e., not in perfect reception conditions. For practical use, horizontal and vertical polarizations are used for the cross-polarized 2×2 scheme. MIMO performance was evaluated mainly targeting UHDTV transmission assuming fixed roof top reception with the required carrier-to-noise ratio (CNR) of 20 dB, which is equivalent to the operational value of the current DTTB for fixed reception in Japan.

The results, such as the simulations, laboratory and field experiments, were analyzed in order to obtain the recommendation of MIMO parameters, and we assessed practical gain of MIMO in several reception scenarios. Optimum MIMO configuration parameters for ATSC 3.0 were provided. A large-scaled MIMO channel measurements were conducted in Osaka, Japan, and 8-tap MIMO channel models were created as a simple deterministic model for practical use.

6.1.1. Broadcast MIMO channel estimation

We assessed the MIMO performance by simulations and provided an optimum configuration for MIMO regarding the waveform parameters, e.g., Pilot Pattern (PP), Fast-Fourier Transform (FFT) size and Guard Interval (GI) for ATSC 3.0. The performance evaluation and optimization of MIMO channel estimation were performed in a single frequency network (SFN) fixed reception and NGH mobile outdoor channel regarding pilot boosting, pilot encoding and channel interpolation.

The recommended practice for MIMO parameter selection obtained in this study is summarized in Table 6.1. Note that the optimum pilot boosting greatly improves the performance especially with higher D_X: the number of carriers between the scattered pilot bearing carriers, and D_Y: the number of symbols between the scattered pilots in a single pilot bearing carrier, and that the optimum boosting is an independent parameter from the

Table 6.1 Recommended practice for MIMO parameters for ATSC 3.0

Channel	Two path SFN (fixed)	NGH outdoor (mobile)
FFT size	16k, 32k	8k, 16k
GI	to be selected according to required coverage	
Pilot boosting	boost3	
Pilot encoding	Null Pilot	Walsh-Hadamard
Frequency Interpolation	DFT	linear
Pilot pattern	larger D_X	smaller D_Y

Modulation and Coding (MODCOD). The recommended pilot boosting is boost3 for Null Pilot (NP) encoding and Walsh-Hadamard (WH) encoding.

Although the encoding scheme and the frequency interpolation do not make much difference in lower signal-to-noise ratio (SNR) region, NP encoding and linear frequency interpolation is the best combination in fixed and mobile reception for SNRs below 10 dB in a precise sense. WH encoding provides a better performance in mobile reception conditions especially at high SNRs.

In a fixed SFN channel, Null Pilot encoding provides better performance than Walsh-Hadamard encoding and larger D_X SP pattern is the best configuration. The larger FFT size can reduce the pilot overhead and achieve lower required SNR in a time invariant SFN channel. In long echo SFN channel, Discrete Fourier Transform (DFT) interpolation provides better performance than linear interpolation in terms of the frequency interpolation at the receiver.

In contrast, WH encoding with smaller D_Y SP pattern is the best configuration in a high Doppler time varying mobile channel. The smaller FFT size and linear interpolation at the receiver can achieve the lowest required SNR.

NP encoding is rapidly degraded especially with (16k FFT, D_Y=4) or (32k FFT D_Y=2) in time varying channel because of the virtually doubled D_Y. On the other hand Walsh-Hadamard encoding with linear frequency interpolation can be severely degraded in long echo SFN channel because of the virtually doubled D_X

6.1.2. Broadcast MIMO signal processing

We evaluated a decision threshold demapping algorithm that reduces complexity in the Log Likelihood Ratio (LLR) calculation for Non-Uniform Quadrature Amplitude Modulation (NUQAM)s. The degradation in required CNR was assessed by simulations using the MIMO channel snapshots actually captured in an urban area, Tokyo. The results showed that the degradations of NUQAMs are equivalent to those of conventional

Quadrature Amplitude Modulations (QAMs), and that the degradation is further mitigated with 4096 NUQAM. Therefore, this complexity reduction algorithm is applicable to MIMO system for practical use.

The performance evaluation of the three MIMO precoding blocks in ATSC 3.0, i.e., Stream Combining (SC), IQ Polarization Interleaving (IQPI) and Phase Hopping (PH), was carried out in physical layer simulations. The correspondence table obtained in this study is shown in Table 6.2, where a check mark indicates that the MIMO precoding block provides over 1 dB gain in the channel. The results showed that SC provides some gains with QPSK and 16QAM in in a PI channel and that IQPI provides small gain only in an extremely high PI over 10 dB channel with 64QAM. PH shows no gain in a PI channel. Consequently, MIMO precoding gain obtained with a higher order modulation in a practical channel with a PI of 10 dB or less is vanishing. In a small Cross Polarization Discrimination (XPD) lower than 6 dB channel, SC and PH provide some gains with QPSK and 16QAM. Whereas IQPI shows no gain on XPD deterioration. Therefore, MIMO precoding gain is negligible with a higher order modulation in a practical fixed reception with a XPD of 6 dB or more. Evaluation results with MIMO channel snapshots captured in an urban area showed that SC provides gains only with Quadrature Phase Shift Keying (QPSK) and code rate 13/15, but IQPI and PH provide no gains. For the reasons described above, MIMO precoding is effective with a lower order modulation, e.g., QPSK and 16QAM in channels where PI are high or XPD are low.

As a feasibility study Digital Terrestrial Television Broadcasting (DTTB) network for 2×2 cross-polarized SM MIMO, an advanced SFN scheme based on Space Time Coding (STC) was verified in laboratory and field experiments. To evaluate 4×2 distributed MIMO system performance, two experimental stations were set up in Hitoyoshi area, Kumamoto Prefecture. We compared two SFN schemes: STC-SFN and conventional SFN without coding at three points within the area of overlap covered by both the Hitoyoshi and the Mizukami stations. The results confirmed that the required received power of STC-SFN is up to 3 dB better than that of the conventional SFN when the transmission capacity is set to 91.8 Mbps with 4096QAM modulation with the desired-to-undesired signal ratio (DUR) of the main wave and the SFN wave is adjusted to 6 dB.

Table 6.2 Correspondence table of MIMO channels where each MIMO precoding is effective

MIMO Precoding	Channel				
	PI		XPD		snapshots
	10 dB or less	over 10 dB	below 6 dB	6 dB or more	
Stream Combining	✓	✓	✓		✓
IQ Polarization Interleaving		✓			
Phase Hopping			✓		

6.1.3. Broadcast MIMO practical gain and channel modeling

We compared the fixed reception performance of SISO and MIMO in laboratory experiments and large-scale field experiments in Tokyo with an advanced ISDB-T system. It should be emphasized that the transmit power for MIMO is twice as that for SISO in this thesis. The amount of improvement in transmission capacity was 7.3 dB at a minimum when MIMO is introduced to enhance transmission robustness. Alternatively, the transmission capacity can be doubled by introducing MIMO requiring a slight increase in received power of 0.9 dB at a maximum compared with SISO. To distribute a VVC-based 8K program within a 6-MHz channel, an increased received power of 3.7 dB were required compared with SISO with a required CNR of 20 dB to achieve 60 Mbps order transmission capacity in the worst case for 28 reception points evaluated in urban areas.

The fixed reception performance comparison between SISO and MIMO was carried out by physical layer simulation with the MIMO channel snapshots of 101 points captured in Osaka with an advanced ISDB-T system. MIMO with a required CNR of 18 dB provides almost the same robustness as SISO with a required CNR of 20 dB, therefore the MIMO capacity gain reaches approximately 1.8 times. With MIMO parameters that have the same transmission capacity as SISO, the performance gain in transmission robustness is approximately 7 dB. When comparing the performance gain with a constant transmission power, the robustness gain decreases by 3 dB, i.e., the MIMO gain is reduced to 4 dB.

The measurements on electric field strength at 101 points showed that the 50-percentile difference in the field strengths between horizontal and vertical polarizations was 0 dB. The 50-percentile absolute difference in the field strengths was about 2 dB. The Cross Polarized Isolation (XPI), which is defined as the ratio of the received signal power of co-polarized transmitted signal and that of cross-polarized transmitted signal, was approximately 7.5 dB, 13 dB and 10 dB for horizontal reception, vertical reception

and the average. With 8-tap MIMO and SISO channel models created in this study, MIMO practical gain over SISO was assessed by simulations. The MIMO capacity gain obtained at the required CNR of 20 dB is 1.7 to 1.8 times in 50, 80, 90, 95-percentile channels. However, The MIMO capacity gain decreases to 1.3 times in 99-percentile channel at 20 dB CNR. Therefore the introduction of MIMO requires careful consideration when 99-percentile location probability should be covered, because in order to achieve a 99% coverage, it is necessary to select robust parameters, which reduces the MIMO capacity gain obtained.

6.2. Future Work

MIMO broadcasting has not been commercialized mainly due to the absence of a strong market because MIMO broadcasting system requires additional investments, such as the initial cost of transmitter and receiver equipment. However, in recent years, it has become standard for smartphones and tablets to have multiple receive antennas. Therefore, by targeting portable/mobile devices, viewers are able to receive MIMO broadcasts signals without additional investment, because MIMO is a breakthrough to greatly increase transmission capacity. Although the study focused on evaluating fixed reception MIMO broadcast in this study, it can be considered to evaluate MIMO broadcast in mobile broadband specification, such as 5G Broadcast, targeting portable/mobile devices.

In the broadcast MIMO channel estimation study, it was confirmed that the equivalent D_Y is doubled in NP encoding scheme, thus the performance in the time varying channel is severely degraded. In this thesis, we evaluated the MIMO capacity gain over SISO with the same SP overhead for SISO and MIMO. As a further study, the MIMO capacity gain can be assessed by doubling the pilot overhead compared to SISO keeping the same resolution of channel estimation as with SISO. In this case, the capacity gain due to the introduction of MIMO will be decreased. As a consequence it is estimated that the capacity gain will be smaller than the value of 1.7 times obtained in this thesis.

Regarding MIMO transmit/receive signal processing, there is room for consideration regarding the combination of each MIMO precoding block. In this thesis, we evaluated fundamental performance of each precoding block of ATSC 3.0. However it would be possible to evaluate the performance of two or three precoding combinations. In addition, we evaluated the performance with Maximum Likelihood Detection (MLD) as an ideal

detection method, however when combining each precoding, it is necessary to study demapping complexity reduction for the practical implementation at the receiver.

Finally, in the broadcast MIMO practical gain and channel modeling, further measurement campaign is desirable. Due to the measurement time constraints, we only measured 28 reception points in Tokyo and 101 reception points in Osaka. The 99-percentile of the 101 points means that the reception point is the second worst case in the MIMO channel snapshots. In order to select more appropriate reception point corresponding to each percentile, it is recommended to increase the number of samples.

Annex A: Ph.D. Dissertation Related Projects

At the time of writing this thesis, the development of the Ph. D. dissertation is in the framework of various research projects. A brief description of the related research projects, contributions and disseminations are following.

Technical Forums

[F1] ATSC Forum

The author is conducting his dissertation at the iTEAM of the Universitat Politècnica de València, which is a member of the ATSC project. ATSC is working to coordinate television standards among different communications media focusing on digital television, interactive systems, and broadband multimedia communications. ATSC is also developing digital television implementation strategies and presenting educational seminars on the ATSC standards.

[F2] 3GPP

The author is conducting his dissertation at NHK, which is a member of the Third Generation Partnership Project (3GPP). 3GPP is working to standardize cellular telecommunications network technologies, including radio access, the core transport network, and service capabilities - including work on codecs, security, quality of service and thus to provide complete system specifications.

[F3] ITU-R

The author is conducting his dissertation at NHK, which is a member of International Telecommunication Union Radiocommunication Sector (ITU-R). Over 5000 specialists from telecommunication and ICT organizations and administrations throughout the world, participate in the Radiocommunication Study Groups to prepare technical bases for Radiocommunication Conferences, develop ITU-R Recommendations (radiocommunication standards) and Reports and compile radiocommunication Handbooks.

Research Projects

[P1] Research and Development of Technology Encouraging Effective Utilization of Frequency for Ultra High Definition Satellite and Terrestrial Broadcasting System

In this project, 2×2 MIMO field test carried out terrestrial 8K transmissions (91 Mbps) at over a single UHF-band channel (6 MHz bandwidth). The analysis of the 2×2 MIMO propagation characteristics, in particular the variability of the required field strength and the degradation in required CNR was conducted. The project period is from Apr. 2014 to Mar. 2017.

[P2] Research and Development for Advanced Digital Terrestrial TV Broadcasting System

The author is conducting his dissertation at NHK, which is a member of a Japanese national research project which is funded by the Ministry of Internal Affairs and Communications in Japan. This project is aiming at the second generation of ISDB-T. The project period is from Apr. 2016 to Mar. 2019.

[P3] 5G-Xcast

The author is conducting his dissertation at the iTEAM of the Universitat Politècnica de València, which is the project manager of 5G-Xcast, the 5G-PPP project focusing on point-to-multipoint transmissions technologies to support large-scale consumption of mass multimedia services for upcoming 5G broadband system. The project period is from June 2017 to May 2019.

References

[1] "ATSC Digital Television Standard A/53," Advanced Television System Committee Std., Sep. 1995.

[2] "Terrestrial integrated services digital broadcasting (ISDB-T) - Specifications of channel coding, framing structure, and modulation," ARIB Std., Sep. 1998.

[3] "Digital Audio Broadcasting (DAB); Data Broadcasting - MPEG-2 TS streaming," ETSI Std. TS 102 427, Rev. 1.1.1, Jan. 2005.

[4] "Framing structure, channel coding and modulation for digital terrestrial television (DVB-T)," ETSI Std. EN 300 744, Rev. 1.6.1, Jan. 2009.

[5] I. Eizmendi, M. Velez, D. Gómez-Barquero, et al, "DVB-T2: The Second Generation of Terrestrial Digital Video Broadcasting System," IEEE Trans. Broadcast., vol. 60, no. 2, pp. 258-271, June 2014.

[6] "DTT Deployment Data," https://dvb.org/solutions/dtt-deployment-data/, Mar. 2023.

[7] D. Gómez-Barquero, "Cost efficient provisioning of mass mobile multimedia services in hybrid cellular and broadcasting systems," Ph.D. dissertation, Universitat Politècnica de València, 2009.

[8] "DVB-T2 - 2nd Generation Terrestrial Broadcasting," DVB Fact Sheet, 2015.

[9] ATSC, Press Release, "Evaluating Detailed 'Physical Layer' Technical Proposals for Next-Generation ATSC 3.0 TV Transmission System," Oct. 2013

[10] "The Future of Terrestrial Broadcasting," European Broadcasting Union, Tech. Rep. V 1.1, Nov. 2011.

[11] "Digital dividend: Insights for spectrum decisions," International Telecommunications Union, Tech. Rep., Aug. 2012.

[12] "Evolved Universal Terrestrial Radio Access (E-UTRA) and Evolved Universal Terrestrial Radio Access Network (E-UTRAN); Overall description (release 9)," 3GPP TS 36.300 V9.10.0, Dec. 2012.

[13] "Final Acts," World Radiocommunication Conference 2012 (WRC-12), Geneva, 2012.

[14] Report ITU-R BT.2302-1, "Spectrum requirements for terrestrial television broadcasting in the UHF frequency band in Region 1 and the Islamic Republic of Iran," Mar. 2021.

[15] RESOLUTION 235 (WRC-2015), “Review of the spectrum use of the frequency band 470-960 MHz in Region 1,” 2015.

[16] Recommendation ITU-R BT.2020; “Parameter values for ultra-high definition television systems for production and international programme exchange,” Oct. 2015.

[17] Recommendation ITU-R BS.2051; “Advanced sound system for programme production,” Feb. 2014.

[18] ATSC, Press Release, “Evaluating Detailed ‘Physical Layer’ Technical Proposals for Next-Generation ATSC 3.0 TV Transmission System,” Oct. 2013

[19] L. Fay, L. Michael, D. Gomez-Barquero, N. Ammar, and M. W. Caldwell, “An overview of the ATSC 3.0 physical layer specification,” IEEE Trans. Broadcast., vol. 62, no. 1, pp. 159-171, Mar. 2016.

[20] K. J. Kim et al., “Low-Density Parity-Check Codes for ATSC 3.0," IEEE Trans. Broadcast., vol. 62, no. 1, pp. 189-196, Mar. 2016.

[21] C. E. Shannon, “A mathematical theory of communication," Bell Syst. Tech. J, vol. 27, pp. 379-423, 1948.

[22] B. Bross, “Overview of the HEVC Video Coding Standard," in Next Generation Mobile Broadcasting, D. Gomez-Barquero, Ed. Boca Raton, FL, USA: CRC Press, 2013, pp. 713-748.

[23] Joint Video Experts Team (JVET). [Online]. Available: https://www.itu.int/en/ITU-T/studygroups/2017-2020/16/Pages/video/jvet.aspx

[24] R. W. Chang and R.A. Gabby, “A Theoretical Study of Performance of an Orthogonal Multiplexing Data Transmission Scheme,” IEEE Trans on Commun., COM-16, pp. 529-540, 1968.

[25] S. B. Weinstein and P. W. Ebert, “Data Transmission by Frequency Division Multiplexing using the Discrete Fourier Transform,” IEEE Trans on Commun. COM-19, pp. 628-634, 1971.

[26] R. Gallager, “Low-density parity-check codes," IRE Transactions on Information Theory, vol. 8, no. 1, pp. 21-28, Jan. 1962.

[27] A. Sato, et al., “Transmission Performance Evaluation of LDPC coded OFDM over Actual Propagation Channels in Urban Area -Examination for Next-generation ISDB-T-,” 2017 IEEE International Symposium on Broadband Multimedia Systems and Broadcasting (BMSB), Cagliari, Italy, June 2017.

[28] S. Alamouti, “A simple transmit diversity technique for wireless communications,” IEEE J. Select. Areas Commun., vol. 16, no. 8, pp. 1451–1458, Oct. 1998.

[29] J. Robert, “Terrestrial TV Broadcast Using Multi-Antenna Systems," Ph.D. dissertation, Technical University Braunschweig, 2013.

[30] M. Slimani, J. Robert, P. Schlegel, U. Reimers, R. Burow, F. Kattanek, R. Pfeffer, and L. Stadelmeier, “Results of the DVB-T2 Field Trial in Germany," IEEE Trans. Broadcast., vol. 61, no. 2, pp. 177-194, June 2015.

[31] D. Gomez-Barquero, C. Douillard, P. Moss, V. Mignone, "DVB-NGH: The Next Generation of Digital Broadcast Services to Handheld Devices," IEEE Trans. Broadcast., vol.60, no.2, pp.246-257, June 2014.

[32] D. Gómez-Barquero (ed.), “Next Generation Mobile Broadcasting,” CRC Press, 2013.

[33] DVB Document A160, “Digital Video Broadcasting (DVB); Next Generation Broadcasting System to Handheld, Physical Layer Specification (DVB-NGH),” Nov. 2012.

[34] P. Moss and T. Y. Poon, “Overview of the Multiple-Input Multiple-Output Terrestrial Profile of DVB-NGH," in Next Generation Mobile Broadcasting, D. Gomez-Barquero, Ed. Boca Raton, FL, USA: CRC Press, 2013, pp. 549-580.

[35] D. Gomez-Barquero et al, “MIMO for ATSC 3.0,” IEEE Trans. Broadcast., vol. 62, no.1, pp. 298-305, Mar. 2016.

[36] S. Saito et al, “8K Terrestrial Transmission Field Tests Using Dual-Polarized MIMO and Higher-Order Modulation OFDM,” IEEE Trans. Broadcast., vol. 62, no.1, pp. 306-315, Mar. 2016.

[37] A/322:2017, ATSC Standard: Physical Layer Protocol, June 2017.

[38] K. Manolakis, et al, “Performance Evaluation of a 3GPP LTE Terminal Receiver,” Proc. 14th European Wireless Conference, Prague, Czech Republic, 2008.

[39] GSA, “LTE Broadcast (LTE Multicast) market status report," Information papers, Oct. 2014.

[40] M. Marques da Silva, A. Correia, R. Dinis, N. Souto, and J. C. Silva, “Transmission Techniques for 4G Systems,” Boca Raton, FL, USA: CRC Press, Inc., Nov. 2012.

[41] C. Hoymann et al., “LTE release 14 outlook,” IEEE Communications Magazine, vol. 54, no. 6, pp. 44-49, June 2016.

[42] 3GPP, “3GPP enhancement for TV service (Release 14),” Tech. Rep. 22.816, v.14.1.0, Mar. 2016.

[43] 3GPP, “New SID on LTE-based 5G terrestrial broadcast,” RP-181706, Sep. 2018.

[44] 3GPP, “Study on scenarios and requirements for next-generation access technologies,” Tech. Rep. 38.913, v.14.3.0, Aug. 2017.

[45] 3GPP, “New WID on LTE-based 5G terrestrial broadcast,” RP-190732, Mar. 2019.

[46] M. Nakamura et al., “A study on the transmission system for advanced ISDB-T,” IEEE International Symposium on Broadband Multimedia Systems and Broadcasting 2019, June 2019.

[47] A. Goldsmith, S. A. Jafar, N. Jindal, and S. Vishwanath, “Capacity limits of MIMO channels,” IEEE J. Sel. Areas Commun., vol. 21, no. 5, pp. 684–702, Jun. 2003.

[48] A. J. Paulraj, D. A. Gore, R. U. Nabar, and H. Bolcskei, “An overview of MIMO communications-a key to Gigabit wireless,” Proceedings of the IEEE, vol. 92, no. 2, pp. 198-218, Feb. 2004.

[49] “Requirements for Evolved UTRA (E-UTRA) and Evolved UTRAN (E-UTRAN) (Release 9)", 3GPP TR 25.913 V9.0.0, Dec. 2009.

[50] “Requirements for Further Advancements for Evolved UTRA (E-UTRA) (Release 10)”, 3GPP TR 36.913 V10.0.0, Apr. 2011.

[51] I. W. Group et al., “IEEE standard for local and metropolitan area networks. part 16: Air interface for fixed broadband wireless access systems," IEEE Std, vol. 802, pp. 16-2004, 2004.

[52] E. Perahia, “IEEE 802.11n development: History, process, and technology," IEEE Communications Magazine, vol. 46, no. 7, 2008.

[53] J. G. Andrews, S. Buzzi, W. Choi, S. V. Hanly, A. Lozano, A. C. Soong, and J. C. Zhang, “What will 5G be?" IEEE Journal on selected areas in communications, vol. 32, no. 6, pp. 1065-1082, 2014.

[54] D. Vargas, “Transmit and Receive Signal Processing for MIMO Terrestrial Broadcast Systems,” Ph.D. dissertation, Universitat Politècnica de València, 2016.

[55] E. Garro, J. Joan Gimenez, S.-I. Park, and D. Gomez-Barquero, “Scattered Pilot Performance and Optimization for ATSC 3.0,” IEEE Trans. Broadcast., vol. 63, no. 1, pp. 282-291, Mar. 2017.

[56] D. Vargas, D. Gozalvez, D. Gomez-Barquero, and N. Cardona, “MIMO for DVB-NGH, The Next Genaration Mobile TV Broadcasting,” IEEE Communications Magazine, vol. 51, no. 7, pp. 130-137, July 2013.

[57] D. Vargas , Y. J. D. Kim, J. Bajcsy, D. Gomez-Barquero, and N. Cardona, “A MIMO-Channel-Precoding Scheme for Next Generation Terrestrial Broadcast TV Systems,” IEEE Trans. Broadcast., vol. 61, no. 3, pp. 445-456, Sep. 2015.

[58] J. D. Mitchell, P. N. Moss, and M. J. Thorp, “A dual polarisation MIMO broadcast TV system,” BBC White Paper WHP 144, Jan. 2006. [Online]. Available: https://www.bbc.co.uk/rd/publications/whitepaper144

[59] J. Boyer, P. G. Brown, K. Halyer, M. Lopez Garcia, J. D. Mitchell, P. N. Moss, and M. J. Thorp, “MIMO for broadcast - Results from a high-power UK trial,” BBC White Paper WHP 157, Oct. 2007. [Online]. Available: https://www.bbc.co.uk/rd/publications/whitepaper157

[60] M. Taguchi, K. Murayama, T. Shitomi, S. Asakura, and K. Shibuya, “Field experiments on dual-polarized MIMO transmission with ultra-multilevel OFDM signals toward digital terrestrial broadcasting for the next generation” IEEE International Symposium on Broadband Multimedia Systems and Broadcasting 2011, June 2011.

[61] T. Shitomi, K. Murayama, M. Taguchi, S. Asakura, and K. Shibuya, “Technology for next-generation digital terrestrial broadcasting - Field experiments of dual-polarized MIMO-OFDM transmission using LDPC codes-,” IEEE International Symposium on Broadband Multimedia Systems and Broadcasting 2012, June 2012.

[62] P. Moss, T. Y. Poon, and J. Boyer, “A simple model of the UHF cross-polar terrestrial channel for DVB-NGH,” Research & Development White Paper WHP 205, Sep. 2011.

[63] P. Moss, “MIMO technology in Broadcasting—and an Application in Programme-Making,” in Proc. IEEE Broadcast Technol. Soc. Gold Workshop Next Gener. Broadcast., Cagliari, Italy, Mar. 2013.

[64] P. Moss, “2-by-2 MIMO Fixed Reception Channel Model for Dual-Polar Terrestrial Transmission,” BBC White Paper WHP 161, Jan. 2008. [Online]. Available: https://www.bbc.co.uk/rd/publications/whitepaper161

[65] Recommendation ITU-R BT.2073-0, “Use of the high efficiency video coding (HEVC) standard for UHDTV and HDTV broadcasting,” 2015.

[66] Y. Matsuo, K. Iguchi, and K. Kanda, “Pre-processing equipment of 8K video codec with low-pass filtering and noise reduction functions,” 18th IEEE International Symposium on Signal Processing and Information Technology (ISSPIT), Dec. 2018.

[67] H. Nyquist, “Certain Topics in Telegraph Transmission Theory,” Reedited manuscript, Proceedings of the IEEE, vol. 90, no. 2, pp. 280-305, Feb. 2002.

[68] “Research and Development of Technology Encouraging Effective Utilization of Frequency for Ultra High Definition Satellite and Terrestrial Broadcasting System,” Ministry of Internal Affairs and Communications, Japan, 2014-2017.

[69] “Research and Development for Advanced Digital Terrestrial TV Broadcasting System,” Ministry of Internal Affairs and Communications, Japan, 2016-2019.

[70] S. Nakahara, M. Okano, M. Takada, and T. Kuroda, “Digital transmission scheme for ISDB-T and reception characteristics of digital terrestrial television broadcasting system in Japan,” IEEE Trans. Consumer Electronics, vol. 45, no. 3, pp. 563-570, Aug. 1999.

[71] 3GPP, “Physical channels and modulation (Release 8),” Tech. Spec. 36.211 v.1.0.0, Mar. 2007.

[72] G.D.Forney, L.-F. Wei, “Multidimensional constellations. I. Introduction, figures of merit, and generalized cross constellations,” IEEE Journal on Selected Areas in Communications, vol. 7, no. 6, pp. 877–892, Aug. 1989.

[73] G.J. Foschini, “Layered Space-time Architecture of Wireless Communication in a Fading Environment when using Multiple Antennas,” Bell Labs. Tech. J., vol. 1, no. 2, pp. 41-59, 1996.

[74] R.V.L. Hartley, “Transmission of Information,” Bell System Technical Journal, 1928.

[75] H. Jin, A. Khandekar, and R. McEliece, “Irregular Repeat-accumulate Codes,” Proc. 2nd Int. Symp. Turbo Codes, Related Topics, pp. 1-8, 2000.

[76] T. Richardson and R. Urbanke, “Multi-edge Type LDPC Codes,” Proc. Workshop Honoring Prof. Bob McEliece 60th Birthday, Pasadena, CA, USA, pp. 24–25, 2002.

[77] Recommendation ITU-R BT.1869-0, “Multiplexing Scheme for Variable-length Packets in Digital Multimedia Broadcasting Systems,” 2010.

[78] ARIB STD-B44 ver. 2.1, Transmission System for Advanced Wide Band Digital Satellite Broadcasting (ISDB-S3), 2016.

[79] ETSI EN 302 755 V1.4.1, Digital Video Broadcasting (DVB); Frame Structure, Channel Coding and Modulation for a Second Generation Digital Terrestrial Television Broadcasting System (DVB-T2), 2015.

[80] 3GPP, "LTE-based 5G terrestrial broadcast; Overall description; (Release 16)," Tech. Rep. 36.276 v.0.2.0, Nov. 2019.

[81] ETSI 102 831, "Digital Video Broadcasting (DVB); Implementation guidelines for a second generation digital terrestrial television broadcasting system (DVB-T2)," Aug. 2012.

[82] C. E. Shannon, "A mathematical theory of communication," Bell Syst. Tech. J, vol. 27, pp. 379-423, 1948.

[83] P. A. Dighe, R. K. Mallik, and S. S. Jamuar, "Analysis of transmit-receive diversity in Rayleigh fading," Proc. IEEE GLOBECOM 2001, vol. 2, pp. 1132-1136, Nov. 2001.

[84] V. Tarokh, N. Seshadri, and A. R. Calderbank, "Space-time codes for high data rate wireless communication: performance criterion and code construction," IEEE Trans. Inform. Theory, vol. 44, no. 2, pp. 744-765, Mar. 1998.

[85] J. G. Proakis, "Digital Communications," McGraw-Hill, 3rd Edition, 1995.

[86] A. van Zelst and T. C. W. Schenk, "Implementation of a MIMO OFDM-based wireless LAN system," IEEE Trans. Signal Processing, vol. 52, no. 2, pp. 483-494, Feb. 2004.

[87] H. Sampath, P. Stoica, and A. Paulraj, "Generalized linear precoder and decoder design for MIMO channels using the weighted MMSE criterion," IEEE Trans. Commun. vol. 49, no. 12, pp. 2198-2206, Dec. 2001.

[88] G. D. Golden, G. J. Foschini, R. A. Valenzuela, and P. W. Wolniansky, "Detection algorithm and initial laboratory results using V-BLAST space-time communication architecture," Electron. Lett. vol. 35, no. 1, pp. 14-16, Jan. 1999.

[89] S. Roger, "Design and Implementation of Efficient Algorithms for Wireless MIMO Communication Systems," Ph.D. dissertation, Universitat Politecnica de Valencia, Valencia, Spain, July 2012.

[90] D. Seethaler, G. Matz, and F. Hlawatsch, "An efficient MMSE-based Demodulator for MIMO Bit-Interleaved Coded Modulation," in IEEE Globecom, Dallas, USA, Nov. 2004.

[91] Report ITU-R BT.2389-0: "Guidelines on measurements for digital terrestrial television broadcasting systems," Feb. 2016.

[92] Recommendation ITU-R BT.2036-1: “Characteristics of a reference receiving system for frequency planning of digital terrestrial television systems,” July 2016.

[93] Recommendation ITU-R BT.419-3: “Directivity and polarization discrimination of antennas in the reception of television broadcasting,” June 1990.

[94] L. Michael and D. Gomez-Barquero, “Bit-Interleaved Coded Modulation (BICM) for ATSC 3.0,” IEEE Trans. Broadcast., vol. 62, no. 1, pp. 181-188, Mar. 2016.

[95] M. K. Ozdemir and H. Arslan, “Channel estimation for wireless OFDM systems,” IEEE Commun. Surveys Tuts., vol. 9, no. 2, pp. 18–48, 2nd Quart., 2007.

[96] M. J. Fernandez-Getino Garcia, J. M. Paez-Borrallo and S. Zazo, “DFT-based channel estimation in 2D Pilot Symbol Aided OFDM Wireless Systems,” Proc. IEEE VTC Spring, vol. 2, pp. 810-814, 2001.

[97] A. Dowler, A. Doufexi, and A. Nix, “Performance evaluation of channel estimation techniques for a mobile fourth generation wide area OFDM systems,” Proc. IEEE VTC Fall, Vancouver, Canada, 2002.

[98] N. Login et al., “Non-Uniform Constellations for ATSC 3.0,” IEEE Trans. Broadcast., vol. 62, no. 1, pp. 197-203, Mar. 2016

[99] S. Kwon, S. I. Park, J. Lee, H. M. Kim, N. Hur, and J. Kim, “Simplified Non-uniform Constellation Demapping Scheme for the Next Broadcasting System,” IEEE International Symposium on Broadband Multimedia Systems and Broadcasting (BMSB 2015), June 2015.

[100] M. Fuentes, D. Vargas and D. Gomez-Barquero, \Low-Complexity Demapping Algorithm for Two-Dimensional Non-Uniform Constellations," IEEE Trans. Broadcast., vol. 62, no. 2, pp. 375-383, June 2016.

[101] C. Barjau, M. Fuentes, T. Shitomi, and D. Gomez-Barquero, “MIMO Sphere Decoding With Successive Interference Cancellation for Two-Dimensional Non-Uniform Constellations,” IEEE Communication Letters, vol. 21, no. 5, pp. 1015-1018, May 2017.

[102] F. Tosato and P. Bisaglia, “Simplified soft-output demapper for binary interleaved COFDM with application to HIPERLAN/2”, IEEE International Conference on Communications, Conference Proceedings, vol. 2, pp. 664-668, May. 2002.

[103] C. Douillard and C. A. Nour, “Bit-interleaved coded modulation in next-generation mobile broadcast standard DVB-NGH”, in Next Generation Mobile Broadcasting, D. Gómez-Barquero, Ed. Boca Raton, FL, USA: CRC Press, 2013, pp. 321-354.

[104] Recommendation ITU-R BT.1306-6: “Error-correction, Data Framing, Modulation, and Emission Methods for Digital Terrestrial Television Broadcasting,” Nov. 2011.

[105] D. Vargas, S. Moon, W. Ko, and D. Gomez-Barquero. “Enhanced MIMO Spatial Multiplexing with Phase Hopping for DVB-NGH," Next Generation Mobile Broadcasting, D. Gomez-Barquero Ed. Boca Raton, FL, USA: CRC Press, 2013, pp. 609-634.

[106] T. Shitomi, S. Saito, S. Asakura, A. Satou, M. Okano, and K. Tsuchida, “Field Experiments of Dual-Polarized MIMO-OFDM Transmission Using Non-Uniform Constellations”, IEEE International Conference on Consumer Electronics (ICCE 2016), Jan. 2016.

[107] A D. Plets et al., “On the methodology for calculating SFN gain in digital broadcast systems,” IEEE Trans. Broadcast., vol. 56, no. 3, pp. 331–339, Sep. 2010.

[108] A S. Jeon et al., “Definition and properties of the erasure effect in single frequency network with two synchronized transmitters,” IEEE Antennas Wireless Propag. Lett., vol. 13, no. 1, pp. 439–442, Mar. 2014.

[109] S. Jeon et al., “Formulating the net gain of SISO-SFN in the presence of erasure effect,” IEEE Trans. Broadcast., vol. 61, no. 2, pp. 323–326, Jun. 2015.

[110] T. Shitomi et al., “A study on advanced single frequency network technology using STC-SDM transmission,” in Proc. IEEE BMSB, pp. 1-5. London, U.K., 2013.

[111] J.-S. Baek et al., “Efficient pilot patterns and channel estimations for MIMO-OFDM systems,” IEEE Trans. Broadcast., vol. 58, no. 4, pp. 648–653, Dec. 2012.

[112] Report ITU-R BT. 2383-4: “Typical frequency sharing characteristics for digital terrestrial television broadcasting systems in the frequency band 470-862 MHz,” Mar. 2022.

[113] N. Shirai et al., “Laboratory experiments and large-scale field trials for evaluating advanced ISDB-T,” IEEE International Symposium on Broadband Multimedia Systems and Broadcasting 2019, June 2019.

[114] Recommendation ITU-R P.1546-5: “Method for point-to-area predictions for terrestrial services in the frequency range 30 MHz to 3000 MHz,” Sept. 2013.

[115] J. J. Gimenez et al., “5G new radio for terrestrial broadcast: A forward-looking approach for NR-MBMS,” IEEE Trans. Broadcast., vol. 65, no. 2, pp. 356-368, June 2019

[116] Report ITU-R BT.2343-8: “Collection of field trials of UHDTV over DTTB networks,” Mar. 2023.

[117] K. Takahashi, et al.: “Static Field Test Results for Advanced Terrestrial Broadcasting in Japan,” in Proc. IEEE BMSB, Jeju, Korea, 2020.

[118] M. Patzold, U. Killat, F. Laue, and Y. Li, “On the statistical properties of deterministic simulation models for mobile fading channels,” IEEE Transactions on Vehicular Technology, vol. 47, no. 1, pp. 254-269, Feb. 1998.

[119] Report ITU-R BT.2265-1, “Guidelines for the assessment of interference into the broadcasting service,” Nov. 2014.